Shaping magnetic fields with superconductor-metamaterial hybrids

Ph.D. Thesis in Physics of

Jordi Prat Camps

under the supervision of
Dr. Àlvar Sánchez
and
Dr. Carles Navau

Departament de Física
Universitat Autònoma de Barcelona

Bellaterra, June 2015

Al Toni, la Queralt i al Marc
A la resta de la meva família i als meus amics

Agraïments

En el moment en què escric aquestes paraules m'adono que, finalment, s'està apunt d'acabar una etapa de la meva vida. Una etapa comparable a una carrera de fons; ha estat un esforç sostingut i continu que ha ocupat bona part de la meva vida durant els darrers anys. De fet, tot i que porti 4 anys dedicat a la recerca continguda en aquest treball, la "carrera" en qüestió va començar fa molt més temps. La carrera la vaig començar molt abans que sabés, fins i tot, que la voldria córrer.

Ara que estic a prop del final, la sensació que tinc mentre escric aquestes paraules és d'autèntica felicitat i agraïment. Vull per tant aprofitar aquest espai per donar les gràcies d'una manera molt sincera a totes les persones que m'han acompanyat en aquesta aventura; sense l'entorn que he tingut estic segur que avui no estaria escrivint aquestes línies.

Vull començar donant les gràcies a tots els amics i companys de Manresa. Sorprèn pensar que amb alguns d'ells ens coneixem des de la nostra etapa a l'Oms... No vull deixar d'esmentar alguns noms, tot demanant disculpes ja d'entrada per tots els que no hi sou i hi hauríeu de ser: David, Josep Àngel, Margarita, Nil, Gemma, Nasi, Mei, Serra, Mario, Toni, Guille, Coro, Guzman... així com a la resta de companys de l'Oms i el Peguera. Vull aprofitar l'ocasió per enviar un càlid record a la "família" de l'Oms i de Prat (en especial a la Gemma Vilaseca i els seus) i a la gent i els professors de l'institut Lluís de Peguera. També vull plasmar un agraïment molt sincer per uns bons amics com són la Laura i l'Stefano, així com també per l'Enric Sarri i la seva família.

Seguidament vull donar les gràcies als amics que he fet durant els anys que porto a la Autònoma. No em refereixo només als companys de carrera sinó també als companys de cotxe, de festes i de moltes altres experiències; així com també als col·legues de doctorat, amb els que hem compartit dinars, somriures i preocupacions a parts iguals: Guillem, Sebastià, Dani, Alba, Albert, Sergi, Toni, Roger, Juanfra, Mònica i especialment la Marina. Vull plasmar un agraïment molt sincer per dos grans amics que han viscut tot

aquest treball d'una manera molt propera; l'Àlex i el Parra. També vull enviar una càlida abraçada al grup d'amics de Barcelona amb qui, en poc temps, hem viscut nombroses i intenses experiències. Vull dirigir un agraïment especialment sincer i profund a la Cristina, així com també a la Maria Oliva i als seus.

En aquest punt vull dedicar unes línies a la que ha estat la meva "segona casa" durant els últims anys; el Grup d'Electromagnetisme de la Universitat Autònoma de Barcelona. I és que em sento molt afortunat d'haver pogut formar part d'aquest petit grup, del que tant he après i amb el que tant he crescut. Us ho vull agrair molt sincerament perquè, segons el meu parer, la millor qualitat d'aquest grup són les persones que el formen i amb qui he tingut la sort de coincidir: Joan, Fernando, Jordi, Mª Josep, Chen, Guillem, Sebastià, Nuria, Carles i Àlvar. Vull dedicar un agraïment molt especial als meus tutors d'aquest treball, el Carles i l'Àlvar. No només per tot el què m'heu ensenyat sinó per la manera com ho heu sabut fer, guiant-me però concedint-me l'espai suficient com perquè mai perdés el rumb i a l'hora pogués pensar-lo per mi mateix. Però sobretot us vull agrair la vostra qualitat humana, qualitat que transcendeix les vostres virtuts científiques i que impregna de joia el record que guardaré d'aquesta experiència. Aquest agraïment també el vull estendre a la resta de família Sánchez-Pascual; Anna, Pau i Bernat; per haver-me fet partícip d'una gran lliçó de vida. En última instància també vull agrair al *Ministerio de Educación, Cultura y Deporte* d'Espanya la beca de *Formación de Profesorado Universitario (FPU)* rebuda (AP2010-2556), que m'ha permès el finançament durant aquests anys.

I finalment, vull plasmar un agraïment profund i sincer pel que ha estat i segueix sent un dels pilars més fonamentals de la meva vida, i del que em sento un autèntic privilegiat: la meva família. Començant per els meus avis Josep i Angeleta, i Joan i Rosa. No m'equivoco si dic que heu estat un referent i una inspiració per mi. M'heu deixat una gran petjada de valors tant essencials com la bondat, la generositat i l'esforç. També als meus oncles Artur i Nuri, i Joan (Miquel) i Mª Àngels, junt amb les meves cosines Marta, Eva i Judit. M'heu donat moltíssims bons moments i m'heu ajudat a somriure en ocasions en què em costava. I en última instància i molt especialment vull donar les gràcies a les persones amb qui més he compartit. Al Toni, el meu pare, per exercir a més a més de "pare" científic i alimentar la meva curiositat des de ben petit. Però sobretot per transmetre'm els valors de la humilitat i la bondat més pura. A la meva mare Queralt, per exercir d'autèntic pilar vital i donar-me l'equilibri i la tranquil·litat que tant m'ha fet créixer. I al meu germà Marc, per omplir-me i complementar-me d'una manera que tant sols una ànima bessona pot fer. A vosaltres especialment us dedico tot aquest treball. Gràcies de tot cor.

Jordi Prat Camps
Bellaterra, Juny de 2015.

Preamble

Magnetism is very important in various areas of science and technology, covering a wide range of scales and topics. Magnetism explains the flow of solar winds or the shielding of cosmic rays by the Earth's magnetosphere. At the opposite limit, magnetic fields are used to cold individual atoms and bring them to their fundamental quantum state. At an intermediate scale, a vast variety of everyday technologies base their operation in magnetic fields. Examples range from electromagnetic turbines, transformers and engines to medical techniques or data storage systems. Therefore, the ability to master and control magnetic fields represents a major chance to improve all of them.

In this thesis we present a new "toolbox" to shape magnetic fields and obtain novel and interesting effects. The work is inspired by the recent developments in the field of light manipulation, which are based on two key factors. On one hand the progress in building artificial materials with engineered microstructure (*metamaterials*) that exhibit exotic effective electromagnetic properties. On the other, the development of a theory (*transformation optics*) that determines the electromagnetic material properties required to obtain the desired effect. The combination of these factors has led to the realization of electromagnetic devices that could not be imagined some years before like invisibility cloaks, illusion devices that transform the image of an object into another, or electromagnetic analogous of black holes, for example.

This work presents the theoretical development and the experimental realization of various novel devices to control magnetic fields. Their design is based on different strategies; transformation optics theory is combined with solutions directly obtained from Maxwell equations, and ideal designs are turned into real devices taking advantage of the properties that magnetic materials offer to shape magnetic fields. At this point it is worth to remark the significant role played by superconducting materials. Among other features, superconductors ideally expel magnetic fields from their interior. This property, complemented with that of the ferromagnetic materials to concentrate magnetic fields,

has turned superconducting and ferromagnetic materials into the main building blocks of the different devices presented in this work.

The contents of this thesis are organized as follows. In chapter 1 we present a brief introduction on electromagnetism, focusing on the magnetostatic case. Ferromagnetic and superconducting materials are briefly described and transformation optics technique is introduced.

Chapter 2 covers the cloaking of magnetic fields. Analogous to the concept of an "invisibility" cloak for light, a cloak for static magnetic fields would prevent magnetic fields to penetrate in its interior and would make the cloak itself and its content magnetically undetectable from the exterior. A feasible design of magnetic cloak (*antimagnet*) is first developed. It is designed with transformation optics and is discretized in a series of shells that could be made of superconducting and ferromagnetic materials. We demonstrate that a simpler cylindrical bilayer structure consisting of an interior superconducting shell surrounded by a ferromagnetic one also cloaks magnetic fields. An experimental demonstration of such bilayer cloak is reported. Its properties are also experimentally studied for low-frequency magnetic fields, confirming that designs conceived for static fields can also be useful for low-frequency waves.

In chapter 3 we present our research on magnetic field concentration. Based on transformation optics, we present the analytical development of a cylindrical shell that concentrates an external applied field in its interior hole. Its properties are compared to the existing strategies to concentrate magnetic fields, showing a large and systematic improvement. The same shell expels the magnetic field of sources that are placed in its interior hole. Combining some of these shells we demonstrate that the field of a source (e.g. a magnet) can be concentrated at a distance from it. Although concentrating shells require magnetic permeabilities not directly found in natural materials, we show that they can be realized using superconducting and ferromagnetic pieces. Some shells are built and their properties to shape magnetic fields are experimentally demonstrated. The properties of these shells are also discussed for low-frequency time-dependent magnetic fields, showing that they allow to increase the magnetic coupling between circuits. This feature is applied to the case of wireless transfer of power, experimentally demonstrating that shells enhance the transferred power and the efficiency of the transfer.

In chapter 4 we develop *magnetic hoses*. Different from electromagnetic waves that easily propagate in waveguides or optical fibers, magnetic fields rapidly decay as one moves far from the source. Our proposal allows to transfer static magnetic fields to arbitrary distances. Combining transformation optics theory with numerical calculations, we present different hose designs. A feasible proposal consisting of only two parts (a ferromagnetic core surrounded by a superconducting shell) is studied in detail and is completed with analytical developments. Finally, the experimental realization of two of such hoses is reported and their transfer properties are measured.

Chapter 5 contains our research on magnetic wormholes. Inspired by cosmological wormholes, that connect two points in space through a path that is out of the conven-

tional 3D space, we study an analogous effect for static magnetic fields. The magnetic wormhole magnetically connects two points in space through a path that is magnetically undetectable. Such structure is not directly designed with transformation optics but is obtained by combining different magnetic materials; it is composed of an interior magnetic hose surrounded by a spherical superconducting shell and a spherical ferromagnetic *metasurface*. 3D numerical calculations are presented to demonstrate its properties and the experimental realization of an actual magnetic wormhole is reported, together with the measurements that validate its properties. Practical applications of the device are also discussed.

Finally, chapter 6 contains the global conclusions of this thesis.

Contents

CHAPTER 1

Introduction to essential concepts

In this chapter we present an introduction to some essential concepts involved in this thesis. We review the basic notions of electromagnetism and magnetic materials, giving an special attention to superconducting materials. We also present the technique of *transformation optics*, which will be applied to design and study different devices considered in this work.

1.1 Introduction to relevant electromagnetism concepts

1.1.1 Maxwell equations

The four Maxwell equations can be written in differential form as [1]

$$\nabla \times \mathbf{E} = -\frac{\partial \mathbf{B}}{\partial t}, \tag{1.1}$$

$$\nabla \times \mathbf{H} = \mathbf{J_f} + \frac{\partial \mathbf{D}}{\partial t}, \tag{1.2}$$

$$\nabla \cdot \mathbf{D} = \rho_{\mathrm{f}}, \tag{1.3}$$

$$\nabla \cdot \mathbf{B} = 0, \tag{1.4}$$

where $\mathbf{E}$ is the electric field, $\mathbf{D}$ the displacement field, $\mathbf{H}$ is the magnetic field, $\mathbf{B}$ is the magnetic induction, $\mathbf{J}_{\mathrm{f}}$ is the free current density and ρ_{f} is the free charge density. Some of these magnitudes are related through the following constitutive equations

$$\mathbf{B} = \mu_0 \left(\mathbf{H} + \mathbf{M}\right), \tag{1.5}$$

$$\mathbf{D} = \varepsilon_0 \mathbf{E} + \mathbf{P}, \tag{1.6}$$

where $\mathbf{M}$ is the magnetization of the material, $\mathbf{P}$ is the electric polarization of the material, μ_0 is the vacuum magnetic permeability and ε_0 is the vacuum electric permittivity. When no material is present $\mathbf{M} = \mathbf{P} = 0$, and simply $\mathbf{B} = \mu_0\mathbf{H}$ and $\mathbf{D} = \varepsilon_0\mathbf{E}$. The four Maxwell equations (1.1)-(1.4) plus the constitutive equations (1.5, 1.6) and the Lorentz force equation totally describe classical electromagnetic phenomena [1].

1.1.2 The static magnetic case

When none of the electromagnetic magnitudes changes over time, all the derivatives with respect to the time become zero and the four Maxwell equations decouple. In these *static* conditions electric and magnetic fields become independent from each other. *Magnetostatic* problems are described by the following two equations

$$\nabla \times \mathbf{H} = \mathbf{J}_\mathrm{f}, \tag{1.7}$$

$$\nabla \cdot \mathbf{B} = 0, \tag{1.8}$$

together with the constitutive relation (1.5). These equations lead to the following boundary conditions that fields have to satisfy at the interface between two magnetic media

$$\mathbf{n} \times (\mathbf{H_1} - \mathbf{H_2}) = \mathbf{K}_\mathrm{f}, \tag{1.9}$$

$$\mathbf{n} \cdot (\mathbf{B_1} - \mathbf{B_2}) = 0, \tag{1.10}$$

where subscripts 1 and 2 refer to mediums 1 and 2 in the interface, respectively. $\mathbf{K}_\mathrm{f}$ is the free surface current density and $\mathbf{n}$ is a unitary vector perpendicular to the interface that points outwards medium 2. Equations (1.7) and (1.9) can be written in terms of the magnetic induction using Eq. (1.5) as

$$\nabla \times \mathbf{B} = \mu_0(\mathbf{J}_\mathrm{f} + \mathbf{J}_\mathrm{M}), \tag{1.11}$$

$$\mathbf{n} \times (\mathbf{B_1} - \mathbf{B_2}) = \mu_0(\mathbf{K}_\mathrm{f} + \mathbf{K}_\mathrm{M}), \tag{1.12}$$

where $\mathbf{J}_\mathrm{M}$ and $\mathbf{K}_\mathrm{M}$ are the magnetization current density and the magnetization surface current density, respectively

$$\mathbf{J_M} \equiv \nabla \times \mathbf{M}, \tag{1.13}$$

$$\mathbf{K_M} \equiv \mathbf{n} \times (\mathbf{M_1} - \mathbf{M_2}). \tag{1.14}$$

Magnetic materials can be described through the magnetic susceptibility tensor, $\overline{\overline{\chi}}_m$, defined as

$$\mathbf{M}(\mathbf{r}) = \overline{\overline{\chi}}_m \mathbf{H}(\mathbf{r}). \tag{1.15}$$

In general, the relationship between the magnetic field and the magnetization inside actual materials can be cumbersome, depending on the magnitude and the direction of

the field, and also on the position in the material. If materials are assumed linear, homogeneous and isotropic the susceptibility becomes a constant scalar magnitude. Applying Eq. (1.15) to the constitutive relation (1.5) we find

$$\mathbf{B} = \mu_0 \left(\mathbb{1} + \overline{\overline{\chi}}_m\right) \mathbf{H} = \mu_0 \, \overline{\overline{\mu}} \, \mathbf{H}, \tag{1.16}$$

where $\overline{\overline{\mu}} \equiv \mathbb{1} + \overline{\overline{\chi}}_m$ is the magnetic relative permeability tensor.

Absence of free currents: magnetic poles

In many actual situations there are no free currents in the magnetic materials, i.e. $\mathbf{J_f} = 0$. This allows to rewrite Eqs. (1.7)-(1.10) in terms of $\mathbf{H}$ using Eq. (1.5)

$$\nabla \times \mathbf{H} = 0, \tag{1.17}$$

$$\nabla \cdot \mathbf{H} = \rho_{\mathrm{M}}, \tag{1.18}$$

$$\mathbf{n} \times (\mathbf{H_1} - \mathbf{H_2}) = 0, \tag{1.19}$$

$$\mathbf{n} \cdot (\mathbf{H_1} - \mathbf{H_2}) = -\sigma_{\mathrm{M}}, \tag{1.20}$$

where ρ_{M} and σ_{M} are the volume and surface magnetic poles densities, respectively. They are defined as

$$\rho_{\mathrm{M}} \equiv -\nabla \cdot \mathbf{M}, \tag{1.21}$$

$$\sigma_{\mathrm{M}} \equiv \mathbf{n} \cdot (\mathbf{M_1} - \mathbf{M_2}) \tag{1.22}$$

This establishes a clear analogy between the magnestostatic case with no free currents and the electrostatic case. The magnetic material, thus, can be fully substituted by the corresponding magnetic poles densities and the magnetic field can be calculated through

$$\mathbf{H} = \mathbf{H}_{\mathrm{a}} + \mathbf{H}_{\mathrm{d}}, \tag{1.23}$$

where $\mathbf{H}_{\mathrm{a}}$ is the field created by external sources (if any) and $\mathbf{H}_{\mathrm{d}}$ is the demagnetizing field created by the poles

$$\mathbf{H}_{\mathrm{d}}(\mathbf{r}) = \frac{1}{4\pi} \int_V \rho_M(\mathbf{r}') \frac{\mathbf{r} - \mathbf{r}'}{|\mathbf{r} - \mathbf{r}'|^3} dV' + \frac{1}{4\pi} \int_S \sigma_M(\mathbf{r}') \frac{\mathbf{r} - \mathbf{r}'}{|\mathbf{r} - \mathbf{r}'|^3} dS'. \tag{1.24}$$

The analogy with the electrostatic case is completed by considering that Eq. (1.17) allows to write the magnetic field as the gradient of a scalar magnetic potential, ϕ_{m}, as

$$\mathbf{H} = -\nabla \phi_{\mathrm{m}}. \tag{1.25}$$

1.2 Magnetic materials

Magnetic materials can be classified depending on the relationship between the magnetic field and the magnetization appearing in the material. Here we describe the main macroscopic features of two of these materials that will be referred throughout this work.

- *Diamagnets:* The magnetization and the field have opposite directions, so that the susceptibility is negative and its magnitude is usually very small. The maximum negative susceptibility is $\chi_m = -1$ for perfect diamagnets. These materials expel magnetic field lines, making $\mathbf{B} = 0$ in its interior. Ideal superconducting materials have zero magnetic induction field in their interior and can be considered, in some cases, as perfect diamagnets, as will be discussed in the following section.

- *Ferromagnets:* The magnetization is aligned with the field and the magnitude of the susceptibility is large. In actual ferromagnetic materials, even when the field is removed, part of the magnetization (the remanent magnetization) is retained. This results in complex non-linear hysteresis loops in which the magnetization not only depends on the existing magnetic field but also on the previous magnetic states. Ferromagnetic materials are classified depending on their remanent magnetization and also on the coercitive field that has to be applied in the opposite direction to make $\mathbf{M} = 0$. Materials with large remanent magnetizations and coercitive fields are called *hard* ferromagnets and that with small remanent magnetizations and coercitive fields are called *soft*.

  When the temperature of a ferromagnet is increased beyond a certain value (the *Curie* temperature), magnetization practically vanishes due to thermal agitation and the material becomes *paramagnetic*. In these conditions a small magnetization appears aligned with the applied field ($\chi_m \gtrsim 0$) and it disappears in absence of field.

  For small applied fields, soft ferromagnetic materials can be modeled with a linear relationship between $\mathbf{M}$ and $\mathbf{H}$, i.e. considering a constant scalar susceptibility. Ferromagnetic materials exist with a wide range of susceptibility values, ranging from $\chi_m \simeq 0$ to effectively infinite. *Ideal soft* ferromagnets are considered to have a constant infinite susceptibility, $\chi_m \to \infty$, which implies zero magnetic field in their interior ($\mathbf{H} = 0$) to keep a finite magnetization.

1.2.1 Superconductors

Superconductivity is a thermodynamic state of some materials that, when they are cooled below a critical temperature T_c, present two properties simultaneously. On one hand they exhibit zero electric resistivity [2]. On the other they present, in principle, a diamagnetic behavior, excluding and expelling the magnetic induction field from their interior except in an outermost layer of thickness λ [3], as is discussed below.

Superconductors can be classified in different ways, one possibility is depending on their critical temperature. The first superconducting materials that were discovered were metals like mercury, lead or niobium, whose critical temperatures were below 10K. Other alloys and compounds also demonstrated to have superconducting properties, even though at temperatures not higher than 30K. All these materials are now known

as low-temperature superconductors. In 1986 J. G Bednorz and K. A. Müller discovered superconductivity in cuprate oxides. This boosted the research on the topic and soon some other ceramic compounds demonstrated superconductivity at much higher temperatures, such as YBaCuO-123 at T_c =92K [4] or BiSrCaCuO-1112 at T_c =105K [5]. These materials, with transition temperatures above the boiling temperature of the liquid nitrogen (77K), are know as high-temperature superconductors.

Regarding the magnetic properties of the superconducting materials, they can be divided into type-I and type-II superconductors. When a magnetic field smaller than a certain critical field H_c is applied to a type-I superconductor below its critical temperature, some shielding currents appear in the surface of the material. These currents extend, in principle, over a thickness depth λ and make the magnetic induction inside the material $\mathbf{B} = 0$. In the shell of flowing currents the magnetic induction decreases exponentially towards the interior of the superconductor. This state is called the Meissner state. For fields higher than H_c, superconducting properties disappear.

Type-II superconductors exhibit a richer behavior. For fields smaller than a critical field $H_{c,1}$ they present the Meissner state. However, for fields between $H_{c,1}$ and another certain critical field $H_{c,2}$, partial flux penetration occurs inside the superconductor in the form of bundles of flux that are surrounded by superconducting currents forming vortices. This is called the mixed state. For fields higher than $H_{c,2}$ superconductivity disappears. In the mixed state, the movement of the vortices (caused by a transport current, for example) dissipates energy and resistive losses appear. However, vortices can be fixed in impurities and defects inside the superconductors, which act as pinning centers. Actually, defects are artificially introduced at will to produce this effect and minimize ohmic losses [6, 7].

Superconductors are studied with different models. The BCS theory [8], proposed by J. Bardeen, L. Cooper and R. Schrieffer in 1957, microscopically explains the origin of the superconductivity and successfully describes the low-temperature superconductivity. However, it is unable to explain high-temperature superconductors. Differently, the Ginzburg-Landau theory [9] explains the phenomena occurring near second-order phase transitions and, thus, describes approximately superconductors at temperatures near T_c. Other phenomenological models are used to understand and design superconducting parts and devices in a more practical way. The London theory [10] explains the Meissner effect and is used to model the superconducting shielding currents appearing in the type-I superconductors and also in the type-II for $H < H_{c1}$. On the other hand, the critical-state model was formulated to describe the mixed state of superconductors with strong pinning [11, 12]. It assumes that any electromagnetic force induces a macroscopic constant current density, J_c, in the superconducting material. This simple model, proposed by C. P. Bean in 1962, has been proved to explain many magnetic measurements performed in such superconductors [13, 14, 15, 16, 17]. Intuitively, for a uniform field applied to an infinite superconducting slab (starting with zero field and current), this model shows that the magnetic field decays linearly towards the interior of the material

with a slope J_c [12]. The model also predicts a strong non-linear and hysteretic behavior so that the current distribution for a given applied field not only depends on this field but also on all the previous magnetic states.

In spite of the complicated phenomenology shown by superconducting materials, throughout this work we will only exploit their property to expel magnetic field from their interior. For this reason we will consider them as ideal diamagnets, having a constant $\chi_m = -1$ ($\mu = 0$). Although this is not strictly true for any superconducting material, actual superconductors effectively exhibit this property in many practical situations. This is the case of type-I superconductors with small values of London penetration depths (λ) compared to their size, or type-II superconductors with large critical current densities J_c and fields significantly smaller than $H_{c,2}$. The application of the ideas presented in this work for strong magnetic fields or for particular materials requires a deeper and more accurate study that is beyond the scope of this thesis.

1.3 Transformation optics

Transformation optics is an emerging technique for the design of advanced electromagnetic media [18]. It is based on the form invariance of Maxwell equations under coordinate transformations and provides an intuitive way to manipulate the electromagnetic propagation. It plays an analogous role to the Snell law; this traditional design tool of optics visualizes the propagation of light in terms of rays that are deviated by different transparent media. This intuitive picture has been of vital importance in the design progress of optical devices and explains why it is still used nowadays, in spite of its simplified assumptions [19].

Transformation optics provides an analogous intuitive tool for the manipulation of electromagnetic fields on all length scales, exact to the level of Maxwell equations. It is based on the fact that Maxwell equations keep their form in any transformed coordinate system, as long as the permittivity and permeability tensors are properly modified.

Suppose electromagnetic fields propagating in a cartesian space, $\mathbf{x}$, following a certain path (Fig. 1.1**a**). If we now consider a transformed space, $\mathbf{x}'$, in which electromagnetic fields describe a different trajectory (Fig. 1.1**b**), Maxwell equations maintain the same form if the constitutive parameters in this transformed space are [18, 20, 21, 22, 23]

$$\mu'(\mathbf{x}') = \frac{\Lambda\,\mu(\mathbf{x})\,\Lambda^{\mathrm{T}}}{\det\Lambda}, \qquad \varepsilon'(\mathbf{x}') = \frac{\Lambda\,\varepsilon(\mathbf{x})\,\Lambda^{\mathrm{T}}}{\det\Lambda}, \tag{1.26}$$

where $\mu(\mathbf{x})$ and $\varepsilon(\mathbf{x})$ are the permeability and permittivity distributions in the original cartesian space. Λ is the Jacobian transformation matrix whose elements are

$$\Lambda_{ij} = \frac{\partial x_i'}{\partial x_j}. \tag{1.27}$$

Therefore, if these permeability and permittivity values $\mu'(\mathbf{x}')$ and $\varepsilon'(\mathbf{x}')$ are placed in

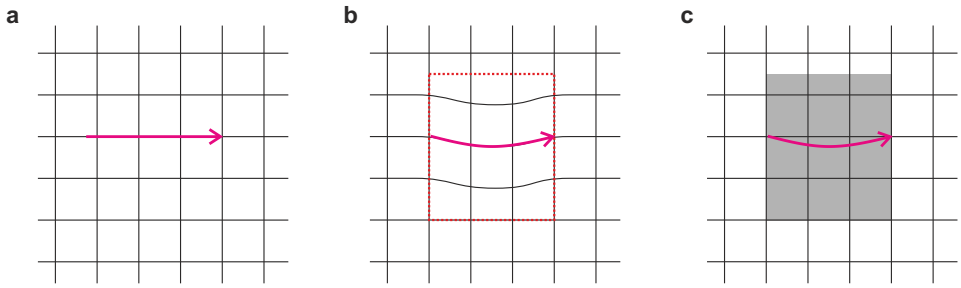

Figure 1.1: Sketch showing how transformation optics is applied to shape electromagnetic fields. The propagation of electromagnetic fields in an original cartesian space, (**a**), is changed by transforming the space (**b**). If the appropriate material parameters are placed in the original space (dark region in **c**), electromagnetic propagation occurs as if the space was effectively transformed.

the original undistorted space, electromagnetic fields will propagate in the same fashion as if they were propagating in the transformed space (see Fig. 1.1**c**). Fields that fulfill Maxwell equations in this transformed space are [18, 22, 23]

$$\mathbf{H}'(\mathbf{x}') = (\Lambda^{\mathrm{T}})^{-1}\,\mathbf{H}(\mathbf{x}), \qquad \mathbf{E}'(\mathbf{x}') = (\Lambda^{\mathrm{T}})^{-1}\,\mathbf{E}(\mathbf{x}), \tag{1.28}$$

being $\mathbf{H}(\mathbf{x})$ and $\mathbf{E}(\mathbf{x})$ the field distributions in the original cartesian space. This shows how this technique allows to design devices to master electromagnetic fields with almost complete freedom. From a practical point of view, though, complicated transformations imply cumbersome anisotropic spatial-dependent permittivities and permeabilities.

This form invariance of Maxwell equations was first used to simplify numerical electromagnetic simulations by adapting computer codes from cartesian to cylindrical geometries [24]. However, with the advances in the realization of materials with exotic electromagnetic properties, the technique was coined as *transformation optics* and emerged as an extraordinary tool to determine the material properties needed to master electromagnetic fields [20, 21]. Since its appearance, transformation optics has been applied to design cloaks with different shapes [20, 21, 25, 26, 27, 28, 29, 30, 31, 32], electromagnetic concentrators [31, 33, 34, 35], rotators [35, 36, 37], wave-shape transformers [38, 39, 40], waveguides [41, 42], or even devices mimicking celestial objects [43, 44] like electromagnetic black holes [45, 46, 47] or wormholes [48], among other devices. It has also been used to design structures for controlling the flow of surface plasmon polaritons at metallic surfaces [49, 50, 51, 52].

It is worth to mention that a similar work considering 2D geometrics optics was presented almost simultaneously [53] to the transformation optics theory [20]. The mold of optic rays presented in that work can be understood as a particular limit of the more general theory of transformation optics, which considers the full Maxwell equations. Precisely because of this fact, this latter theory can be applied to control not only electromagnetic waves but also electric and magnetic fields in the static case. Throughout this thesis transformation optics theory will be used to determine the magnetic perme-

abilities required to control static magnetic fields in different ways.

Beyond electromagnetism, transformation optics ideas have also been extended to other physical systems in which the governing equations have a similar form-invariance under space transformations [54]. Some examples include the control of acoustic waves [55, 56, 57, 58, 59], fluid waves [60, 61], elastic waves [22, 62, 63, 64, 65] or thermal diffusion [66, 67, 68], among others.

CHAPTER 2

Cloaking magnetic fields

Invisibility is one of the ancient dreams of mankind. Making things invisible and hide them from view is an appealing idea that has appeared frequently in literature and films. Although attractive, this dream belonged to the realm of science fiction for many years. During the last decades of the 20th century important advances in the realization of materials with exotic properties were made. Artificial media with engineered microstructure, known as *metamaterials*, demonstrated anomalous electromagnetic properties not available in natural materials [69, 70, 71]. All this opened the way to manipulate electromagnetic fields in ways that could not be imagined some years before, realizing negative refraction [72, 73, 74, 75, 76, 77] or sub-wavelength focusing [76], among others effects.

In 2006 two independent works demonstrated that, for ray optics [53] and electromagnetic waves [20], light could be bended and guided in an almost arbitrary way through media with changing optical properties. The theory, called *transformation optics* [20], was based on the form of Maxwell equations and its invariance under space transformations; the material parameters required to control the light in a certain way could be derived from a space transformation that yielded the desired wave propagation.

One of the first applications of this theory was to design an *invisibility cloak* [20, 53, 78, 79]; a device that suppresses the scattering appearing when any electromagnetic wave hits an object. This cloak from transformation optics was designed by expanding and redistributing the space around a given region so that light rays were diverted around a zone that was rendered invisible. Although this was the first realistic approach to an invisibility cloak, the required material parameters were cumbersome, and anisotropic and fine-tuned inhomogeneous permittivities and permeabilities were needed. Moreover, they implied additional fundamental problems such as superluminal phase velocities

and extremely narrow bandwidths [80, 81, 82, 83]. Despite all these difficulties, ideas were experimentally demonstrated by constructing a simplified version of a cloak for microwave waves [26]. This boosted the research on cloaking and, more generally, on the enormous possibilities offered by the theory of transformation optics.

The initial idea of perfect cloaking by means of total scattering suppression for any impinging wave evolved to more practical approaches, in which some requirements were simplified to obtain more feasible and functional designs. For example, considering the geometric-optics limit and applying non-Euclidean space transformations without singularities, a broad bandwidth cloak for light rays was designed [84]. Restricting the directionality of the cloak important simplifications were also obtained. This is the concept behind the carpet cloak [85], which consists on placing a desired object under a reflective surface an hiding the bump with the cloak so that appears completely flat. In this scenario, quasi-conformal transformations were applied to minimize the anisotropy of the required materials, leading to a broadband cloaking effect. This was demonstrated for microwaves [86] and also for optical frequencies [87, 88]. More simplified cases were also considered, applying geometric optics to design unidirectional or multidirectional cloaks [89, 90]. In these cases natural birefringent materials were used to shape light rays and demonstrate the effect in the visible spectrum. An alternative path to achieve electromagnetic invisibility is the scattering cancellation approach. This consists on canceling the most important terms of the scattering caused by an object, which can be achieved by using less demanding materials [83]. Plasmonic and mantle cloaks are based on this principle [91, 92] and have been thoroughly studied and experimentally validated [93, 94], mainly in the microwave regime.

The science of invisibility has also been exported to other physical systems in which the concept of an undetectable cloak may also be useful [95]. This is the case of acoustic waves, governed by the elasto-dynamic equations [22, 55], for which different cloaks have been studied and built [55, 58]. Transformation optics has also been applied to mold the heat flow, not only to build thermal cloaks but other devices like heat concentrators [96, 66, 97, 98]. Interestingly, diffusion equations that govern the flow of heat are very similar to those for the propagation of light in diffusive mediums, like fog or frosted glass. This has led to the recent realization of a broadband cloak for visible light in diffusive scattering medium [99].

The concept of the invisibility cloak was also considered in the limit case of zero frequency. In 2007 Wood and Pendry [100] introduced the idea of *magnetic cloaking*. They showed that in the dc case (electromagnetic waves in the limit of zero frequency), for which the electric and magnetic effects decouple, a magnetic cloak for concealing static magnetic fields without disturbing the external field could be designed by transformation optics and would require only to tune the magnetic permeability (μ) of the material. In particular this would require a material with anisotropic and position-dependent permeability values, smaller than 1 in one direction and larger than 1 in

the perpendicular direction. A $\mu < 1$ could be achieved by arrays of superconducting plates [100, 101, 102], whereas $\mu > 1$ could be obtained with ferromagnetic materials. However, no method was presented to achieve the required position-dependent values in perpendicular directions simultaneously and, for this reason, no magnetic cloak had been designed nor fabricated then.

This eventual magnetic cloaking would have not only scientific interest but also important technological applications, since magnetic fields are fundamental to many everyday technologies, from energy generators or transformers to magnetic memories or medical tests. Many of these technologies are based on a precise spatial distribution of magnetic field, which should not be perturbed by magnetic objects—not only by magnets but also by any material containing iron or steel, for example.

In this chapter we present different strategies to cloak static magnetic fields. Our main goal is to explore and develop feasible designs that can be realized with actual materials and existing technologies.

A parallel work for the static electric case has also been done in recent years. Cloaks and other devices for dc electric fields have been fabricated using resistor networks [103, 104, 105].

2.1 The antimagnet

The first proposal for cloaking static magnetic fields [100] was based on the cloak for electromagnetic fields [20]. Wood and Pendry showed that the permeabilities required for an electromagnetic cloak would also work for static magnetic fields. Electromagnetic cloaks were originally designed applying linear space transformations, leading to inhomogeneous and anisotropic permeability components for the shell [20]. For example, the permeabilities

$$\mu_\rho = \frac{\rho - R_1}{\rho}, \qquad \mu_\varphi = \frac{\rho}{\rho - R_1}, \tag{2.1}$$

would result in a cylindrical cloak with inner and outer radii R_1 and R_2, respectively. Notice this cloak requires fine-tuned permeability components that depend on the position within the material. Moreover, at the inner surface ($\rho \to R_1$), the material needs to be extremely anisotropic with $\mu_\rho \to 0$ and $\mu_\varphi \to \infty$. This makes any practical implementation very difficult.

We address the problem of magnetic cloaking by defining more precisely our goal. Rather than a magnetic cloak—null interior field and external field undistorted—we want to design an *antimagnet* [106], defined as a material forming a shell that encloses a given region in space while fulfilling the following two conditions

i The magnetic field created by any magnetic element inside the inner region—e.g. a permanent magnet—should not leak outside the region enclosed by the shell.

ii The system formed by the enclosed region plus the shell should be magnetically undetectable from outside (no interaction—e.g. no magnetic force—with any external magnetic source).

In addition to these two conditions, the antimagnet should also be realizable with actual materials. For this reason we first explore whether other permeability arrangements - simpler than that of Eq. (2.1), which require inhomogenous and anisotropic materials- can cloak magnetic fields [28]. In particular we will investigate alternative space transformations that yield homogeneous cloaking shells.

2.1.1 Homogeneous anisotropic shell to cloak magnetic fields

Consider the following cylindrical non-linear space transformation between $\rho = R_0$ and $\rho = R_2$

$$\begin{cases} \rho' = R_2 \left(\frac{\rho}{R_2}\right)^k, \\ \varphi' = \varphi, \qquad\qquad \rho \in [R_0, R_2) \\ z' = z, \end{cases} \tag{2.2}$$

which relocates the space between $\rho'(\rho = R_0) = R_1$ and $\rho'(\rho = R_2) = R_2$ if k fulfills the relation

$$R_0 = R_2 \left(\frac{R_2}{R_1}\right)^{-\frac{1}{k}}. \tag{2.3}$$

If $R_0 < R_1$ this corresponds to a compression of the space between R_1 and R_2, as sketched in Fig. 2.1**b**. The parameter k ranges from 0 (when $R_0 \to 0$) to 1 ($R_0 \to R_1$). To keep the transformed space continuous, the space $\rho < R_0$ is linearly expanded through

$$\begin{cases} \rho' = \frac{R_1}{R_0}\rho, \\ \varphi' = \varphi, \qquad\qquad \rho \in [0, R_0) \\ z' = z. \end{cases} \tag{2.4}$$

From the final transformed space (Fig. 2.1**c**) notice this would work as a cloaking shell; the field outside would be unperturbed and the field inside could be made arbitrarily small by choosing a small R_0 and compressing the field between R_1 and R_2. Applying equations (1.26) and (1.27) of transformation optics theory we find the permeability tensors required to obtain this behavior. Expressed in the usual cylindrical basis they are

$$\mu' = \begin{pmatrix} k & 0 & 0 \\ 0 & \frac{1}{k} & 0 \\ 0 & 0 & \frac{1}{k}\left(\frac{\rho'}{R_2}\right)^{\frac{2}{k}-2} \end{pmatrix}, \qquad \rho' \in [R_1, R_2) \tag{2.5}$$

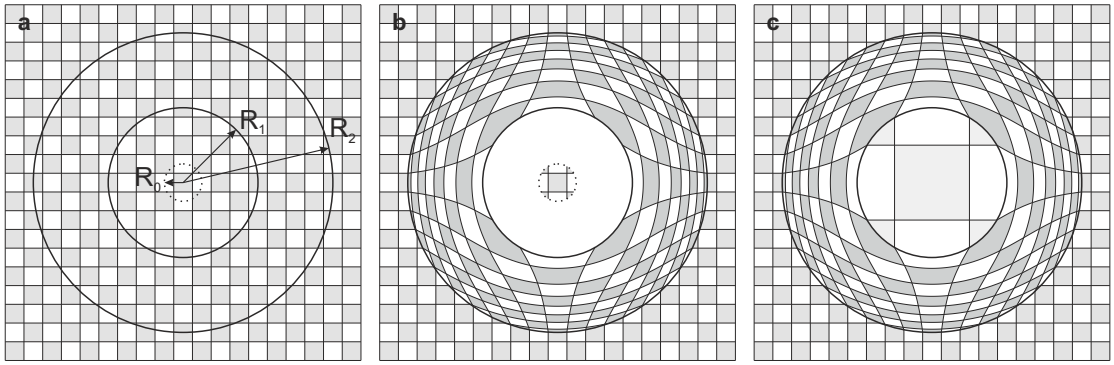

Figure 2.1: Sketch of the space transformations that lead to a cloak with homogeneous and anisotropic permeability components.

$$\mu' = \begin{pmatrix} 1 & 0 & 0 \\ 0 & 1 & 0 \\ 0 & 0 & \left(\frac{R_1}{R_2}\right)^{\frac{2}{k}-2} \end{pmatrix}. \qquad \rho' \in [0, R_1) \tag{2.6}$$

Since we assume translational symmetry along the z-axis, no parameter can depend on the z coordinate. Moreover, we assume the fields are in the xy plane and there are no z-components, so that only the 2x2 upper-left minor of the permeability tensor is relevant. This means that a homogeneous anisotropic cylindrical shell with permeability components fulfilling $\mu_\rho\,\mu_\varphi = 1$ (which we name a *conjugate* shell) keeps any externally applied magnetic field (with z-translational symmetry) undistorted. The field in all regions of space can be calculated from transformation optics [Eq. (1.28)] finding

$$\mathbf{H}'\left(\rho', \varphi'\right) = \left(\frac{R_2}{R_1}\right)^{1-\mu_\varphi} \mathbf{H}\left(\left(\frac{R_2}{R_1}\right)^{1-\mu_\varphi} \rho', \varphi'\right), \qquad \rho' \in [0, R_1) \tag{2.7}$$

$$\begin{cases} H'_\rho\left(\rho', \varphi'\right) = \mu_\varphi \left(\frac{R_2}{\rho'}\right)^{1-\mu_\varphi} H_\rho\left(\left(\frac{R_2}{\rho'}\right)^{1-\mu_\varphi} \rho', \varphi'\right), \\ H'_\varphi\left(\rho', \varphi'\right) = \left(\frac{R_2}{\rho'}\right)^{1-\mu_\varphi} H_\varphi\left(\left(\frac{R_2}{\rho'}\right)^{1-\mu_\varphi} \rho', \varphi'\right), \end{cases} \qquad \rho' \in [R_1, R_2) \tag{2.8}$$

$$\mathbf{H}'\left(\rho', \varphi'\right) = \mathbf{H}\left(\rho', \varphi'\right), \qquad \rho' \in [R_2, \infty) \tag{2.9}$$

where we have used that $\mu_\rho = k$ and $\mu_\varphi = 1/k$, according to Eq. (2.5). $\mathbf{H}(\rho, \varphi)$ is the external applied field expressed in the cylindrical basis.

Equation (2.9) confirms the external field is not distorted by the shell. In its interior, Eq. (2.7) shows that the field can be arbitrarily reduced by increasing the angular permeability of the shell, and in the limit case $\mu_\varphi \to \infty$ (and $\mu_\rho \to 0$) the interior

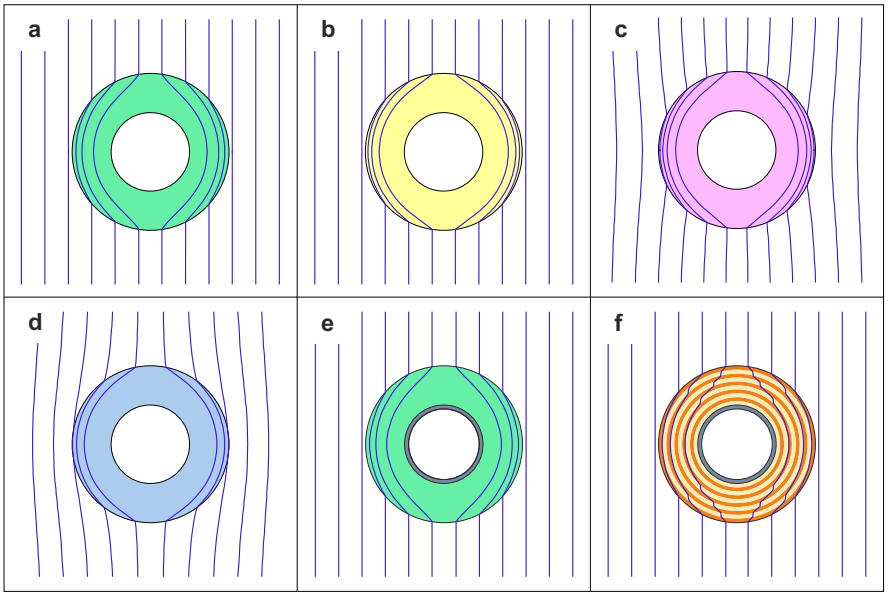

Figure 2.2: Numerical calculations of field lines (blue) for a uniform magnetic field applied to different cylindrical shells, having (**a**) $\mu_\varphi = 1/\mu_\rho = 6$, (**b**) $\mu_\varphi = 1/\mu_\rho = 10$, (**c**) $\mu_\varphi = 12$ and $\mu_\rho = 1/6$, (**d**) $\mu_\varphi = 6$ and $\mu_\rho = 1/16$. (**e**) An ideal superconducting shell (gray) is placed inside a shell with $\mu_\varphi = 1/\mu_\rho = 6$, showing no external field distortion. (**f**) An antimagnet made of 5 FM layers (orange) with $\mu^{\mathrm{FM}} = 6$ and 5 SC layers (yellow) with $\mu_\rho^{\mathrm{SC}} = 0.104$ and an inner superconductor with $\mu = 0$ (gray).

field is totally canceled. This limit corresponds to a space transformation in which $R_0 \to 0$, meaning that a one-dimensional line is expanded into a cylindrical region. Transformations involving such singular transformations have been typically applied to design electromagnetic cloaks [20, 26, 53, 100] [see that of Eq. (2.1) for example], which result in extreme anisotropic parameters and cause intrinsic causality problems of the involved propagating waves [81, 107, 108, 109]. Although these problems do not apply to our static problem, the limit case $\mu_\varphi = 1/\mu_\rho \to \infty$ has other practical drawbacks involving, for example, extreme values of field at the outermost surface of the shell. To design a feasible magnetostatic cloak, thus, it will be sufficient to choose a small value of $\mu_\rho > 0$ (see Fig. 2.2**a** and **b** for numerical calculations[1] of shells with $\mu_\varphi = 1/\mu_\rho = 6$ and $\mu_\varphi = 1/\mu_\rho = 10$, respectively).

In this way we have found a simpler homogeneous anisotropic arrangement of permeabilities ($\mu_\varphi = 1/\mu_\rho$ with $1 \gg \mu_\rho > 0$) that allows to cloak any externally applied magnetic field.

This result can be alternatively found solving the two magnetostatic Maxwell equations (1.7, 1.8). For this purpose we consider a cylindrical shell with constant radial and angular relative permeabilities μ_ρ and μ_φ, respectively, in the particular case of a

[1] All numerical calculations included in this thesis have been performed with the finite-elements software COMSOL Multiphysics, AC/DC module.

uniform external applied field $\mathbf{H}_a = H_a\hat{x}$. Since there are no free currents, a magnetic scalar potential is defined as $\mathbf{H} = -\nabla\phi$. Potential inside ($\rho < R_1$) and outside the shell ($\rho > R_2$) has to satisfy the Laplace equation. Since the shell is assumed anisotropic, the potential within the shell material ($R_1 < \rho < R_2$) does not fulfill the Laplace equation but the following one

$$\rho^2\frac{\partial^2\phi}{\partial\rho^2} + \rho\frac{\partial\phi}{\partial\rho} + \left(\frac{\mu_\varphi}{\mu_\rho}\right)\frac{\partial^2\phi}{\partial\varphi^2} = 0. \tag{2.10}$$

The solution of this equation can be found following a similar procedure as for the Laplace equation using separation of variables. Considering that the potential at $\rho \to 0$ has to be finite, at $\rho \to \infty$ has to tend to the applied one ($-H_a\,\rho\cos\varphi$) and imposing the four boundary conditions [Eqs. (1.9, 1.10)] at the surfaces $\rho = R_1$ and $\rho = R_2$, we can find the solution of the potential in the three different regions. We are interested in the external field distortion and the field inside the shell, where potential is

$$\phi(\rho,\varphi) = -A\rho\cos\varphi, \qquad \rho < R_1 \tag{2.11}$$

$$\phi(\rho,\varphi) = \left(-H_a\rho + \frac{B}{\rho}\right)\cos\varphi, \qquad \rho > R_2 \tag{2.12}$$

being A and B constants related to the real[2] positive-defined auxiliary variables $p \equiv \sqrt{\mu_\rho\mu_\varphi}$ and $u \equiv \sqrt{\mu_\varphi/\mu_\rho}$ as

$$A = H_a\frac{-4p(R_2/R_1)^{1+u}}{(-1+p)^2 - (1+p)^2(R_2/R_1)^{2u}}, \tag{2.13}$$

$$B = H_a\frac{(-1+p^2)R_2^2[1-(R_2/R_1)^{2u}]}{(-1+p)^2 - (1+p)^2(R_2/R_1)^{2u}}. \tag{2.14}$$

Equation (2.11) indicates that the field inside the shell is always uniform and has the direction of the external applied field. The external distortion caused by the shell, the second term of the Eq. (2.12), has a dipolar shape (i.e. is the same expression as the potential created by a line dipole with magnetic moment per unit length $\eta\hat{x}$, with η proportional to the constant B). The only case for which $B = 0$, and thus there is no distortion, is for $\mu_\varphi = 1/\mu_\rho$ (apart from the trivial case $R_1 \to R_2$). Then $p = 1$ and $u = \mu_\varphi$, simplifying A so that the field inside the shell is

$$\mathbf{H}_{\text{in}} = \left(\frac{R_2}{R_1}\right)^{1-\mu_\varphi} H_a\hat{x}, \tag{2.15}$$

same as in Eq. (2.7). For non-conjugate permeabilities, we first consider the case of $\mu_\rho\,\mu_\varphi > 1$ ($p > 1$). Then $B > 0$ and the distortion corresponds to a dipole with magnetic moment in the direction of the applied field, so that the total field lines are attracted by the shell (a distortion similar to that caused by a ferromagnetic material, see Fig. 2.2**c**). For $\mu_\rho\,\mu_\varphi < 1$ ($p < 1$), $B < 0$ and the distortion corresponds to a dipole in the opposite direction, expelling the total field lines (similar to the distortion of a

[2]Throughout this work we will restrict to positive values of magnetic permeability.

diamagnetic material, see Fig. 2.2**d**). The conjugate case $\mu_\rho\,\mu_\varphi = 1$ is the middle case in which lines are kept exactly uniform. Notice this last discussion on the distortion for non-conjugate shells cannot be done from transformation optics results. In that case the transformation keeps the external space undistorted and, thus, results only consider cases in which the external field is unperturbed.

In view of these results, a homogeneous anisotropic shell with $\mu_\varphi = 1/\mu_\rho$ and $1 \gg \mu_\rho > 0$ will be the starting point for the design of the antimagnet. Although such shell provides magnetic cloaking, leaving any external field unperturbed, this is not an antimagnet because the magnetic field created by a source in its interior would leak to the exterior. To avoid this we introduce a superconducting layer at the inner surface of the shell, modeled with a zero relative permeability ($\mu = 0$). Then, applying magnetostatic boundary conditions at its inner surface, it can be demonstrated that condition (i) is fulfilled. Introducing such a superconducting layer does not substantially modify the property of cloaking, as long as the angular permeability is sufficiently larger than 1, because in this case magnetic field is mostly excluded from the interior part of the shell and, thus, the distortion caused by the superconductor is very small (see Fig. 2.2**e**).

In this way an antimagnet design is being outlined: an inner superconducting layer and an outer homogeneous shell. However, this scheme alone cannot yet solve our goal of a feasible design, because the outer shell would require fine-tuned anisotropic permeability values and such kind of materials are not available.

It is worth to remark that a similar development can be done considering an homogeneous anisotropic spherical shell. If the two magnetostatic Maxwell equations are solved for a uniform external applied field, we find the exterior field is undistorted if the relative permeability components of the shell (in the spherical base) fulfill

$$\mu_\varphi = \mu_\theta = \frac{1}{2}\left(1 + \frac{1}{\mu_r}\right). \tag{2.16}$$

Notice this non-distortion condition is essentially different from that for the cylindrical case ($\mu_\varphi = 1/\mu_\rho$). Actually, this solution for the spherical case cannot be obtained from transformation optics theory applying a radial space transformation analogous to that used for the cylinder. The field inside the shell is found to be

$$\mathbf{H}_{\text{in}} = \left(\frac{R_2}{R_1}\right)^{2-2\mu_\theta} \mathbf{H}_a. \tag{2.17}$$

This shows that, for the spherical case, an homogeneous anisotropic shell fulfilling Eq. (2.16) with $\mu_\varphi = \mu_\theta \gg 1$ also acts as a magnetic cloaking shell.

2.1.2 Antimagnet design

The cylindrical homogeneous anisotropic shell with permeability components $\mu_\varphi = 1/\mu_\rho$ cannot be directly realized with existing magnetic materials. Such fine-tuned

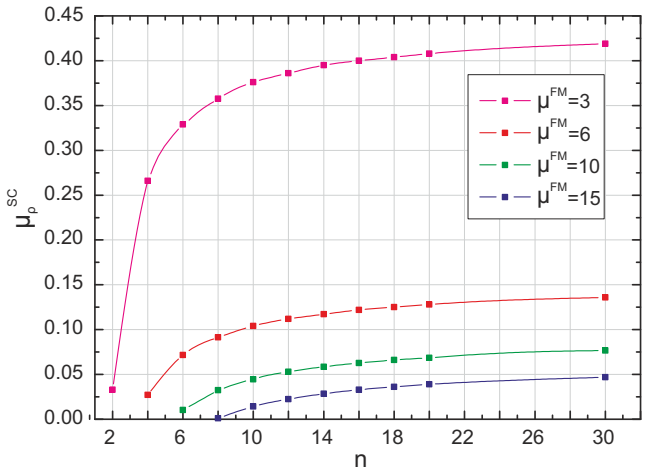

Figure 2.3: Optimum values of μ_ρ^{SC} as a function of the number of layers and for different values of μ^{FM}.

magnetic anisotropy will be obtained from an artificially engineered material, which we can consider it as a magnetic metamaterial [106].

For this purpose we make use of two kinds of cylindrical layers: one type consisting of a uniform and isotropic ferromagnetic (FM) material with constant relative permeability ($\mu_\rho^{\mathrm{FM}} = \mu_\varphi^{\mathrm{FM}} \equiv \mu^{\mathrm{FM}}$) and a second type having a constant value of radial permeability $\mu_\rho^{\mathrm{SC}} < 1$ and $\mu_\varphi^{\mathrm{SC}} = 1$. The first (isotropic) kind of layers could be made of a soft magnetic material (e.g. a steel), and the second one could be realized with arrays of superconducting (SC) plates [100, 101, 102]. These arrays exhibit a smaller-than-one relative permeability in the direction perpendicular to the plates (tunable by changing the distances between them) and no magnetic response in the parallel direction. Alternating these two kinds of layers we can outline a shell with the required effective anisotropic permeabilities; a large angular permeability provided by the ferromagnetic layers and a smaller-than-one radial permeability from the superconducting ones.

To find the appropriate values of permeabilities for the two kinds of layers we follow a numerical optimization method. First we fix the radii of the shell (R_1 and R_2) and the number of layers, n, into which the shell is being discretized. An ideal superconductor with $\mu = 0$ is placed inside and a certain permeability for the FM layers $\mu^{\mathrm{FM}} > 1$ is set. Considering a uniform external applied field, the radial permeability of the other layers, μ_ρ^{SC}, is tuned so that the external field is not distorted. For the particular case of $\mu^{\mathrm{FM}} = 6$ and a shell of $n = 10$ layers, we find the optimum $\mu_\rho^{\mathrm{SC}} = 0.104$. The numerical simulation of this case is shown in Fig. 2.2**f**, demonstrating the external applied field is undistorted whilst field lines are diverted around the inner cloaked region. Notice the optimum $\mu_\rho^{\mathrm{SC}} = 0.104$ is smaller than the conjugate value of permeability of the FM layers $1/\mu^{\mathrm{FM}} = 1/6 \simeq 0.167$. This is understood by taking into account that these FM layers are isotropic and they also provide an extra radial permeability that has to be

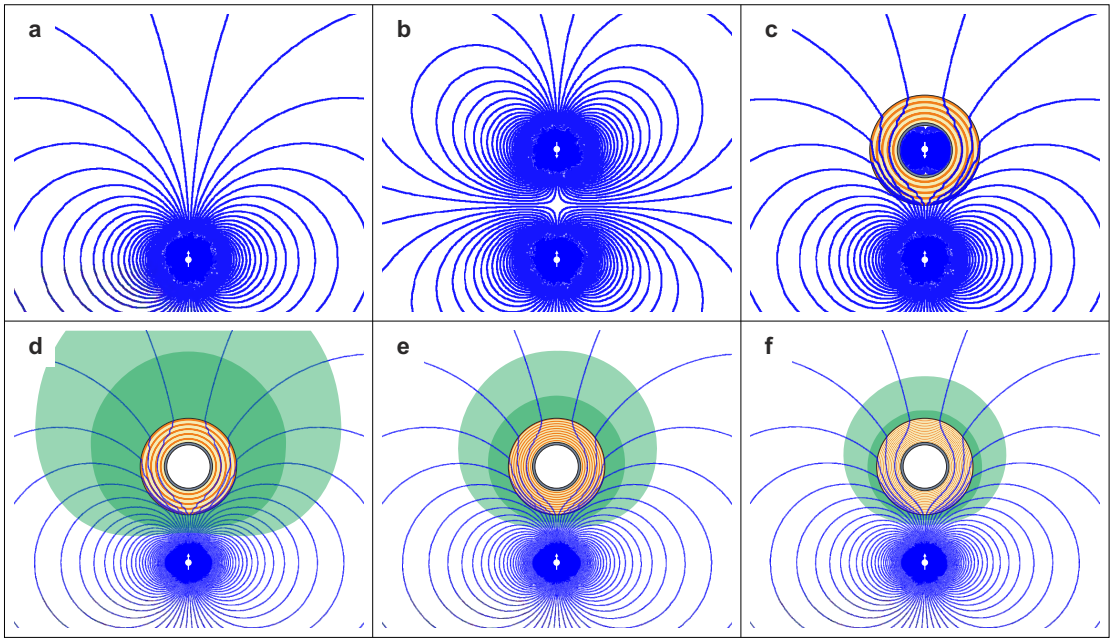

Figure 2.4: (**a**) The field of a line dipole (white) is clearly modified when a second dipole (**b**) is placed pointing to the opposite direction. (**c**) When an antimagnet surrounds one of the dipoles, the external field distribution is the same as when there was a single dipole. The distortion caused by antimagnets with different number of layers is calculated, for $n = 10, 20$ and 30 (**d**, **e** and **f**, respectively). Light and dark green regions indicate points where the distortion (calculated as the difference between the total field and the field of the dipole, $|\,\mathbf{B} - \mathbf{B}_{\rm dip}\,| \,/\, |\,\mathbf{B}_{\rm dip}\,|$) exceeds 1% and 3%, respectively.

compensated by a smaller radial permeability of the SC layers.

The result of cloaking with ten layers and $\mu^{\rm FM} = 6$ is not unique; the same procedure could be done for other values of permeability of the FM layers and for different number of layers. In Fig. 2.3 we show the optimum values of $\mu_\rho^{\rm SC}$ as a function of the number of layers and for different $\mu^{\rm FM}$ [110]. From this plot notice that the optimum values of $\mu_\rho^{\rm SC}$ tend to saturate when the number of layers increases. This indicates that, for a uniform applied field, the discretized system approaches the ideal homogeneous anisotropic shell.

Finally, it is only left to study the performance of antimagnets when non-uniform fields are applied. This is demonstrated in panels of Fig. 2.4, where (**a**) the magnetic field lines created by a line dipole (with translational symmetry along the z-axis) is shown. Field lines created by two dipoles are clearly different, as shown in **b**. When one of the two dipoles is surrounded by an antimagnet (**c**) the field outside it is the same as when only one of them was present; the field of the surrounded dipole does not leak to the exterior and the field of the external dipole is unaffected by the shell. Although field lines in Fig. 2.4**c** do not show a clear distortion, the performance of antimagnets for non-uniform applied fields have to be analyzed carefully, since the optimized $\mu_\rho^{\rm SC}$ values have been obtained only considering uniform applied fields. For this purpose

we calculate the distortion caused by antimagnets with different number of layers (see Fig. 2.4**d-f**) when the field of a line dipole is applied near the external surface. We see that in this case a certain field distortion appears, and this is more important near the device. The larger the number of layers it has, the less distortion it causes. This can be understood by reminding that the homogeneous anisotropic shell does not distort any external applied field. As long as the angular permeability is large enough so that the effect of the inner SC can be neglected, the distortion caused by the antimagnet is only related to the discretization of the shell. For this reason, the larger the number of layers (i.e. the better discretization), the less the external field distortion. In addition, the discretization of the shell becomes more critical when the applied is more inhomogeneous (for example when the dipole is nearer to the antimagnet), making necessary the use of more layers.

In this way we have found a feasible design of antimagnet, which allows to magnetically cloak any magnetic material (even a source of magnetic field) for any externally applied magnetic field. Interestingly, Narayana and Sato made an experimental realization of such metamaterial-based static magnetic cloaks, using a material composed of artificially patterned superconducting and soft ferromagnetic elements [111].

2.2 SC-FM bilayer to cloak uniform applied fields

In the previous section we designed antimagnets that cloak any external applied field in an approximate way because of its discretized design. The more inhomogeneous the applied field is, the larger the number of layers required to minimize the distortion. However, as seen in Fig. 2.3, uniform applied fields can be cloaked considering small numbers of layers. In this section we explore whether systems consisting of only two homogeneous isotropic layers can cloak uniform applied fields [112].

2.2.1 Analytical derivation

Consider two concentric cylindrical shells (with translational symmetry along the z axis), made of linear homogeneous isotropic magnetic materials with relative permeabilities μ_1 (internal) and μ_2 (external). The interior shell has an inner radius R_0 and outer one R_1, and the external shell has an inner and outer radii R_1 and R_2, respectively. A uniform field is applied $\mathbf{H}_a = H_a\hat{x}$ and we define a scalar magnetic potential $\mathbf{H} = -\nabla\phi$ because there are no free currents. Since materials are homogeneous and isotropic, potential has to fulfill the Laplace equation in all regions of space plus the corresponding boundary conditions. Imposing the potential at $\rho \to 0$ is finite, at $\rho \to \infty$ tends to the applied one ($-H_a\,\rho\cos\varphi$) and setting the magnetostatic boundary conditions at the interfaces between the materials we can find the solution of the potential in all regions of space (inside the interior hole, within the two different shells and outside them). In

particular, inside the hole and outside the bilayer the potential is

$$\phi(\rho,\varphi) = -A\rho\cos\varphi, \qquad \rho < R_0 \tag{2.18}$$

$$\phi(\rho,\varphi) = \left(-H_a\rho + \frac{B}{\rho}\right)\cos\varphi, \qquad \rho > R_2 \tag{2.19}$$

where A and B are constants that depend on the permeabilities of the two shells and on the radii. This shows the field inside the shell is always uniform, as in the case of an homogeneous anisotropic shell [sect. 2.1.1, Eq. (2.11)]. Interestingly, the expression of B indicates there is a combination of positive permeabilities of the shells for which the distortion of the external applied field is zero

$$\mu_2 = \frac{\mathcal{K}}{2(R_1^2-R_2^2)[(1-\mu_1)R_0^2-(1+\mu_1)R_1^2]} + \frac{\sqrt{-4\mu_1[(1-\mu_1)R_0^2-(1+\mu_1)R_1^2][(1-\mu_1)R_0^2+(1+\mu_1)R_1^2](R_1-R_2)^2(R_1+R_2)^2+\mathcal{K}^2}}{2(R_1^2-R_2^2)[(1-\mu_1)R_0^2-(1+\mu_1)R_1^2]}, \tag{2.20}$$

being $\mathcal{K}$ an auxiliary parameter defined as

$$\mathcal{K} \equiv (\mu_1^2-1)(R_0^2-R_1^2)(R_1^2+R_2^2). \tag{2.21}$$

Even though this combination of permeabilities leads to zero external field distortion, a magnetic cloak requires that fields do not penetrate into the interior hole. This can be ensured by setting the permeability of the inner shell to zero, i.e. considering the inner shell is an ideal superconductor. As explained in section 2.1, this magnetically decouples interior and exterior regions, also preventing the field of an inner magnetic source to leak to the exterior. In this particular case of $\mu_1 = 0$ expressions of A and B are

$$A = 0, \tag{2.22}$$

$$B = H_a R_2^2 \frac{(\mu_2+1)R_1^2-(\mu_2-1)R_2^2}{(\mu_2-1)R_1^2-(\mu_2+1)R_2^2}. \tag{2.23}$$

Notice that B does not depend on the inner radius of the ideal superconducting shell because the field is completely expelled from it. More interestingly, we can find a value of μ_2 for which $B = 0$, so that the external field is exactly undistorted [112]

$$\mu_2 = \frac{R_2^2+R_1^2}{R_2^2-R_1^2}. \tag{2.24}$$

This relevant result shows that a uniform external applied field can be exactly cloaked using only two layers made of homogeneous isotropic materials; an inner superconducting layer surrounded by a soft ferromagnetic one with relative permeability $\mu_2 > 1$ given by Eq. (2.24). In Fig. 2.5**a** we show the numerical calculation of a cylindrical bilayer system

that exactly cloaks a uniform applied field. The two separate parts distort the field; the exterior ferromagnetic shell attracts field lines (**b**) and the inner superconductor expels them (**c**). The compensation occurs only for a particular permeability, and it is possible because the distortions of the two materials are opposite but exhibit the same spatial dependence [113].

An analogous analytical derivation can be done considering two concentric spherical shells. If the inner one is an ideal superconductor, the permeability of the outer shell for which the external applied field is exactly undistorted is [112]

$$\mu_2 = \frac{2R_2^3 + R_1^3}{2(R_2^3 - R_1^3)}. \tag{2.25}$$

When the applied field is non-uniform, the exact compensation no longer occurs and the bilayer slightly distorts the field (see the numerical calculation for the field of a line dipole and a cylindrical bilayer cloak in Fig. 2.5**d**). Actually, the more inomogenous the applied field is, the larger the distortion caused by the bilayer. However, this distortion is much less than that caused by the inner superconducting shell alone, for example. Moreover, numerical calculations indicate that this distortion can be reduced by thinning

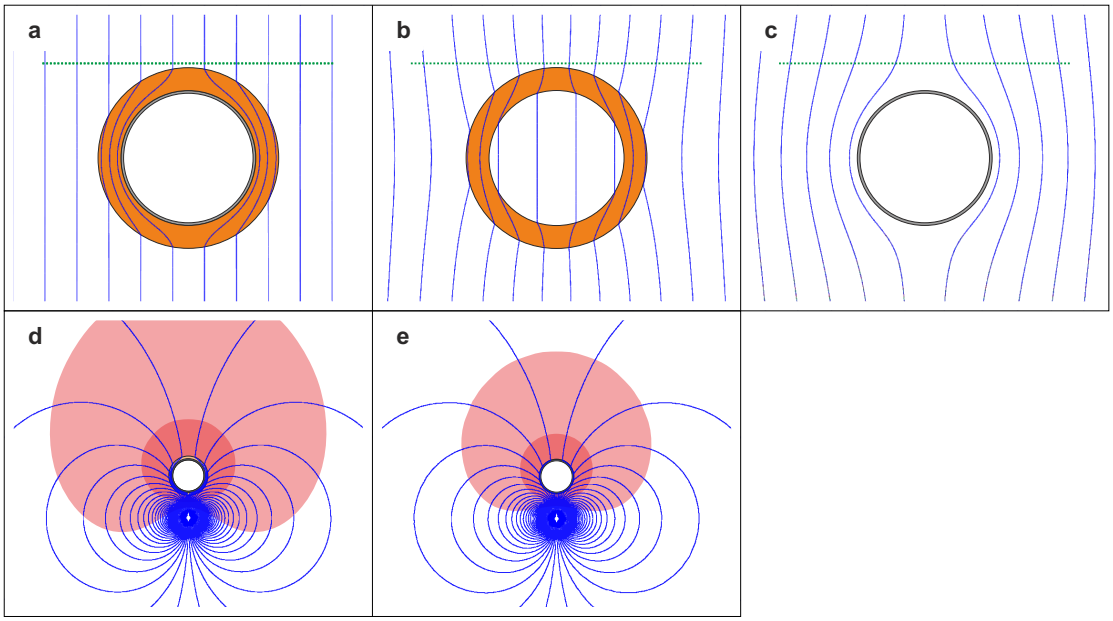

Figure 2.5: (**a**) Numerical calculation of a cylindrical bilayer cloak consisting of an exterior ferromagnetic shell (orange) with $\mu_2 = 3.54$ and an inner ideal superconducting shell (gray), with $R_1/R_1 = 1.34$ and fulfilling Eq. (2.24). The FM and SC parts alone distort the field attracting field lines (**b**) and expelling them (**c**), respectively. Calculations showing the distortion regions caused by cylindrical bilayers with (**d**) $R_2/R_1 = 1.15$ and (**e**) $R_2/R_1 = 1.025$, when the field of a line dipole (placed at a distance of $2.5R_1$ from the center of the bilayer) is applied. Light (dark) pink regions indicate where distortion is larger than 1% (5%).

the exterior ferromagnetic shell (see Fig. 2.5**e**), $R_2 \to R_1$, and using the corresponding μ_2 given by Eq. (2.24) ($\mu_2 \to \infty$). A deeper study on the distortion caused by spherical bilayer cloaks for non-uniform applied fields is found in chapter 5.

2.2.2 Experimental realization

A cylindrical bilayer cloak was built to experimentally demonstrate its cloaking properties. This experimental work was performed in collaboration with the group of F. Gömöry in the Slovak Academy of Sciences.

Instead of the uniform superconducting and ferromagnetic cylindrical shells proposed in the ideal bilayer, the inner shell consisted of few turns of high-temperature superconducting tape, and the outer layer was composed of few turns of an iron-based commercial alloy sheet. The superconducting layer was made of two turns of a superconducting tape 12mm wide, which contained a 1μm thick layer of cuprate superconductor ReBCO. The superconductor was wrapped on top of a cylindrical plastic former of diameter $\Phi_{\text{in}} = 12.5$mm and an insulating kapton layer was inserted between the turns. The outer ferromagnetic layer was made of seven turns of a $Fe_{18}Cr_9Ni$ alloy sheet, having a thickness of 100μm. A 215μm thick kapton layer was introduced between them (see Fig. 2.6**a**). The final radii ratio of the bilayer was $R_2/R_1 = 1.34$, which would require a $\mu_2 = 3.54$ [calculated through Eq. (2.24)]. Although the relative permeability of the ferromagnetic sheet was measured between 11 and 18, the alternation of the sheet with the kapton layers (with no magnetic response) decreased the effective permeability of the whole set, approaching it to the theoretical required value. The length of the bilayer cloak was $L = 12$mm.

The uniform applied field was created by a pair of race-track electromagnets, and the bilayer was placed between them. The vertical component of the field, B_y, was measured by a Hall probe in the median plane of the bilayer along the line transversal to its axial length (green dashed line in Fig. 2.6**b**). Three different measurements were performed: (i) FM only at room temperature (i.e. superconducting tape over its critical temperature, thus electromagnetically inactive), (ii) SC only at 77K (removing the exterior FM shell and submerging the device into liquid nitrogen) and (iii) SC-FM bilayer at 77K.

The calculated vertical component of the field along the measuring line for the three cases is plotted in Fig. 2.6**c**, assuming an exact bilayer with ideal parameters and the dimensions used in the experiments. The superconductor and the ferromagnet repel and attract field lines so the vertical component of the magnetic field in the central region tends to be smaller and larger than the applied field, respectively. When the bilayer is complete, the applied field is unaffected. Results of our experiments (Fig. 2.6**d** and **e**) show that the magnetic signature of our bilayer cloak practically left the applied field of 40mT unaffected, and the measured distortion was much smaller than that for the cases of the SC or the FM alone. The small deviations observed in the experiments probably

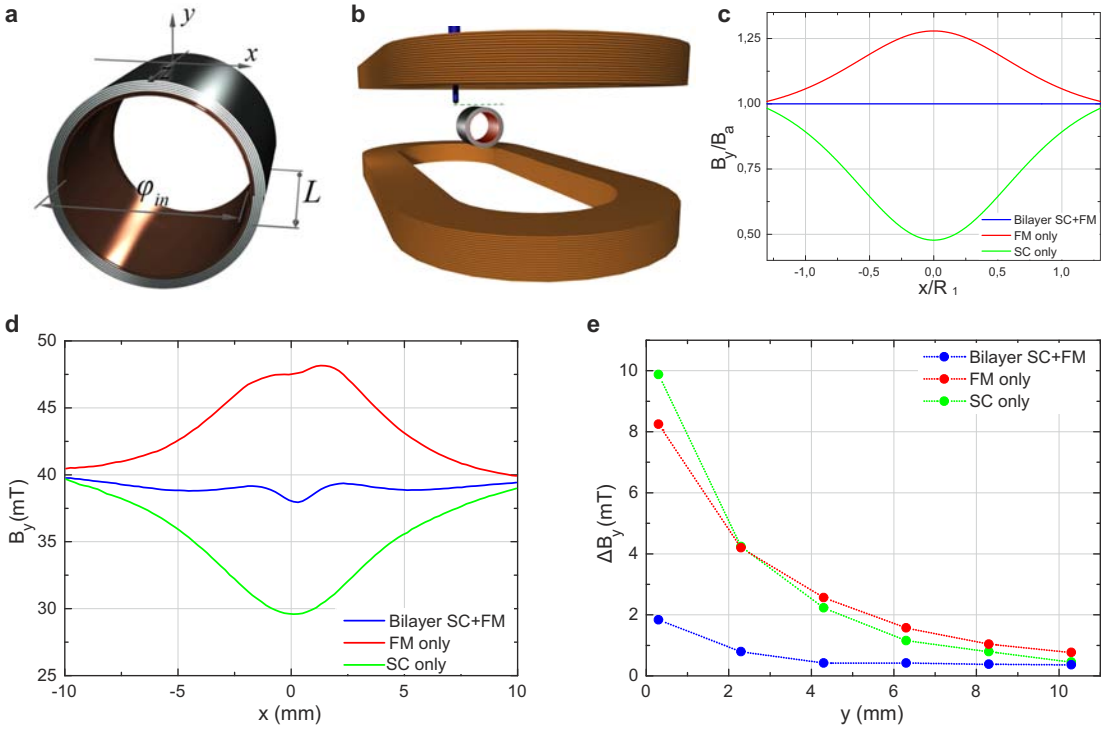

Figure 2.6: (**a**) Illustration of the bilayer cloak, showing the different turns of SC and FM materials. (**b**) Sketch of the experimental setup; electromagnets are shown in brown and the support for the Hall probe in blue. (**c**) Calculated vertical y-component of field along the line at 0.3mm above the surface of the bilayer, as indicated by the dashed line in **b**. Parameters were $R_2/R_1 = 1.34$, $\mu_1 = 0$ and $\mu_2 = 3.54$, corresponding to values for an exact cloak. (**d**) Measured vertical component of field for an applied field of 40mT. (**e**) Difference between maximal and minimal values of the vertical component of field for scans taken from $x = -10$ to 10mm at various heights y. In all cases red lines correspond to measurements of the FM alone (at room temperature), green lines of the SC alone (at liquid nitrogen temperature) and blue lines correspond to measurements of the complete SC-FM bilayer cloak (performed at liquid nitrogen temperature).

resulted from the short length of the bilayer, comparable to its diameter, and also from the nonideal behavior of the SC and FM materials. The magnetic undetectability of the bilayer was also substantial at some distance from it, as can be seen from the mapping at different vertical heights above the surface (Fig. 2.6**e**).

These experiments demonstrated that magnetic fields can be cloaked with a simple bilayer structure made of superconductors and ferromagnetic materials. Results were obtained using only commercially available materials, for fields as large as 40mT and at liquid-nitrogen temperatures, indicating that these ideas may be readily applied to actual technologies. In fact, a bilayer magnetic cloak based on this research is already being used in some accelerator-based nuclear physics experiments performed at the Department of Physics and Astronomy of Stony Brook University [114, 115].

The design could also be applied to other practical problems. For example, after an appropriate development, a magnetic bilayer cloak could allow patients with pacemakers or cochlear implants to use medical equipment based on magnetic fields, such as magnetic resonance imaging. The cloak would prevent magnetic fields to affect the implanted devices and would not distort the image of the rest of the body.

Apart from these applications for magnetic fields, results of this research have inspired new cloaking strategies that have been applied to other areas. Similar bilayer structures made of bulk materials have been used to build different thermal cloaks [97, 98]. A bilayer cloak for diffusive light has also been realized recently [99].

2.3 SC-FM bilayer for low-frequency time-dependent applied fields

The SC-FM bilayer cloak of section 2.2 was designed assuming magnetostatic conditions. In this section we study whether this simple but powerful solution for static magnetic fields can be extended to other frequency regions [116]. Obviously, a direct translation to optical, infrared or even microwave regions is impossible, because the electric and magnetic fields are intertwined. Here we study the performance of the SC-FM bilayer cloak for low-frequency time-dependent applied magnetic fields. In this regime, valid for frequencies up to thousands of Hz, the involved wavelength is much larger than any size of the device so the field distribution is quasistatic. This part of the electromagnetic spectrum has a particular technological interest, since most of the electromagnetic technology (electric generators, transformers, etc.) works in these conditions.

2.3.1 Bilayer construction and measurements

A longer SC-FM bilayer cloak was made in order to reduce the end effects. Four pieces of SC coated conductor were used to build the interior layer and a FM foil (made of steel with 18% Cr and 18% Ni) the outer one (see Fig. 2.7**a**). The final dimensions were $R_1 = 10.7$mm, $R_2 = 12.1$mm and $L = 70$mm. The performance of this bilayer cloak was first studied for a uniform static magnetic field of 21mT, obtaining similar results to that for the cloak discussed in section 2.2.2.

Then, a time-dependent uniform magnetic field was applied, following the calibration-free method for ac magnetization loss measurements described in [117]. An oscillatory input current, i_{ac}, with frequency f created the time-dependent applied magnetic field, and the voltage induced in the pick-up coils with the same frequency (first harmonic) due to the magnetic response of the cloak, u_{s}, was measured. The part of the voltage in phase with the applied current, $u_{\mathrm{s,loss}}$, is related to the electromagnetic losses in the sample. The out-of-phase part of the voltage, $u_{\mathrm{s,ind}}$, is proportional to the time derivative of the magnetic flux in the pick-up coils due to the presence of the cloak. In the experiment the two components were measured by a lock-in technique for different

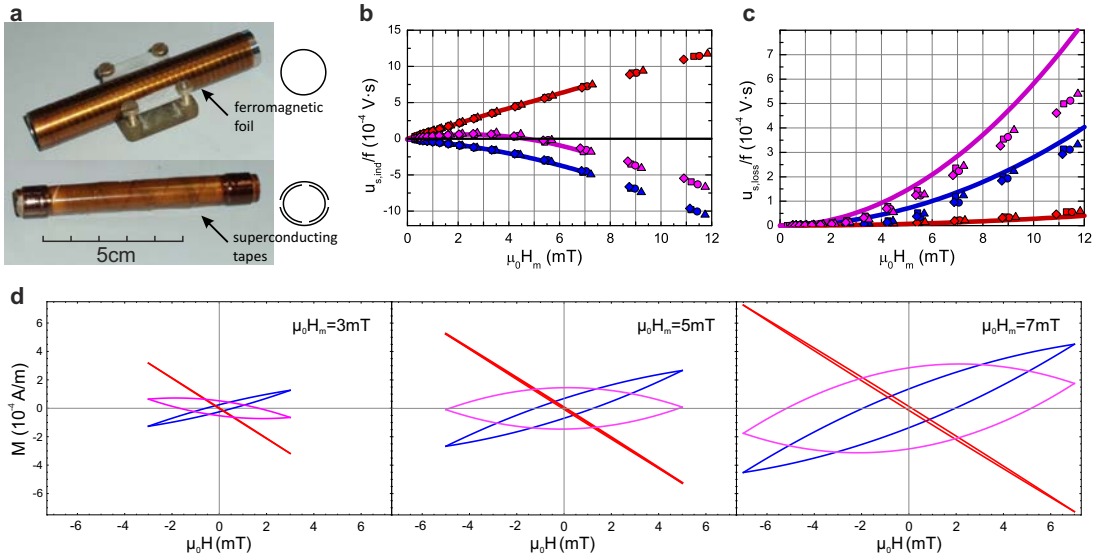

Figure 2.7: (**a**) Picture of the two parts forming the magnetic cloak. (**b**) Measured voltage component $u_{\mathrm{s,ind}}/f$ for the SC, the FM and the SC-FM bilayer (red, blue and purple symbols, respectively) together with the corresponding fitting curves (solid lines). (**c**) Measured component $u_{\mathrm{s,loss}}/f$ (symbols) with plots (solid lines) of Eq. (2.28) using the fitting parameters. Square, circle, triangle and diamond symbols correspond to measurements at different frequencies of 144, 72, 36 and 18Hz, respectively. (**d**) Calculated Rayleigh loops using Eq. (2.26) and the fitting parameters for different values of maximum field H_{m}.

amplitudes of applied field (ranging from 0 to 12mT) and at different frequencies (f between 18 and 144Hz). Measurements were performed for three different cases: (i) the FM layer only, (ii) the SC only and (iii) the SC-FM bilayer. Results are shown in Figs. 2.7**b** and **c**.

2.3.2 Interpretation of the results by the Rayleigh model

The values of $u_{\mathrm{s,ind}}$ for the SC and the FM parts alone have opposite signs and non-negligible values even for small applied fields. For the SC-FM bilayer, values are close to zero for fields up to 7mT, showing that the contributions from the two constituting parts cancel each other, in analogy to the cancellation occurred in the static case. Differently, regarding the resistive part of the signal, $u_{\mathrm{s,loss}}$, the signal of the bilayer increases continuously and is larger than that of its two constituting parts separately. Since this part of the signal is related to the dissipated energy, this means the bilayer has a hysteretic behavior characterized by a certain magnetization loop with a non-zero width, which would make the bilayer cloak detectable.

The behavior of the bilayer and its constituting parts can be understood more deeply by deducing the basic features of their magnetization loops. For low applied fields, superconductors and ferromagnetic materials can be modeled by a Rayleigh model [118],

which assumes the ascending and descending branches of the magnetization loop can be approximated to

$$M = (\chi_a + \eta H_{\rm m})\, H \pm \frac{1}{2}\eta \left(H^2 - H_{\rm m}^2\right), \tag{2.26}$$

where M is the magnetization of the sample, H is the applied field, $H_{\rm m}$ is the maximum applied field and χ_a and η are two independent parameters. By comparing this expression with that of the fundamental loop one can relate the two measured voltage components with the different parameters of the model through [14, 116, 119]

$$-\alpha \frac{u_{\rm s,ind}}{f} = \chi_a H_{\rm m} + \eta H_{\rm m}^2, \tag{2.27}$$

$$\alpha \frac{u_{\rm s,loss}}{f} = \frac{1}{2}\eta H_{\rm m}^2, \tag{2.28}$$

being α a calibration constant that depends on the susceptometer. By fitting the signals $u_{\rm s,ind}/f$ to second grade polynomials we determined the parameters $-\chi_a/\alpha$ and $-\eta/\alpha$ for each case using Eq. (2.27) (see the fitting solid lines in Fig. 2.7**b**). These parameters were used to calculate $u_{\rm s,loss}/f$ through Eq. (2.28); results are plotted in solid lines in Fig. 2.7**c**, showing consistency with the measurements for low fields.

Using these fitting parameters the corresponding Rayleigh loops were plotted through Eq. (2.26) for different values of maximum applied field $\mu_0 H_{\rm m}$ =3, 5 and 7mT (see Fig. 2.7**d**). These plots show that the cancellation of $u_{\rm s,ind}$ for the SC-FM bilayer at low fields arises from the compensation of the magnetic response of the SC and FM parts. As seen from the loops, the magnetization at the maximum amplitude of applied field for the SC and the FM parts separately are approximately equal with opposite signs. For the SC-FM bilayer they cancel each other making $u_{\rm s,ind}$ close to zero for fields up to 7mT. For larger fields, the FM contribution dominates and $u_{\rm s,ind}$ is no longer zero.

On the other hand, the non-negligible signal $u_{\rm s,loss}$ measured even at low fields for the SC-FM bilayer reveals losses during the cycle. Most of the losses come from the ferromagnet, as can be seen from the signals of $u_{\rm s,loss}$ for the SC and the FM parts alone and also from the corresponding loops, because loops for the FM are much thicker than that for the SC. These losses should mainly arise from the FM magnetic hysteresis rather than eddy currents associated to the electrical conductivity, because $u_{\rm s,loss}$ is proportional to the frequency. Loops show the compensation of the SC and FM parts forming the bilayer at the maximum amplitude of applied field is almost perfect, but at other points of the cycle their response is different and a net magnetic moment appears, making the bilayer magnetically detectable. This imbalance is mainly caused by the non-linear response of the FM part. If ferromagnetic materials with smaller hysteresis (magnetically softer) were selected, the cancellation of the FM and the SC parts would better extend to the whole cycle, and the width of the SC-FM bilayer loops would be very much reduced, leading to smaller values of $u_{\rm s,loss}$. In this case there would be a cancellation of the two components of the measured voltage and the cloak (and its content) would be magnetically undetectable along the entire cycle.

These experiments show that, in addition to the full electromagnetic regime and the simpler static case, a third regime of non-zero frequencies exists in which fields are actually oscillating but still the advantages and the solutions obtained for the static case can be used. Therefore, the important advantages of applying transformation optics to the static case can be extended to the low-frequency range of the electromagnetic spectrum, opening the way to novel applications in electromagnetic technology.

2.4 Chapter summary and conclusions

The "invisibility" concept traditionally associated to visible light can be generalized and extended to other cases of large scientific and technological interest. Applied to the static magnetic case, we have shown that feasible solutions employing actual commercial materials can be found for cloaking magnetic fields.

The problem has been first addressed with transformation optics theory, and we have shown that magnetic fields can be cloaked with an homogeneous anisotropic shell. The properties required for such shell can be approximated using superconducting and ferromagnetic materials. In this line we have presented *antimagnets* that cloak any magnetic material (even a source of field) and can be realized using existing technologies and materials. A general strategy to discretize homogeneous and anisotropic shells has been introduced, showing a whole family of solutions that lead to cloaking of magnetic fields.

Important alternative and simpler solutions for magnetic cloaking have been found by solving the magnetostatic Maxwell equations. It has been analytically demonstrated and experimentally confirmed that a bilayer system composed of an inner superconducting shell surrounded by a ferromagnetic one is able to cloak uniform magnetic fields. This design cannot be derived from transformation optics and reveals that in the static case there is room to find alternative solutions requiring less demanding materials.

Interestingly, we have shown that the simpler solutions for the static case can also be valid for time-varying fields of low frequency. Experimental measurements have shown that the bilayer magnetic cloak is partially undetectable for frequencies up to some KHz. Moreover, the imperfections of the cloaking effect in our experiment have not arisen from an intrinsic limitation of the design but from the non-linear response of the particular ferromagnetic materials used, something that could be eventually improved. These experiments, thus, have demonstrated that the simpler solutions for static magnetic fields could also be useful for low-frequency waves, extending the application of the different cloaks presented in this chapter.

To sum up, we have developed different magnetic cloaks that can be realized with adequate combinations of existing superconducting and ferromagnetic materials. The experimental validation of the ideas, not only in the static magnetic case but also for low-frequency waves, indicates that results of this research could be readily applied

to different technologies in which is desirable to magnetically shield a region without distorting the existing field distribution.

CHAPTER 3

Concentration of magnetic fields

Magnetic fields are found at the basis of key technologies, like magnetic data recording, energy generation, accurate sensing or plasma confinement, for example. An important goal is to concentrate magnetic fields in a desired point or volume of space. This could increase the sensitivity of a sensor or improve the performance of power generators and transformers. Medical techniques based on magnetic fields (like magnetic resonance image or transcranial magnetic stimulation) could also benefit from this property, since many or them are based on the application of strong magnetic fields in particular places of the human body.

Strategies to concentrate electromagnetic fields have been widely investigated for different purposes and following very different approaches. Apart from traditional dielectric lenses, whose concentration properties are tied to the diffraction limit of the electromagnetic wave, light concentrators based on plasmonics have demonstrated an unprecedented ability to concentrate light into deep-subwavelength volumes [120, 121, 122]. Transformation optics has been applied to investigate the concentration properties of some of these devices [50, 51, 52], which could have important applications for efficient light harvesting, subwavelength optics or high-density data storage.

Transformation optics has also been applied to design macroscopic electromagnetic concentrators [31]. The underlying idea is opposite to that of the cloaking; the space is transformed concentrating it into an inner small volume of space. Such electromagnetic concentrator requires fine-tuned inhomogeneous and anisotropic permittivities and permeabilities within the shell volume. Moreover, the inner region where the electromagnetic wave is concentrated also requires materials with particular electromagnetic properties. All this makes this kind of concentrator very impractical.

In this chapter we develop a concentrating shell for static magnetic fields. Our aim

is to present a feasible design and compare its performance with existing strategies for magnetic field concentration. Its application to low-frequency time-dependent magnetic fields will be also discussed.

3.1 Homogeneous anisotropic cylindrical shell for magnetic field concentration

A cylindrical concentrating shell can be designed by transformation optics applying a space transformation closely related to that used to design the homogeneous anisotropic cloaking shell (sect. 2.1.1). Consider an inner and outer radii for the shell R_1 and R_2, respectively. Defining a parameter R_0 between R_1 and R_2 ($R_1 < R_0 < R_2$), the space transformation expressed in Eq. (2.4) corresponds to a compression of the space $\rho \in [0, R_0)$ into $\rho' \in [0, R_1)$, as sketched in Fig. 3.1**b**. In this case the transformation of Eq. (2.2) expands the space $\rho \in [R_0, R_2)$ into $\rho' \in [R_1, R_2)$ (see Fig. 3.1**c**) and keeps the transformed space continuous as long as Eq. (2.3) is fulfilled [123].

From Eq. (2.3) it can be seen the k parameter now ranges from 1 (when $R_0 \to R_1$) to ∞ (when $R_0 \to R_2$). This reveals a beautiful symmetry between the cloaking and concentration cases, since the two effects can be seen as part of a continuous transformation that only depends on a single parameter R_0 [110]. For R_0 between 0 and R_1 ($0 < k < 1$) the space is moved out from the central part and a cloaking region is obtained, whilst for R_0 between R_1 and R_2 ($1 < k < \infty$) the space is concentrated inside the shell.

Owing to this symmetry, material parameters obtained for the cloaking case [Eqs. (2.5) and (2.6)] are also valid for the concentrator. Assuming there are no z-components of field and there is translational symmetry along the z-axis, a cylindrical concentrating shell requires the following relative permeability components (expressed in the usual cylindrical basis)

$$\mu_\rho = k, \qquad \mu_\varphi = 1/k, \qquad \rho' \in [R_1, R_2) \tag{3.1}$$

$$\mu_\rho = 1, \qquad \mu_\varphi = 1, \qquad \rho' \in [0, R_1) \tag{3.2}$$

with $k > 1$. This means that an homogeneous shell with large radial permeability and conjugate angular one concentrates the applied magnetic field in its interior. Interestingly, this magnetic concentrating shell does not require material in the interior region, as indicated by Eq. (3.2). This result contrasts with that of the concentrator for electromagnetic waves [31], which requires filling the interior space with materials having the appropriate permittivity and permeability. For this reason the magnetic concentrator represents an ideal collector for energy harvesting or for increasing the sensitivity of a magnetic sensor placed inside.

Fields in all regions of space can be calculated from transformation optics theory

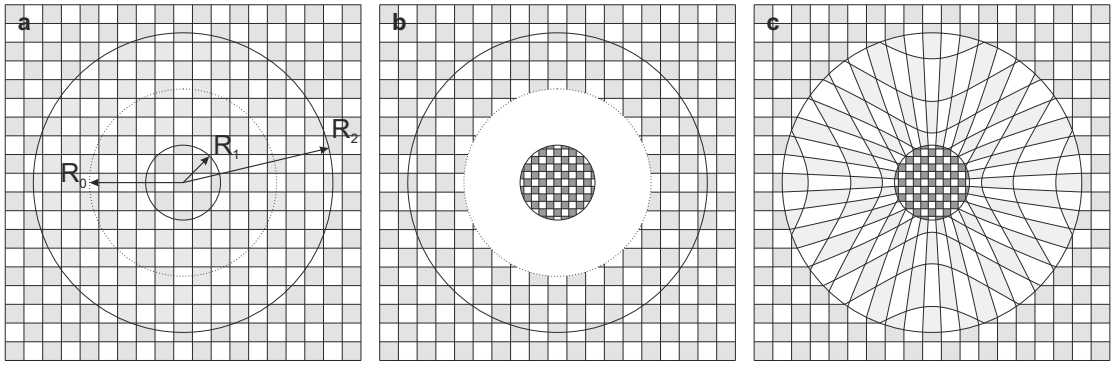

Figure 3.1: Sketch of the space transformations that lead to an homogeneous anisotropic concentrating shell.

obtaining the same expressions as for the cloaking case [Eqs. (2.7)-(2.9)]

$$\mathbf{H}'\left(\rho',\varphi'\right)=\left(\frac{R_2}{R_1}\right)^{1-\mu_\varphi}\mathbf{H}\left(\left(\frac{R_2}{R_1}\right)^{1-\mu_\varphi}\rho',\varphi'\right),\qquad \rho'\in[0,R_1) \tag{3.3}$$

$$\begin{cases} H'_\rho\left(\rho',\varphi'\right)=\mu_\varphi\left(\frac{R_2}{\rho'}\right)^{1-\mu_\varphi}H_\rho\left(\left(\frac{R_2}{\rho'}\right)^{1-\mu_\varphi}\rho',\varphi'\right), \\ H'_\varphi\left(\rho',\varphi'\right)=\left(\frac{R_2}{\rho'}\right)^{1-\mu_\varphi}H_\varphi\left(\left(\frac{R_2}{\rho'}\right)^{1-\mu_\varphi}\rho',\varphi'\right), \end{cases} \qquad \rho'\in[R_1,R_2) \tag{3.4}$$

$$\mathbf{H}'\left(\rho',\varphi'\right)=\mathbf{H}\left(\rho',\varphi'\right),\qquad \rho'\in[R_2,\infty) \tag{3.5}$$

where $\mathbf{H}(\rho,\varphi)$ is the external applied field expressed in the cylindrical basis. These results show the external field is not distorted by the shell [Eq. (3.5)], whilst the field is enhanced in the interior hole [Eq. (3.3)]. Restricting to positive permeabilities, the maximum field concentration is obtained for $k\to\infty$, corresponding to $R_0\to R_2$. In this case the shell requires $\mu_\rho\to\infty$ and $\mu_\varphi\to 0$.

In this case of maximum concentration, if a uniform field $\mathbf{H}_a$ is applied, the field inside the shell is

$$\mathbf{H}_{\text{in}}=\frac{R_2}{R_1}\mathbf{H}_a, \tag{3.6}$$

indicating that strong fields can be obtained by making the inner radius small, for example (see Fig. 3.2**a**).

For non-uniform applied fields, Eq. (3.3) shows not only the field modulus but also its spatial variation increases inside the shell. Consider the case of a line dipole with magnetic moment pointing to the vertical direction $\boldsymbol{\eta}=\eta\,\hat{y}$ aligned with the origin at a distance $y_0=-d$. The vertical component of the field along the y-axis and its gradient are found to be

$$H_y=\frac{\eta}{2\pi}\left(y+d\right)^{-2},\qquad \frac{\partial H_y}{\partial y}=-\frac{\eta}{\pi}\left(y+d\right)^{-3}. \tag{3.7}$$

If a magnetic concentrating shell with $\mu_\rho \to \infty$ and $\mu_\varphi \to 0$ is placed centered at the origin, the field in the interior region and the gradient can be calculated through Eq. (3.3) finding [123]

$$H_y = \frac{R_2}{R_1}\frac{\eta}{2\pi}\left(\frac{R_2}{R_1}y + d\right)^{-2}, \qquad \frac{\partial H_y}{\partial y} = -\left(\frac{R_2}{R_1}\right)^2 \frac{\eta}{\pi}\left(\frac{R_2}{R_1}y + d\right)^{-3}. \tag{3.8}$$

This result shows the field is enhanced by the radii ratio of the shell whilst the gradient is increased by a larger factor corresponding to the square of the radii ratio. Therefore, magnetic concentrating shells could be specially useful to improve sensors that measure gradients of magnetic field, as is the case of some biosensors [124] for measuring the human brain response in magnetoencephalographies [125, 126] or for detecting single magnetic microbeads [127].

3.1.1 Magnetic concentrating shell in terms of magnetic energy redistribution

The concentration properties of this shell can be also understood in terms of magnetic energy redistribution. Consider a certain external applied field and a concentrating shell with $\mu_\rho = 1/\mu_\varphi$. Since the external field is not distorted by the shell [Eq. (3.5)], the magnetic energy density distribution in the external space is unaffected. Within the shell volume, the $\mathbf{H}$ field is given by Eq. (3.4) and the $\mathbf{B}$ field is found to be

$$\begin{cases} B'_\rho\left(\rho',\varphi'\right) = \mu_0\left(\frac{R_2}{\rho'}\right)^{1-\mu_\varphi} H_\rho\left(\left(\frac{R_2}{\rho'}\right)^{1-\mu_\varphi}\rho',\varphi'\right), \\ B'_\varphi\left(\rho',\varphi'\right) = \mu_0\mu_\varphi\left(\frac{R_2}{\rho'}\right)^{1-\mu_\varphi} H_\varphi\left(\left(\frac{R_2}{\rho'}\right)^{1-\mu_\varphi}\rho',\varphi'\right). \end{cases} \tag{3.9}$$

Interestingly, in the case of maximum concentration $\mu_\rho \to \infty$ and $\mu_\varphi \to 0$ expressions simplify and fields are

$$\mathbf{H}'\left(\rho',\varphi'\right) = \frac{R_2}{\rho'} H_\varphi\left(R_2,\varphi'\right)\hat{\varphi}, \tag{3.10}$$

$$\mathbf{B}'\left(\rho',\varphi'\right) = \mu_0\frac{R_2}{\rho'} H_\rho\left(R_2,\varphi'\right)\hat{\rho}, \tag{3.11}$$

showing that the $\mathbf{B}$ field is radial and $\mathbf{H}$ is angular. Therefore, the magnetic energy density $w = \mathbf{B}\cdot\mathbf{H}/2$ is zero in the shell volume, demonstrating that the energy is transferred to the interior hole (see Fig. 3.2**b**), where the field is increased. For non-extreme concentrating shells ($\mu_\rho = 1/\mu_\varphi > 1$), the energy within the shell is not totally expelled towards the interior hole and, thus, the field concentration is reduced.

Ideal FM and SC materials also redistribute the magnetic energy density. Actually, both materials have zero energy density in their interior, because $\mathbf{B} = 0$ inside the SC and $\mathbf{H} = 0$ inside the ideal FM. However, a cylindrical shell made of SC or FM material does not transfer the magnetic energy to the interior hole but expels the energy towards the exterior, as can be seen in Fig. 3.2**c**. The energy (and the field) inside the interior hole is zero, and such shells are used to shield magnetic fields.

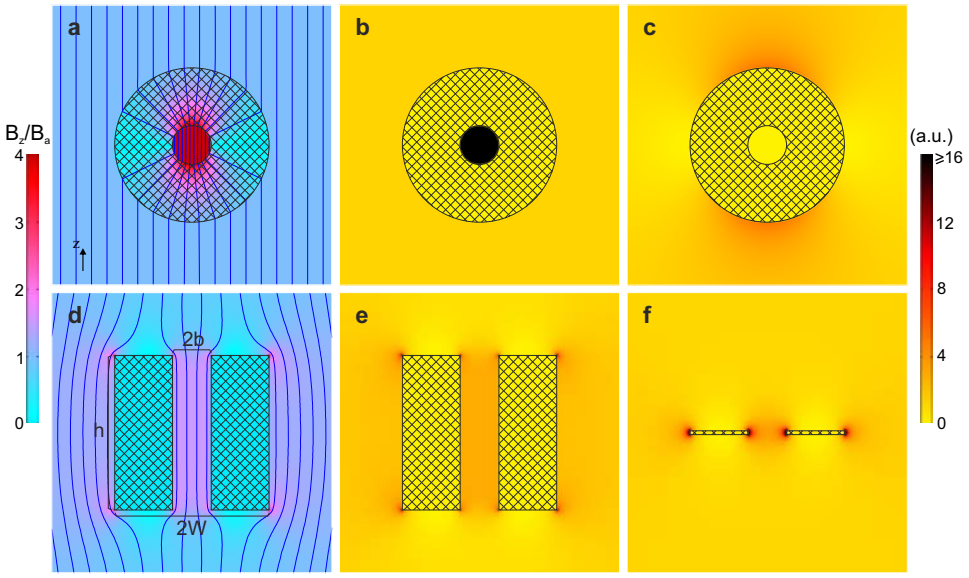

Figure 3.2: Magnetic field lines and their density (in color, normalized to the applied field) for (**a**) an homogeneous anisotropic shell with $\mu_\rho = 1/\mu_\varphi \to \infty$ and $R_2/R_1 = 4$ and for (**d**) two slabs of ideal superconducting material with $\mu = 0$. Plots of magnetic energy density for (**b**) an homogeneous anisotropic shell $\mu_\rho = 1/\mu_\varphi \to \infty$, (**c**) a shell made of ideal soft ferromagnetic material with $\mu \to \infty$, (**e**) two slabs of ideal superconducting material with a height $h = 4b$ and with (**f**) $h = b/10$. In all cases a uniform external field is applied.

3.1.2 Demonstration of maximum field concentration by a conjugate shell

The maximum field concentration of conjugate concentrating shells is achieved when $\mu_\rho \to \infty$ and $\mu_\varphi \to 0$. However, the design from transformation optics only considers the case in which the external applied field is undistorted by the shell. It has to be studied whether non-conjugate cylindrical shells (i.e. shells that distort the external applied field) with arbitrary radial and angular permeability components achieve larger concentration factors.

For this purpose we find the general solution of the magnetostatic Maxwell equations when a uniform field is applied to an homogeneous anisotropic cylindrical shell. This problem was already solved in the second part of sect. 2.1.1. We found that for an applied field $\mathbf{H}_a = H_a\hat{x}$ the field inside the shell is $\mathbf{H}_{\text{in}} = A\hat{x}$, with

$$A = H_a \frac{-4p(R_2/R_1)^{1+u}}{(-1+p)^2 - (1+p)^2(R_2/R_1)^{2u}}, \tag{3.12}$$

$p \equiv \sqrt{\mu_\rho \mu_\varphi}$ and $u \equiv \sqrt{\mu_\varphi/\mu_\rho}$. From this expression, considering a fixed μ_φ, it can be demonstrated [123] that the maximum field in the hole is obtained when $\mu_\rho \to \infty$ and is

$$H_{\text{in}}(\mu_\rho \to \infty, \mu_\varphi) = H_a \frac{2(R_2/R_1)}{2 + \mu_\varphi \ln(R_2/R_1)}. \tag{3.13}$$

This field is larger than that obtained with a conjugate shell with the same angular permeability, $H_{\rm in}(\mu_\rho \to \infty, \mu_\varphi) \geq H_{\rm in}(\mu_\rho = 1/\mu_\varphi, \mu_\varphi)$. Also, for a fixed μ_ρ, the inner field is maximized for $\mu_\varphi \to 0$ and is

$$H_{\rm in}(\mu_\rho, \mu_\varphi \to 0) = H_a \frac{2\mu_\rho (R_2/R_1)}{2\mu_\rho + \ln(R_2/R_1)}, \tag{3.14}$$

which is also larger than that for a conjugate shell with the same radial permeability, $H_{\rm in}(\mu_\rho, \mu_\varphi \to 0) \geq H_{\rm in}(\mu_\rho, \mu_\varphi = 1/\mu_\rho)$. The absolute maximum of both Eqs. (3.13) and (3.14) is found for $\mu_\rho \to \infty$ and $\mu_\varphi \to 0$. This result demonstrates that the maximum field concentration obtained with an homogeneous anisotropic cylindrical shell is found for the extreme conjugate case $\mu_\rho \to \infty$ and $\mu_\varphi \to 0$, which keeps the external field undistorted and increases the inner field by a factor $H_{\rm in}/H_a = R_2/R_1$.

3.1.3 Comparison to existing strategies for field concentration

The field concentration properties of this shell can be compared to the existing strategies to concentrate magnetic fields, which are typically used to increase the sensitivity of different magnetic sensors [128, 129, 130, 131, 132, 133]. The usual concentration strategy is based on two infinite slabs made of superconducting (or ferromagnetic) material, separated by a gap at which flux concentration is produced (see Figs. 3.2**d** and **e**). The field is enhanced at the edges of the slabs, not only on the gap region but also on the exterior ones. When reducing their thickness (h), the contribution from the edges adds up and a rather intense magnetic field is achieved in the gap, although it is not homogeneous but increases towards the edges and decreases at the central region (Fig. 3.2**f**). The thin-film limit case ($h \to 0$) was studied in detail in [134], and the flux per unit length, Φ, and the average z-field in the gap, $\langle B_z \rangle$, were found as a function of the geometrical parameters of the SC strips. These results can be compared with that for the concentrating shell, identifying $b = R_1$ and $W = R_2$ (compare Figs. 3.2**a** and **d**). Results are plotted in Fig. 3.3. This shows the average field inside the concentrator is clearly larger than between two SC strips. Numerical calculations performed considering thick SC slabs show even smaller field concentrations than for the thin limit case. More interestingly, the flux between two strips tends to zero when the gap is narrowed, because field lines are diverted to the exterior limits of the strip. In contrast, the concentrator with $\mu_\rho = 1/\mu_\varphi \to \infty$ achieves a constant flux, $\Phi_a = 2\mu_0 H_a W$, that does not depend on the radii ratio.

These results demonstrate that magnetic concentrating shells provide a completely new strategy to concentrate magnetic fields, achieving a substantial improvement with respect to the existing strategies that are being applied in actual devices and technologies.

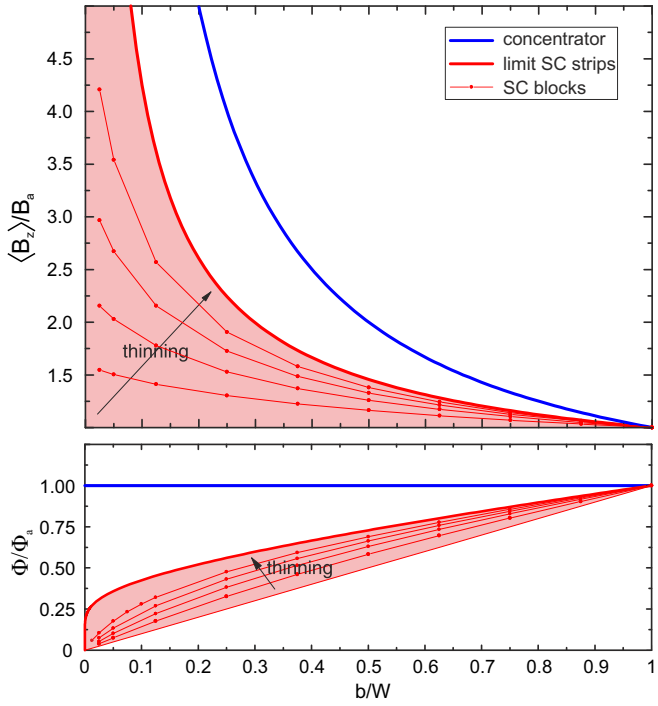

Figure 3.3: (Upper) Plots of the average field $\langle B_z \rangle$ in the gap between two superconducting slabs normalized to the applied field as a function of the gap ratio b/W (red dots). The thin-film limit case is represented with a thick red line and the case of the homogeneous anisotropic concentrator $\mu_\rho = 1/\mu_\varphi \to \infty$ with a thick blue line. (Lower) Plots of the normalized flux for the same cases.

3.2 Field expulsion properties of the shell

In the previous section we discussed the concentration properties of the homogeneous anisotropic magnetic concentrating shell for external applied fields. However, the behavior of such shell when a source of field is placed inside its hole cannot be directly deduced from the previous development based on transformation optics, since the space inside the hole $\rho' < R_1$ is transformed. The space transformation for the concentrating shell keeps the external space $\rho' > R_2$ undistorted, whilst the space inside the shell $\rho' < R_1$ is compressed with respect to the original space, as sketched in Fig. 3.1**c**. If we now take this inner compressed space as the reference, the external space is "expanded" with respect to it. This opens the way to interpret the previous homogeneous anisotropic concentrating shell as coming from an alternative space transformation, keeping the inner space undistorted and expanding the external space.

Consider an inner and outer radii R_1 and R_2, respectively, and a parameter $R_1 < R_0 < R_2$. From an initial undistorted space, the space inside R_1 is not transformed. The space $\rho > R_0$ is expanded to $\rho' > R_2$ through the radial transformation

$$\rho' = \frac{R_2}{R_0}\rho, \qquad \rho \in [R_0, \infty), \tag{3.15}$$

and the space $R_1 < \rho < R_0$ is expanded between $R_1 < \rho' < R_2$ through

$$\rho' = R_1 \left(\frac{\rho}{R_1} \right)^k, \qquad \rho \in [R_1, R_0), \tag{3.16}$$

where k fulfills the following equation to ensure the transformed space is continuous

$$R_0 = R_1 \left(\frac{R_1}{R_2} \right)^{-\frac{1}{k}}. \tag{3.17}$$

In this case $k > 1$, and for the extreme case of maximum space expulsion, $R_0 \to R_1$, then $k \to \infty$. Applying these space transformations, and considering there are no z-components of field, the required relative permeability components in the different regions of space are found

$$\mu_\rho = 1, \qquad \mu_\varphi = 1, \qquad \rho' \in [R_2, \infty) \tag{3.18}$$

$$\mu_\rho = k, \qquad \mu_\varphi = 1/k. \qquad \rho' \in [R_1, R_2) \tag{3.19}$$

Therefore, these space transformations lead to the same homogeneous anisotropic shell with $\mu_\rho = 1/\mu_\varphi > 1$ that was designed to concentrate external applied fields. However, this development demonstrates that when the source of field is inside the hole, the field in the hole is undistorted and the external field is modified by the shell. The analytical expression of the field outside the shell is found from transformation optics theory [Eq. (1.28)] using the space transformation of Eq. (3.15) and is

$$\mathbf{H}'\left(\rho', \varphi'\right) = \left(\frac{R_1}{R_2} \right)^{1-\mu_\varphi} \mathbf{H}\left(\left(\frac{R_1}{R_2} \right)^{1-\mu_\varphi} \rho', \varphi' \right), \qquad \rho' > R_2, \tag{3.20}$$

where $\mathbf{H}(\rho, \varphi)$ is the field created by the source alone. The maximum expulsion is achieved for $k \to \infty$, i.e. for a shell with $\mu_\rho \to \infty$ and $\mu_\varphi \to 0$. In this case one can calculate the field outside the shell when a line dipole (with translational symmetry along the z-axis) is placed inside the shell. Considering that $\mathbf{H}_{\text{dip}}(\boldsymbol{\eta}, \rho, \varphi)$ is the field created by the bare dipole with magnetic moment per unit length $\boldsymbol{\eta}$, it can be demonstrated through Eq. (3.20) that the field outside the shell is [123]

$$\mathbf{H}'\left(\rho', \varphi'\right) = \left(\frac{R_1}{R_2} \right) \cdot \mathbf{H}_{\text{dip}}\left(\boldsymbol{\eta}, \left(\frac{R_1}{R_2} \right) \rho, \varphi \right) = \mathbf{H}_{\text{dip}}\left(\left(\frac{R_2}{R_1} \right) \boldsymbol{\eta}, \rho, \varphi \right). \tag{3.21}$$

This shows that the exterior field is the same as that created by a dipole with a larger magnetic moment, $(R_2/R_1)\boldsymbol{\eta}$. From an energy point of view, the shell acts expelling the magnetic energy that would be within the material towards the exterior. Notice the exterior field can be made arbitrarily large by decreasing the inner radius of the shell. In this situation, the large values of magnetic energy density found close around the dipole are moved to the external space, giving rise to large values of field.

The behavior of these magnetic concentrating shells with $\mu_\rho = 1/\mu_\varphi > 1$ can be simply summarized as follows. When the source of field is located at the exterior, the

shell expels (partially, for $\mu_\rho = 1/\mu_\varphi > 1$, or totally, in the limit $\mu_\rho = 1/\mu_\varphi \to \infty$) the magnetic energy towards the interior hole, where the field is described by Eq. (3.3). On the other hand, when the field source is placed inside the shell, this analogously expels the magnetic energy towards the exterior, where the field follows Eq. (3.20).

3.3 Concentration at a distance

These properties of the shells can be combined to redistribute the magnetic energy in space with a new degree of freedom, resulting in not straightforward distributions of magnetic field. Consider a line dipole in space, which creates a distribution of magnetic energy density as shown in Fig. 3.4**a**. When the dipole is surrounded by one of the shells with $\mu_\rho = 1/\mu_\varphi \to \infty$ the energy is totally expelled towards the exterior (Fig. 3.4**b**). A second shell can be used to collect all the energy density in a region and concentrate it in its interior hole. A large value of energy density (and, thus, of field) can be obtained

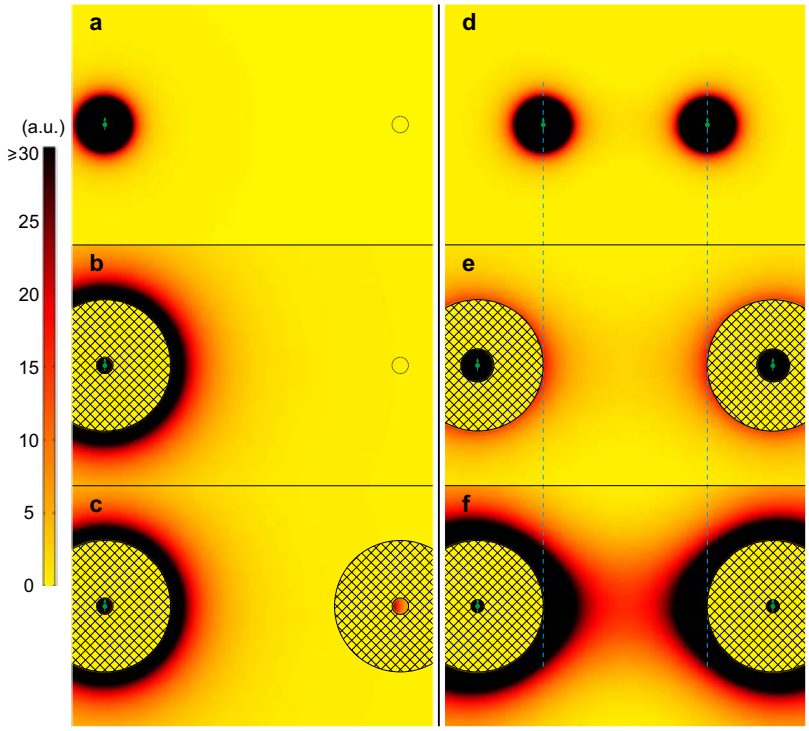

Figure 3.4: Left panels: the magnetic energy density of a line dipole (**a**) is spatially redistributed towards larger radial distances by a concentrating shell with $\mu_\rho = 1/\mu_\varphi \to \infty$ and $R_2/R_1 = 8$ (**b**). (**c**) A second identical shell collects all the energy in its volume and transfers it to its hole. Right panels: (**d**) plot of the magnetic energy density of two identical dipoles separated by a given gap; when separating and enclosing them with concentrating shells of radii ratios $R_2/R_1 = 4$ (**e**), the magnetic energy density between them is similar to that in the original case. When the inner radii of the shells is reduced so that $R_2/R_1 = 10$ (**f**) the field in the middle region is clearly enhanced.

at a point far from the source of magnetic field (see Fig. 3.4**c**). This large energy inside the second shell was originally found at points near the dipole in the initial isolated situation; the use of the shells has allowed to redistribute it in space.

A second example could be the redistribution of the energy between two dipoles. Consider two bare line dipoles separated by a certain distance; the energy distribution is shown in Fig. 3.4**d**. If we surround them with concentrating shells of radii ratios $R_2/R_1 = 4$ and separate each other to keep the same gap of free space, the energy density in the middle space is similar to that in the initial case. Reducing the inner radii of the shells (so that $R_2/R_1 = 10$) the expelled energy is largely increased, and the energy (and the magnetic field) between them is clearly enhanced (see Figs. 3.4**e** and **f**).

These cases are examples of how magnetic concentrating shells could be used to shape magnetic fields in space in new ways. The concentration of field at a distance from the source could be applied, for example, to enhance wireless power transmission techniques based on electromagnetic induction [135]. The performance of the transmission crucially depends on the mutual inductive coupling between the source and the receiver resonators [136], something that could be improved by these shells. This application is discussed in detail in section 3.5. The ability to increase the magnetic field in a region of free space between the sources could be applied to medical techniques like transcanial magnetic stimulation [137, 138], for which large magnetic fields are required at a given position deep in the brain.

3.4 Realization using superconducting and ferromagnetic materials

The ideal homogeneous anisotropic concentrating shells derived in the previous section require materials with very fine-tuned anisotropy, something not directly found in natural materials. In particular, the most favorable concentrator would require $\mu_\rho = 1/\mu_\varphi \to \infty$, i.e. a very large permeability in the radial direction and zero angular permeability. Natural materials exist with large values of magnetic permeability (soft ferromagnets). On the other hand superconducting materials ideally behave as perfect diamagnets, having relative permeabilities close to zero.

The combination of these two materials in a series of alternated and radially displaced pieces (wedges or even rectangular pieces, see Fig. 3.5**a-c**) constitutes a very good approximation to the ideal concentrating shell. In these *metamaterial* concentrating shells, the ferromagnets provide a large permeability in the radial direction whilst the alternated superconductors cancel angular components of the field, leading to an effective $\mu_\varphi = 0$. This is demonstrated by numerical calculations, shown in Fig. 3.5 [123]. For large numbers of pieces (easily achieved in practice using commercially available thin SC strips and high-permeability FM foil), the behavior becomes very similar to the ideal

one [110].

It is worth to remark that configurations consisting of only FM pieces (without the use of superconductors and their associated cryogenics) can also achieve significant field concentrations, as shown in Fig. 3.5**d**. In these cases, magnetic **B**-field lines are radially guided through the FM parts due to the demagnetizing fields appearing as a result of the geometry of the pieces. The shape and the spacing between the pieces determine the properties of the shell.

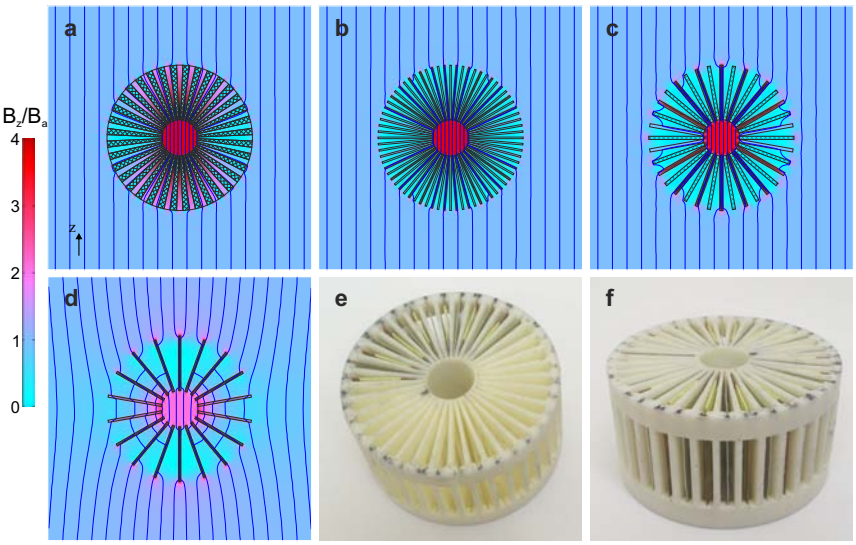

Figure 3.5: Magnetic **B**-field lines and their density (in color, normalized to the applied field) for (**a**) a metamaterial concentrating shell made of 72 wedges of alternating homogeneous and isotropic ideal superconducting ($\mu \to 0$) and ideal soft ferromagnetic ($\mu \to \infty$) materials. (**b**) A similar shell discretized into 72 rectangular prisms and (**c**) discretized into 36 pieces. (**d**) A metamaterial made of only 18 thin ferromagnetic pieces also concentrates the uniform external applied field. (**e**, **f**) Pictures of the constructed metamaterial concentrating shell; the non-magnetic plastic support is shown in white and the SC and the FM pieces are inserted into the 36 lodgings.

3.4.1 Experimental realization

Some concentrating shells were built to demonstrate their properties [139]. We constructed a metamaterial concentrating cylindrical shell made of 36 rectangular prisms of alternated SC and FM materials. The FM pieces were made of commercial high permeability metallic alloy (mu-metal foil 0.3mm thick) and the SC ones were made of a type-II SC coated conductor (SuperPower SCS12050) (see Fig. 3.5**e** and **f**). Pieces were radially distributed and fixed in a non-magnetic 3D-printed plastic support. The resulting metamaterial shell had an approximate interior and exterior radii of $R_1 = 7.5$mm and $R_2 = 30$mm, respectively, and a height of 30mm.

First, a uniform external field was applied by two Helmholtz coils (see the setup

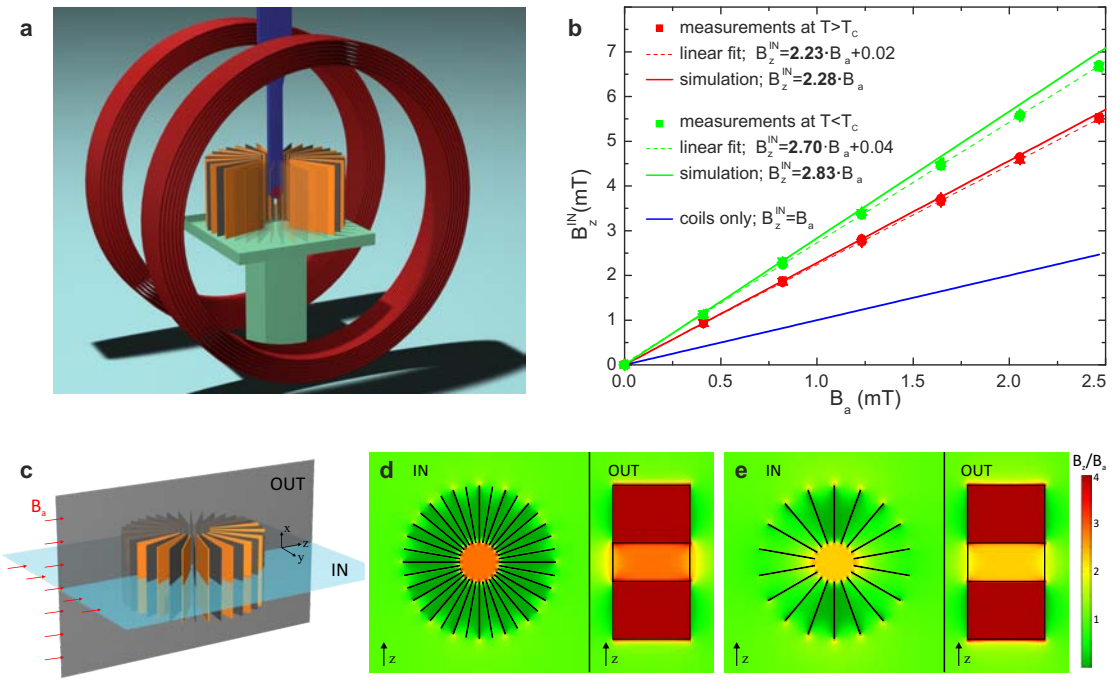

Figure 3.6: (**a**) Sketch of the experimental setup to measure the concentrating properties of the metamaterial shell. Two Helmholtz coils (red) created a uniform field. The shell (SC pieces in orange and FM ones in dark gray) was centered and the Hall probe (blue) measured the field in the central interior point, B_z^{IN}. (**b**) The measured field is plotted as a function of the field applied by the coils, B_{a}, (in symbols) for $T < T_{\mathrm{c}}$ in green and for $T > T_{\mathrm{c}}$ in red (horizontal and vertical error bars ΔB_{a}=0.04mT and ΔB^{IN}=0.002 mT, respectively, have been omitted for clarity). The corresponding linear fits are presented in dashed lines together with the simulations results, in solid lines. The blue line shows the field created by the bare coils. The calculated B_z field component is plotted in the planes IN and OUT, (**c**), for the case of 18 SC+18 FM (i.e. $T < T_c$), (**d**), and for the case of only 18 FM ($T > T_c$), (**e**).

in Fig. 3.6**a**) and the field inside the shell was measured by a Hall probe. Results of the concentrated field as a function of the field applied by the coils are shown in symbols in Fig. 3.6**b**. The field was measured in two different conditions; with the whole device submerged into liquid nitrogen (SCs below its critical temperature, T_{c}, and, thus, activated) and also at room temperature (with the SC parts deactivated). Measurements below T_{c} showed that field was increased by a factor 2.70 (green symbols and dashed fitting line in Fig. 3.6**b**). Although the theoretical enhancement factor should be 4 for an ideal infinitely long metamaterial, this figure was in excellent agreement with the 3D finite-element numerical simulation of the system (green solid line and Fig. 3.6**d**), which considered the actual finite dimensions and assumed ideal magnetic permeabilities for the materials ($\mu_{\mathrm{FM}} \to \infty$ and $\mu_{\mathrm{SC}} \to 0$). The difference in the field concentration factor can be attributed to the finite size of the metamaterial and its discretized nature. Regarding the measurements at room temperature, a concentration factor of 2.23 was achieved even in this case when superconductors were deactivated (red symbols and

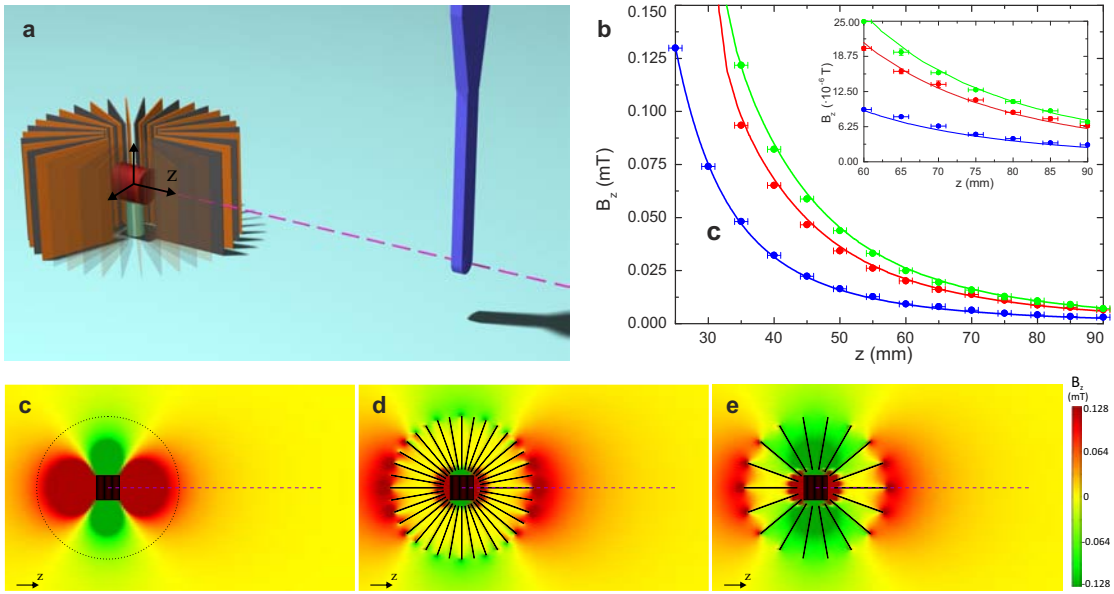

Figure 3.7: (**a**) Sketch of the setup to measure the field expulsion. A small coil (red) was placed inside the shell and fed with a constant current. The B_z field component was measured outside the shell by the Hall probe along the centered line (pink) as a function of the distance to the center z. (**b**) Measurement results are plotted in symbols; blue symbols are the field of the bare coil, green symbols are measurements at $T < T_c$, and red ones at $T > T_c$. Solid lines show results of the corresponding 3D simulations. Plots of the B_z field component in the median plane of these simulations for the case of the coil alone, (**c**), 18 FM+18 SC ($T < T_c$), (**d**), and 18 FM ($T > T_c$), (**e**).

dashed fitting line in Fig. 3.6**b**). The corresponding simulation, shown in Fig. 3.6**e**, considering only the 18 FM pieces, matched very well with these measurements (red solid line).

The field-expulsion properties of the shell were measured by placing a small coil at its center and feeding it with a constant current. The field B_z was measured outside the shell as a function of the distance z (see Fig. 3.7**a**). Measurements below T_c (green symbols in Fig. 3.7**b**) show the expelled field was increased by a factor of around 2.5 with respect to the field of the bare coil (blue symbols). Above T_c, the shell also increased the field in all exterior points by a factor of around 2.0, confirming its good behavior even without superconducting parts. These measurements agreed very well with the corresponding 3D finite-element simulations performed assuming ideal materials (solid lines in Fig. 3.7**b**). Plots of field in the median planes of these numerical calculations are shown in Fig. 3.7**c**, **d** and **e** considering the coil alone, the concentrator with 18 FM pieces and 18 SC ones, and the concentrator with only the 18 FM, respectively.

Finally we measured the field concentration at a distance from the source. For this purpose a second metamaterial shell consisting of only 18 FM pieces (and same radii) was built. The coil creating the field was placed inside the original shell and the field

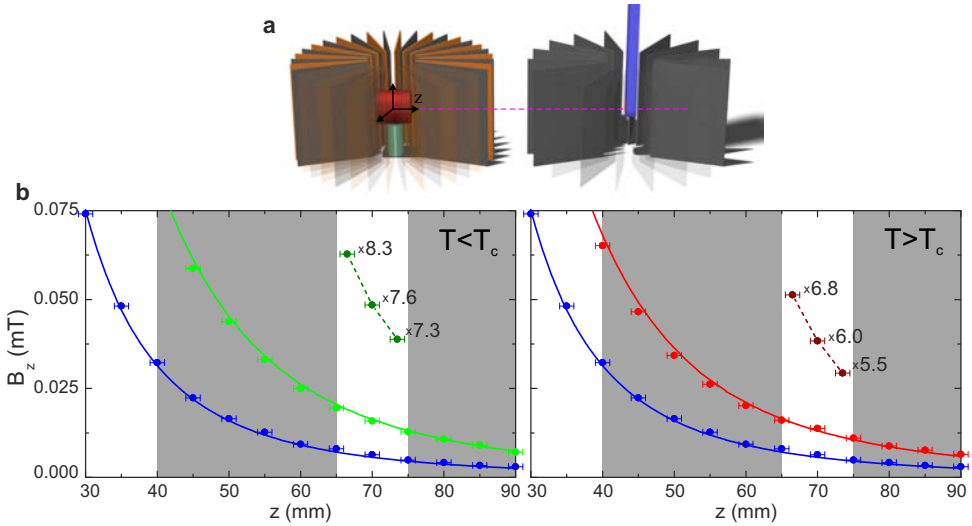

Figure 3.8: (**a**) Sketch of the experimental setup. (**b**) Measurement results (symbols) for the two working conditions; $T < T_c$ (left plot) and $T > T_c$ (right plot). Blue symbols and line correspond to measurements and simulation of the coil alone, light green (red) symbols and line correspond to measurements and simulations of the field expelled by the original metamaterial shell (already shown in the previous figure). Dark green (red) symbols correspond to the field measured inside the second shell when both shells were present. Numbers indicate the enhancement factor of the measured field with respect to the field of the bare coil. Dashed lines are guides for the eye.

was measured with the Hall probe inside the second shell. Both shells were separated a distance of 70mm from center to center (see Fig. 3.8**a**). Measurements are shown in Fig. 3.8**b**, for two cases. When $T < T_c$ (left plot), the shell with the source behaved rather as a full SC-FM metamaterial and, even though the receiver shell was a FM-only metamaterial, the measured transferred field was increased by an average factor of around 7.5 with respect to the field of the bare coil. When $T > T_c$ (right plot), the average factor was still around 6.0. In both cases, plots show that not only the field was magnified in the inner region of the receiver shell but also its gradient, as we theoretically predicted in Sec. 3.1 [139].

These experiments constituted a proof-of-principle of the theory of magnetic concentrating shells. The particular values of field concentration, expulsion and concentration at a distance obtained in these experiments could be clearly improved by considering longer shells and larger radii ratios. Nevertheless they demonstrated that the ideal theoretical magnetic concentrating shells emerged from transformation optics could be turned into real devices using actual commercial materials.

All this work on magnetic concentrating shells has opened a research topic that has been followed by different groups with different approaches. Other strategies to concentrate magnetic fields have been investigated based on transformation optics [140, 141, 142, 143, 144]. Our design of magnetic concentrating shells has also been studied

considering the field created by permanent magnets [145]. Moreover, the concentrating shell concept and its discretization into radially displaced pieces has been extended to other research areas to design concentrators for dc currents [146] or thermal energy harvesting devices [147].

3.5 Increasing the magnetic coupling between circuits by concentrating shells

The magnetic coupling between circuits is a key factor for most basic electromagnetic technologies like transformers or power generators. The performance of a transformer depends, in great measure, on the amount of magnetic field created by the primary circuit that crosses the secondary. Similarly, the magnetic flux crossing the coils of a generator determines the output power of the device. A growing number of technologies to deliver power wirelessly are also based on the magnetic coupling between circuits; a primary circuit creates a low-frequency time-dependent magnetic field that induces a voltage to the secondary. A strong magnetic coupling is pursued to maximize the transferred power and the efficiency.

This magnetic coupling between circuits is rigorously defined in terms of the flux that crosses one of the circuits, Φ_2, when an intensity I_1 circulates through the other circuit. This determines the mutual inductance between them, M_{12}, as $\Phi_2 = M_{12}\, I_1$. The flux Φ that crosses each circuit as a consequence of an intensity I circulating through itself defines the self-inductance, L, as $\Phi = L\, I$.

In this section we discuss how the unique properties of magnetic concentrating shells to distribute and concentrate magnetic energy in space allow to increase the magnetic coupling between circuits. This is applied to the the interesting case of wireless power transmission, experimentally demonstrating that magnetic concentrating shells allow to enhance the transmitted power and the transfer efficiency [148].

3.5.1 Theoretical development

Consider a circuit placed inside a magnetic concentrating shell. For an interior source of field, we demonstrated in section 3.2 that the field distribution inside the shell is not perturbed by the shell itself. Thus, if the circuit carries a certain intensity, the flux crossing the circuit is the same as if it was in free space, i.e. the circuit self-inductance is not modified by the shell. This first conclusion is relevant because, in general, magnetic materials near circuits affect the field distributions and modify their self-inductances. A clear example is the case of a high-permeability magnetic material inserted into a circuit, as happens with the ferromagnetic cores of transformers; the flux is hugely increased as well as the self-inductance of the coils.

Now consider two circuits separated a distance d. Each circuit consists of a couple of

wires separated by distances h_1 and h_2 for the primary and secondary circuits, respectively (see Fig. 3.9**a**). If each of the wires of the primary circuit carries an intensity I in opposite directions, the flux crossing the secondary circuit can be analytically calculated (see the Supplementary Material of [148]). The mutual inductance per unit length between the two circuits is found to be

$$M_{12} = \frac{\mu_0}{4\pi} \ln\left(\frac{4d^2 - (h_1 - h_2)^2}{4d^2 - (h_1 + h_2)^2}\right). \tag{3.22}$$

We now consider the case of two equal circuits, $h_1 = h_2 = h$, in which the primary circuit is surrounded by an ideal cylindrical concentrating shell with $\mu_\rho \to \infty$, $\mu_\varphi \to 0$ and $R_2/R_1 \equiv \alpha$. Applying Eq. (3.20) for the transformed field outside a concentrating shell, the mutual inductance is found

$$M_{12}^{\mathrm{I}} = \frac{\mu_0}{4\pi} \ln\left(\frac{4d^2 - h^2(1-\alpha)^2}{4d^2 - h^2(1+\alpha)^2}\right). \tag{3.23}$$

By comparing this equation (3.23) with the expression for bare circuits (3.22), we see the effect of surrounding the circuit with the concentrating shell is to effectively increase the size of the circuit (distance between wires) from h to αh.

If a second shell with radii ratio $R_2'/R_1' \equiv \beta$ surrounds the secondary circuit, Eq. (3.3) determines the field inside the second shell and the mutual inductance is

$$M_{12}^{\mathrm{II}} = \frac{\mu_0}{4\pi} \ln\left(\frac{4d^2 - h^2(\beta-\alpha)^2}{4d^2 - h^2(\beta+\alpha)^2}\right). \tag{3.24}$$

This expression corresponds to the mutual inductance between two circuits with bigger sizes αh and βh, and separated by the same distance d. For $d \gg h$, the improvement on the mutual inductance tends to $M_{12}^{\mathrm{II}}/M_{12} \to \alpha\beta$.

This enhancement of the mutual inductance, combined with the fact that the shells do not change the self-inductances of the circuits, makes the system with concentrators magnetically equivalent to the same bare circuits separated by a smaller distance d'. This effective distance can be found through Eqs. (3.22) and (3.24) as

$$\frac{d'}{h} = \sqrt{\frac{4\left(\frac{d}{h}\right)^2 - (\beta-\alpha)^2}{4\alpha\beta}}, \tag{3.25}$$

where α and β are the radii ratios of the shells, h is the spacing between the wires (of the two circuits) and d is the distance between their centers. For the particular case of two equal concentrating shells $\alpha = \beta = R_2/R_1$ the effective distance is reduced as $d' = (R_1/R_2)d$.

When circuits are surrounded by concentrators the gap of free space between them is reduced. The previous discussion on the improvement of the mutual inductance by concentrating shells can be rewritten as a function of the gap of free space (g) instead of the distance between the centers of the circuits d (see Fig. 3.9**a**). Considering

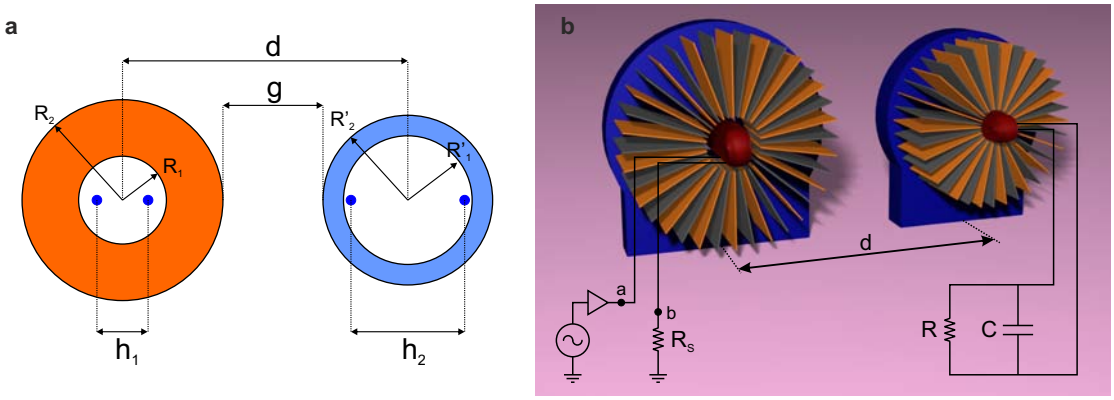

Figure 3.9: (**a**) Sketch of the geometry considered. (**b**) Picture showing the experimental setup to measure the wireless power transfer. Sketches of the primary and secondary circuits are also included. Coils are shown in red, the ferromagnetic parts of the shells in gray and the conducting ones in orange.

that the inner diameter of the shells exactly coincides with the size of the circuits (i.e. $2R_1 = 2R_1' = h$), the improvement on the mutual inductance for the same value of gap, $M_{12}^{\mathrm{II}}(g = d - R_2 - R_2')/M_{12}(g = d - R_1 - R_1')$, is reduced but it is still larger than one. Therefore, although the gap of free space between circuits with concentrators is smaller than for bare circuits, using shells results in an increase of the coupling for the same value of gap [148].

3.5.2 Experimental demonstration of wireless power transfer enhancement

Motivated by the recent explosion of mobile technologies, nowadays there is a huge interest to develop and improve strategies to transfer power wirelessly. One of such strategies that is more extended is based on magnetic induction between two coils; one of the coils creates a time-dependent magnetic field that induces a voltage to a second coil, from which the energy is extracted. This approach, already explored by Tesla more than 100 years ago [149], had a boost some years ago when Soljačić's team demonstrated that significant amounts of power could be efficiently transmitted to large distances (8 times the radius of the coils) using self-resonant coils in a strongly coupled regime [135].

The transmitted power and the efficiency of the energy transfer between the coils crucially depend on the mutual inductance between the circuits [136, 150]. Different strategies have been proposed to increase this coupling and transmit energy to longer distances, for example using "superlenses" to direct the magnetic field. These devices have been realized using metamaterial slabs that exhibit effective negative permeabilities at the frequencies of interest [151, 152].

An alternative strategy we suggest to increase the magnetic coupling is using magnetic concentrating shells. In this section we experimentally demonstrate that these

shells improve the wireless power transfer without significantly modifying the self-inductances of the circuits.

For this purpose we used two metamaterial concentrating shells. One of them (S1) was the shell we made for the static measurements (see Sect. 3.4.1), with radii R_2 =30mm, R_1 =7.5mm and a height of 30mm. Since these new measurements were performed with time-dependent magnetic fields, the shielding properties provided by the superconductors in the static case now could be approximately obtained from conducting materials, without using superconducting parts (and thus avoiding the complications of refrigeration). For this reason 18 rectangular pieces made of copper foil and similar size substituted the original SC pieces. A second shell (S2) was built following the same principle, made of 18 FM pieces alternated with 18 conductive ones. The size of this second shell was R_2' =25mm, R_1' =5mm and height a of 30mm.

Two coils were built to fit inside the shells. They had an elongated shape, approximating to the translational symmetry considered for the analytical development. The coil (C1) fitting inside the shell S1 had a length of 48mm and a thickness of 11mm approximately, and the second coil (C2) fitting inside the shell S2 had the same length and a thickness of 9mm (see Fig. 3.9**b**).

Measurements of self-inductances of the coils

The self-inductances of the two coils were measured in isolated conditions and also placed inside the corresponding shells. The inductance, L, was found by measuring the resonance frequency (f_0) of an RLC circuit as the one sketched in Fig. 3.10**a**. In resonance, voltage signals at points A and B are in phase because the impedance of the circuit is purely real and the following relation between the parameters is fulfilled

$$L = \frac{1}{4\pi^2 C f_0^2}, \tag{3.26}$$

allowing to find the inductance if the capacitor, C, is known. Measurement results are shown in Fig. 3.10**b**, for frequencies between 20 and 40KHz. They demonstrate that the inductance of the first coil C1 was barely modified by the shell S1. Differently, the self-inductance of second coil C2 was more increased by the corresponding shell, probably because in this case the coil was more closely to the FM and the conductive parts forming the shell. A finner discretization of the shell into more pieces could reduce this effect. Nevertheless, these results show that the shells do not change significantly the self-inductance of the coil that are surrounding, even considering their finite length and the discretization.

Wireless power transfer enhancement by concentrating shells

The wireless power transmission between the coils was measured in different situations. The first coil C1 was connected to a primary circuit consisting of a signal

a

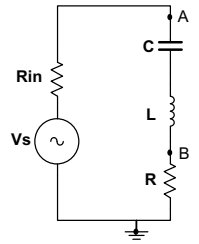

b

	***L* (mT)**
C1 alone	0.15±0.01
C1+S1	0.16±0.01
C2 alone	0.065±0.003
C2+S2	0.071±0.003

Figure 3.10: (**a**) Sketch of the RLC circuit used to measure the self-inductance of the coils. (**b**) Measured self-inductances for frequencies between 20 and 40KHz.

generator and a power amplifier, in series with a shunt resistance, $R_\mathrm{s} = 1\Omega$. The second coil C2 was connected in parallel to a capacitor, $C = 387.4\mathrm{nF}$, and a load resistance, $R = 990\Omega$, forming a resonant secondary circuit (see the sketch in Fig. 3.9**b**). The total power delivered to the system, W_T, and the power dissipated in the load resistance, W_R, were calculated through [153]

$$W_\mathrm{T} = \frac{V_a\, V_b}{2R_\mathrm{s}} \cos\phi_{a\to b}, \tag{3.27}$$

$$W_R = \frac{1}{2}\frac{V_R^2}{R}, \tag{3.28}$$

being V_a (V_b) the amplitude of the voltage at point a (b), $\phi_{a\to b}$ the phase shift between the voltages at points a and b, and V_R the amplitude of the voltage drop in the load resistance (see Fig. 3.9**b**). The final figure-of-merit of the power transfer is the efficiency, η, defined as [151]

$$\eta = \frac{W_R}{W_\mathrm{T}}. \tag{3.29}$$

Three kind of measurements were performed. First the wireless power transfer between the two bare coils was measured as a function of the distance between them, d. The frequency of the signal generator was fixed at the resonant frequency of the secondary circuit $f = 31.75\mathrm{KHz}$. Then, the emitting coil C1 was surrounded by the shell S1 and measurements were repeated at the same frequency. Finally, the receiving coil C2 was also surrounded by the shell S2. In this case the resonant frequency of the secondary circuit was slightly modified to $f = 30.17\mathrm{KHz}$.

The power dissipated in the load resistance and the total power delivered to the system for the three cases are shown in Fig. 3.11**a**. Whilst the total power was approximately constant in all measurements, the power dissipated in the load resistance was clearly increased by the shells. This indicates that the efficiency of the transfer was also enhanced. In Fig. 3.11**b** the efficiency [calculated with Eq. (3.29)] is plotted for the three cases, demonstrating a very significant improvement. Actually, the ratio of improvement was around 5 when using only one shell and around 35 using the two shells (bottom panel).

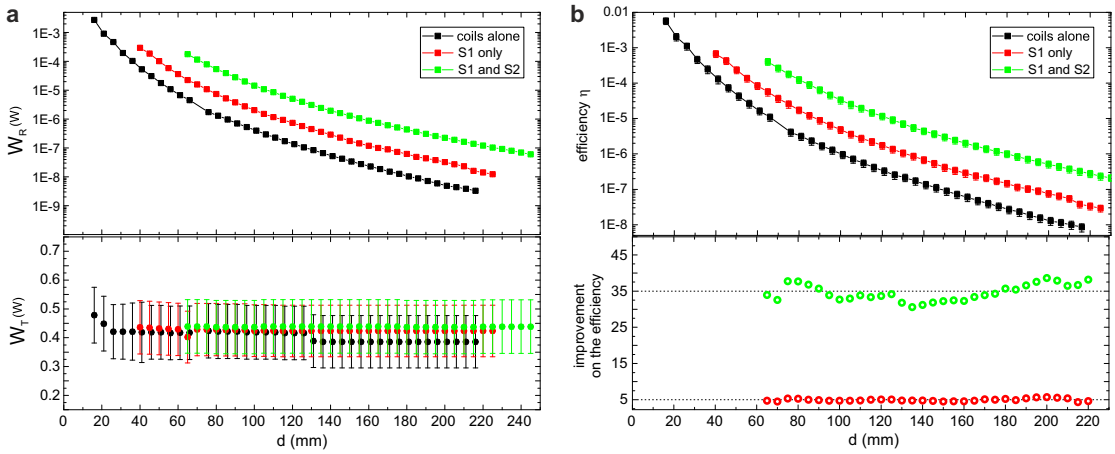

Figure 3.11: (**a**) Measurements of the power dissipated in the load resistance, W_R, and the total power delivered to the system, W_T, as a function of the distance between coils. (**b**) The efficiency of the power transfer is plotted (top), together with the improvement achieved by using one or two concentrating shells (bottom). Black points are measurements of the two coils alone, red points correspond to use only the first shell S1 and green points to use the two shells.

These measurements show how magnetic concentrating shells increase the magnetic coupling between circuits without modifying their self-inductances. Applied to the interesting case of wireless power transfer, shells demonstrate to increase the transmitted power as well as the efficiency in a very significant way. Since the materials forming the concentrating shells are cheap and commercial, and work at room temperature, devices generated from these ideas could be readily applied to different existing technologies.

3.6 Chapter summary and conclusions

Magnetic field concentration is essential in many applications. For example, it is applied in high precision magnetic sensors to increase their sensitivity or in electromagnetic transformers to concentrate fields in the coils and increase their performance. Our research presented in this chapter introduces a completely new approach to magnetic concentration and, for this reason, results are essentially different from that obtained using traditional strategies of magnetic field shaping.

The design of the magnetic concentrating shell discussed in this chapter is based on transformation optics. It has been demonstrated that, for fields applied externally to the shell, the field is concentrated in the interior hole whilst the external field distribution is not distorted. Reinterpreting the same space transformation, a symmetric behavior has been shown for interior field sources so that the same shell expels the field towards the exterior without changing the field inside the hole.

When comparing the field concentration properties of the shell with traditional strategies using gaps between superconducting or ferromagnetic materials, concentrat-

ing shells have demonstrated to improve the figures both in terms of field and magnetic flux enhancement. Combining concentration and expulsion properties, we have also demonstrated that large values of field can be obtained at points far from the sources of field.

We have shown that ideal homogeneous and anisotropic concentrating shells can be accurately discretized into pieces of superconducting and ferromagnetic materials. Following this strategy some shells have been built and their properties to shape static magnetic fields have been experimentally validated.

Finally, we have also discussed the properties of magnetic concentrating shells in terms of magnetic coupling between circuits, for both static and low-frequency electromagnetic fields, showing that they can be used to increase the mutual inductance between distant circuits without changing the circuits self-inductances. This property has been applied to the relevant case of wireless power transfer, experimentally demonstrating that shells increase the transferred power and its efficiency by large factors.

In conclusion, concentrating shells developed in this chapter constitute a new tool the control and shape magnetic fields. Their properties to concentrate and expel fields can be combined to obtain very different effects and could be useful for numerous applications. Increasing the sensitivity of magnetic sensors, transmitting fields to distant positions or improving the wireless power transfer between circuits are only some particular examples in which shells could provide novel possibilities.

CHAPTER 4

Routing of static magnetic fields

Guiding and transferring magnetic fields is an essential requirement in many devices, from large scale transformers to nanoscale magnetic logic devices [154, 155]. Unlike electromagnetic waves that can be routed and transmitted with waveguides or optical fibers to long distances, static magnetic fields rapidly decay with the distance from their source. In this section we develop a new design, called a *magnetic hose*, which allows to transfer static magnetic fields to arbitrary distances following any desired path. A feasible design employing actual materials is proposed and experimentally demonstrated [156].

4.1 The problem

The conventional way to transfer the static magnetic field of a source (e.g. a magnet) is using a ferromagnetic material with high magnetic permeability, as in the transfer of field from the primary to the secondary circuits of a transformer [154]. The transferred field, however, is drastically reduced as the material is lengthened. This is explained by considering that the ferromagnet yields high values of magnetic induction field not only in the longitudinal direction of the material but also in the perpendicular one. For this reason some magnetic field lines inside the ferromagnet exit from the material through its lateral faces, causing that the field transferred to the end decreases with the length (see Fig. 4.1**a** for numerical calculations).

An alternative strategy could consider guiding magnetic field lines through a hollow superconducting tube. However, the transferred field in this case also decreases exponentially with the length of the tube (see Fig. 4.1**a**). Intuitively, the amount of field lines emerged from a source at one end of the tube that go inwards decrease when the

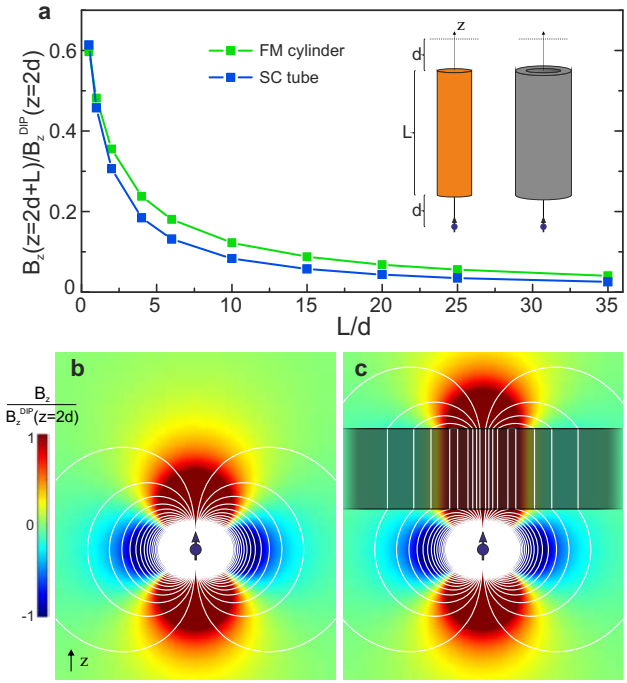

Figure 4.1: (**a**) Numerical calculations of the field transferred by a cylindrical ferromagnet (in orange, with $\mu \to \infty$) and a superconducting tube (in gray, with $\mu \to 0$). Symbols indicate the vertical field on the axis at $z = 2d + L$, $B_z(z = 2d + L)$, normalized to the field created by the bare dipole at a vertical distance $z = 2d$, $B_z^{\mathrm{DIP}}(z = 2d)$. (**b**) Numerical calculation of the field (B_z in colors and field lines in white) of an isolated point dipole. (**c**) When a slab of ideal material with $\mu_x = \mu_y \to 0$ and $\mu_z \to \infty$ is present, the field is vertically shifted.

tube is made long. If the field source (e.g. a point dipole) is introduced inside the tube, and considering that is infinitely long, it can be analytically demonstrated that the field not only does not extend to longer distances but decreases more rapidly [156, 157].

Hence, in contrast to time-dependent electromagnetic fields that can be transmitted and routed to long distances with, for example, optical fibers, a device capable of doing so with static magnetic fields does not exist.

4.2 Magnetic hose

4.2.1 Homogeneous anisotropic material to transfer magnetic fields

We design our device to transfer magnetic fields by transformation optics. Considering cartesian coordinates, we apply the following space transformation that shifts the space in the z-direction

$$z' = z, \qquad z \in (-\infty, z_1) \tag{4.1}$$

$$z' = \frac{z_2 - z_1}{\xi}(z - z_1) + z_1, \qquad z \in [z_1, z_1 + \xi) \tag{4.2}$$

$$z' = z + (z_2 - z_1 - \xi), \qquad z \in [z_1 + \xi, \infty) \tag{4.3}$$

where z_2 and $z_1 < z_2$ are constants and ξ is a small parameter. The x and y coordinates are left untransformed, i.e. $x' = x$ and $y' = y$. This space transformation shifts the space above $z_1 + \xi$ replacing it above z_2 (Fig 4.2**b**), and linearly expands the region between z_1 and $z_1 + \xi$ to keep the transformed space continuous, as sketched in Fig. 4.2**c**. Notice that in the limit case of $\xi \to 0$ this transformation corresponds to a vertical shift of the field above $z > z_1$ transferring it to $z' > z_2$.

Applying transformation optics theory we find the required permeabilities for this control of the field

$$\mu = 1, \qquad z' \in (-\infty, z_1) \tag{4.4}$$

$$\mu_x = \mu_y = \frac{\xi}{z_2 - z_1}, \quad \mu_z = \frac{z_2 - z_1}{\xi}, \qquad z' \in [z_1, z_2) \tag{4.5}$$

$$\mu = 1. \qquad z' \in [z_2, \infty) \tag{4.6}$$

These results show that an homogeneous anisotropic material is required only in the space between $z = z_1$ and $z = z_2$. In the limit case of $\xi \to 0$, a very large permeability is needed in the transfer direction and a zero permeability is required in the perpendicular one ($\mu_x = \mu_y \to 0$ and $\mu_z \to \infty$). In this case, applying tranformation optics expresions [Eq. (1.28)], the field can be found in all regions of space. In particular, the field in the shifted space $z' > z_2$ is

$$\mathbf{H}'(x', y', z') = \mathbf{H}\left(x', y', z' - (z_2 - z_1)\right) \tag{4.7}$$

where $\mathbf{H}(x, y, z)$ is the original field distribution expressed in the cartesian basis. This demonstrates that the field is completely shifted a distance $z_2 - z_1$. Since z_1 and z_2 are arbitrary parameters, the field can be transferred to arbitrary distances (see the numerical calculation for the field of a point dipole in Fig. 4.1**b** and **c**).

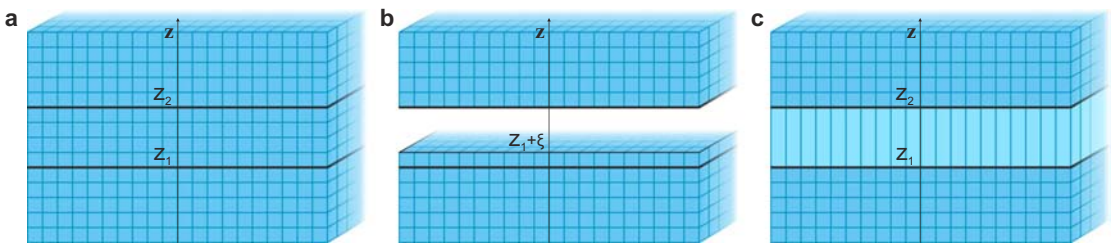

Figure 4.2: Sketch of the space transformations applied to design a material to transfer magnetic fields.

It is worth to notice that for $\mu_x = \mu_y \to 0$ and $\mu_z \to \infty$ the magnetic energy density inside the shell is zero because fields are $\mathbf{H}' = H_x(x', y', z_1)\hat{x} + H_y(x', y', z_1)\hat{y}$ and $\mathbf{B}' = \mu_0 H_z(x', y', z_1)\hat{z}$, yielding $w = \mathbf{B} \cdot \mathbf{H}/2 = 0$. Since the field distribution below the shell is not changed by the material (because the space is not transformed) this indicates the energy distribution is also totally shifted a distance $z_2 - z_1$.

This ideal material obtained from transformation optics meets the goal of transferring the field to any distance but is not a feasible solution, because requires an infinitely wide slab of material and also because the required anisotropic permeability is not directly found in natural magnetic materials. We address these two limitations separately.

4.2.2 Magnetic hose to transfer magnetic fields

In order to attain a feasible design, we first study the field transfer properties of a finite piece of material. We consider the case of a point dipole at a distance d below a cylindrical piece of material with $\mu_\rho \to 0$ and $\mu_z \to \infty$ (see inset in Fig. 4.3**a**). We numerically calculate the field transferred to the opposite end of the material as a function of the radius R of the material and for different lengths L. Results in Fig. 4.3**a** show that the vertical field B_z at a distance d above the top end of the material decreases only slightly when the material length increases and rapidly saturates to a certain value that depends on R. It can be demonstrated that this saturated value is not zero; hence, a part of the magnetic field is always transferred through the hose to arbitrary distances [156]. For $R = 4d$ and lengths up to $L = 10d$ the transferred field is very close to that transferred by an ideal infinite slab. This property is approximately maintained even for radii as small as $R \simeq 2d$.

To circumvent the second limitation regarding the required homogeneous anisotropic permeabilities, we follow a discretization strategy similar to that applied for the magnetic concentrating shells (Sec. 3.4). Considering axial symmetry, the large vertical and zero horizontal permeability components can be effectively obtained by alternating cylindrical shells made of ideal superconducting and soft ferromagnetic materials. Ferromagnetic parts provide a large axial permeability and the alternated superconductors prevent radial components of $\mathbf{B}$ field[1]. The transfer properties of these discretized designs, hereafter named *magnetic hoses*, are demonstrated through numerical calculations. Results of the transferred field as a function of the number of shells, n, are shown in Fig. 4.3**b**. The field of the dipole, located at one end of the hose, that is transferred to the opposite end tends to the ideal behavior with increasing n. More than 90% of the transfer can be achieved with n =20. Remarkably, even with only two shells, the transfer can be as high as 75%. In this bilayer scheme the SC has to be the outer layer, surrounding the FM, in order to prevent that field lines inside the FM core leak outside through the lateral surface.

[1] These superconducting shells should contain a non-superconducting slit along their length to avoid undesired effects appearing in superconducting materials with holey topologies.

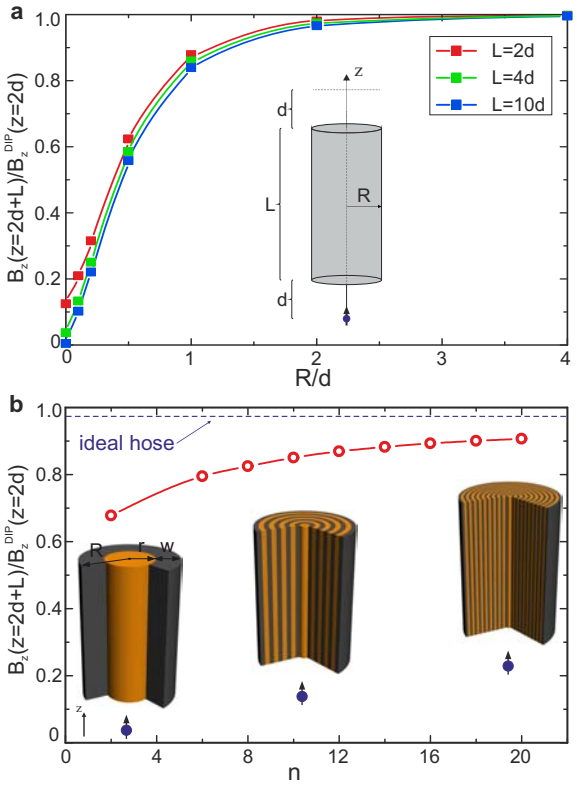

Figure 4.3: (**a**) On-axis vertical field at a distance d above a cylindrical piece of ideal material with $\mu_\rho \to 0$ and $\mu_z \to \infty$, when a vertical dipole is placed at a distance d below it, as a function of the radius R (see inset). Calculation results (in symbols) are shown for different lengths of the material. (**b**) Assuming the same configuration, transferred field results for hoses discretized into different number of shells, n. FM (in orange, with $\mu \to \infty$) and SC (in gray, with $\mu \to 0$) shells have all the same thickness. The field transferred by an ideal hose with the same geometry is indicated. The total radius of the hoses is $R = 2d$ and their length $L = 4d$. All results are normalized to the on-axis vertical field created by an isolated dipole at a vertical distance $z = 2d$, $B_z^{\mathrm{DIP}}(z = 2d)$.

In view of its excellent performance, we focus on the properties of this bilayer FM+SC hose. In this case, the field transfer properties strongly depend on its sizes r and w (see inset in Fig. 4.3**b**). Numerical calculations of this system applying the field of a vertical point dipole at one end of the hose demonstrate that the transferred field at the opposite end is maximum for $r \simeq 0.6d$ and $w \simeq 1.4d$ [156]. Intuitively, a small FM core prevents that all field lines of the dipole go into the material. Conversely, if the FM is too large, field lines turn around in its interior reducing the transferred field. The thickness of the SC is also relevant, tending to concentrate field lines towards the FM core.

This FM+SC bilayer hose can be extended to other topologies considering, for example, more than two ends. In Fig. 4.4 we show numerical calculations of hoses with different shapes and different number of ends. Numbers indicate the numerical average field that goes out of each end $\bar{B}_z \equiv \langle B_z \rangle_S / B_z^{\mathrm{DIP}}(z = d)$ [where $B_z^{\mathrm{DIP}}(z = d) = \mu_0 m/(2\pi d^3)$].

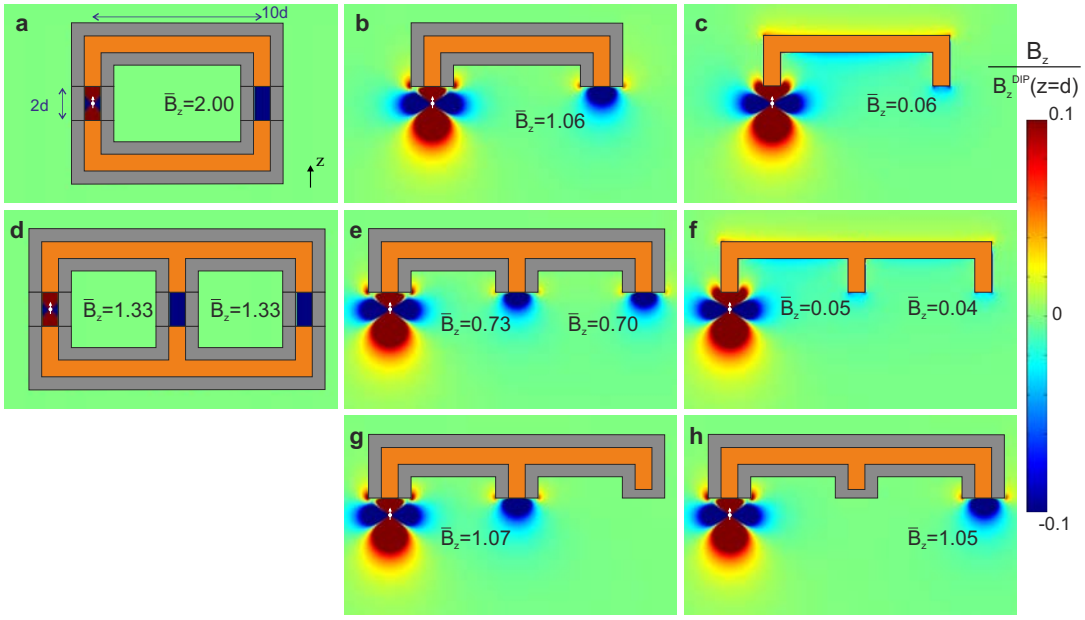

Figure 4.4: Plots of field in the median plane of different 3D numerical calculations. Point dipoles are shown in white, FM parts are represented in orange ($\mu \to \infty$ and $r = d/2$) and SC ones in gray ($\mu \to 0$ and $w = 3d/4$). The vertical field component, B_z, is shown in colors and numbers indicate the average field that goes out of each end normalized to the maximum field of an isolated dipole at distance d; $\bar{B}_z \equiv \langle B_z \rangle_S / B_z^{\mathrm{DIP}}(z = d)$.

Interestingly, the solution of closed hoses as that of Figs. 4.4**a** and **d** can be analytically found by solving the Laplace equation with the appropriate boundary conditions. Imposing that the normal component of the **B** field is 0 at the interior face of the SC, the scalar magnetic potential is constant within the ideal soft FM, and forcing continuity of the potential along the whole closed hose, it can be demonstrated that the field in the gap of empty space inside a single-branch closed hose is uniform with a modulus

$$B_z = \frac{\mu_0 m}{2\pi r^2 (h_\mathrm{s} + h_\mathrm{a})}, \tag{4.8}$$

where m is the magnetic moment of the dipole, $2h_\mathrm{s}$ is height of the region where the dipole is, $2h_\mathrm{a}$ is the height of the empty gap and r is the radius of the FM core (see the Supplemental Material of [156]). Applied to the case of Fig. 4.4**a**, with $h_\mathrm{s} = h_\mathrm{a} = d$ and $r = d/2$, we find that $\bar{B}_z = 2$, in perfect agreement with the numerical calculation.

In the case of Fig. 4.4**d**, the scalar magnetostatic potential is constant within the top and bottom ferromagnetic pieces. For this reason the difference of magnetic potential between the top and bottom ferromagnets in the two empty gaps is the same. This situation is analogous to the electrostatic potential in parallel electric circuits, so an effective gap equivalent to the two parallel gaps can be calculated through the parallel

association formula

$$h_{\mathrm{a}}^{\mathrm{eff}} = \left(\frac{1}{h_{\mathrm{a},1}} + \frac{1}{h_{\mathrm{a},2}} \right)^{-1} . \tag{4.9}$$

Considering $h_{\mathrm{a},1} = h_{\mathrm{a},2} = d$, this yields an smaller effective gap $h_{\mathrm{a}}^{\mathrm{eff}} = d/2$. Applying Eq. (4.8) and taking into account the field is equally divided into the two gaps, we find $\bar{B}_z = 4/3$ in each one, in agreement with the calculations.

These analytical results for closed hoses allow to understand results for open geometries. In Figs. 4.4**b** and **e** the equivalent open geometries show that the average field is reduced respect to the closed cases but follow the same trend. The more ends the hose has, the less average field exits each one. When one of the ends is closed, we recover similar results to that for a single-ended hose (see Figs. 4.4**g**, **h** and **b**). Notice that using the FM cores alone yields tiny field transfer results, and they are reduced with the length.

Beyond this simplest design of a bilayer FM+SC hose, other proposals consisting of a larger number of layers can provide useful properties in some situations. For example, the shape of the field transferred by a bilayer FM+SC hose does not maintain the same spatial distribution as the field that goes into the opposite end. Hoses discretized into a larger number of layers, approaching to the anisotropic ideal design, cause much less distortion on the applied field distribution, and they keep it to the opposite end. These designs consisting of many shells have also demonstrated good transfer results even when superconductors are removed. Several thin ideal FM cylinders separated by air gaps transfer the field to longer distances than equivalent bulk cylinders made of the same ideal FM material. These results open the way to design hoses that work at room temperature and overcome existing strategies to transfer static magnetic fields.

4.2.3 Experimental realization

We built two bilayer FM+SC hoses to demonstrate their field transfer properties. One of them had a length of 60mm and the other of 140mm. The FM core of the short one was made of a commercial soft iron and had a radius of 8mm and a length of 60mm (Fig. 4.5**a**). The SC shell for this hose was made of 17 pieces of superconducting coated conductor, 4mm wide (SuperPower SCS4050). Pieces were parallel arranged with an overlap of 0.5mm, and were all glued on adhesive tape. The resulting SC shell had a rectangular shape of 54x60mm (see Fig. 4.5**b**). The FM core of the long hose was a Co-Fe alloy (VACOFLUX-17 from Vacuumschmelze) with a radius of 9mm and a length of 140mm (Fig. 4.5**d**). The corresponding SC shell was made of 14 pieces of a superconducting coated conductor, 12mm wide (SuperPower SF12050). They were parallel placed with an overlap of 2mm and glued on adhesive tape. Another 13 pieces of a narrower strip (SuperPower SF12050) were fixed on the overlapping lines to avoid field leakage. The resulting rectangular shell had a size of 61x140mm (see Fig. 4.5**e**).

Three different measurements were performed. First, the field transferred by the FM

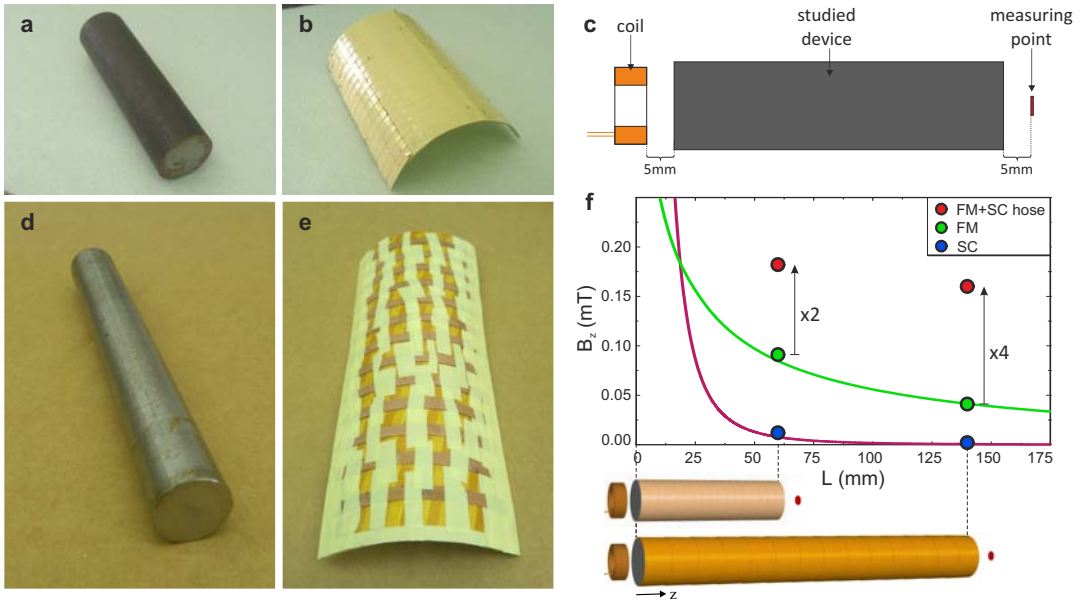

Figure 4.5: Pictures of the FM cores for the short (**a**) and long (**d**) hoses, and pictures of the corresponding SC shells (**b**) and (**e**) , respectively. (**c**) Sketch of the experimental setup. (**f**) Measurement results (in symbols) together with numerical calculations of the field transferred by an ideal soft FM (green line) and the field of the bare coil (purple line).

cores alone was measured at room temperature. Then we measured the field transferred by the SC shells only. For this purpose they were wrapped around plastic formers with the same sizes as the corresponding FMs. Measurements were performed at liquid nitrogen temperature. Finally, SCs were wrapped around the FMs and the field transfer was measured at liquid nitrogen temperature. The field applied at one end of the different devices was created by feeding a coil with a constant current. Devices were placed at a distance $d = 5$mm from the coil and the field was measured by a Hall probe also at a distance $d = 5$mm from the opposite end (see sketch of the setup in Fig. 4.5**c**).

Results of these measurements are shown in symbols in Fig. 4.5**f**, together with calculations of the field created by the bare coil (purple line) and that transferred by an ideal FM cylinder (green line). Measurements show the field transferred along the hose is much larger than that transferred by the FM or the SC alone. As indicated in the figure, for the short hose, the field is enhanced a factor 2 with respect to the FM case. For the long one this factor rises, as predicted by the theory, improving the transfer of the FM by 4 times.

In spite of these good results, measured transferred fields are less than that obtained by numerical calculations using the same experimental dimensions and assuming ideal SC and soft FM materials. If we normalize these measurements to the field created by the coil alone at a distance $2d$ =10mm we find the values in Table 4.1 ("measured" columns). Comparing them with the corresponding numerical calculations ("calculated"

Table 4.1: Measured and calculated transferred field ratios. Numerical calculations assumed the dimensions of the experiments and ideal materials ($\mu^{\mathrm{FM}} \to \infty$ and $\mu^{\mathrm{SC}} \to 0$).

	short length (60mm)		**long length (140mm)**	
	measured ±0.2%	calculated	measured ±0.2%	calculated
$B^{\mathrm{SC}}/B^{\mathrm{coil}}(z=2d)$	1.5%	9%	0.2%	4%
$B^{\mathrm{FM}}/B^{\mathrm{coil}}(z=2d)$	12.1%	11%	5.5%	5%
$B^{\mathrm{hose}}/B^{\mathrm{coil}}(z=2d)$	24.3%	50%	21.4%	43%

columns) we see the field transferred by the hose is less than calculated. Differently, measurements for only the FM agree with the corresponding calculations, indicating that the discrepancy in the field transfer is due to the non-perfect behavior of the SC parts, probably due to the field leaking between the SC strips forming the shell. This effect could be reduced by adding more SC shells and improving the sealing between the SC pieces. Nevertheless, even with these imperfections in such proof-of-principle experiments, the measured transferred field ratio of the hose with respect to the FM increases from 2 to 4 between the short and long studied lengths, validating the theoretical ideas of magnetic field routing presented in this chapter.

The magnetic hoses presented in this chapter are studied in static conditions, with infinite associated wavelength. This allows to scale them up or down arbitrarily. In particular, one could conceive a nanometric hose, which might be useful to increase the magnetic coupling between nanomagnets in magnetic logic schemes [155, 158, 159, 160]. A magnetic nanohose could also be used as a new tool to harness quantum systems, as required in quantum information processing [161], for example. In particular, such a device could be used to address, control, and manipulate the internal state of individual quantum systems, even if they were separated by large distances where optical methods are no longer available. Beyond the transfer of classical magnetic fields, one could also envision a system similar to the one considered in this chapter to magnetically couple distant quantum systems, allowing to separate them by relatively long distances and still strongly interact with each other [162]. The characterization of such a system, however, would require a full quantum treatment of the device.

4.3 Chapter summary and conclusions

Differently from electromagnetic waves that naturally propagate in space, static magnetic fields rapidly decay from their sources. This well-known limitation has important consequences in different magnetic technologies and, for this reason, magnetic fields are usually created near the points where they are required.

A novel strategy to transmit them to large distances has been developed in this chapter. The problem has been first addressed with transformation optics, finding an ideal

but unfeasible solution. Based on numerical calculations, we have demonstrated that a finite cylindrical piece of material with large permeability in the axial direction and zero permeability in the perpendicular one allows to transfer fields to arbitrary distances. A discretization procedure similar to that applied for the magnetic concentrating shells has demonstrated that such magnetic hoses can be built alternating cylindrical superconducting and ferromagnetic shells. The field transfer performance depends on the total number of shells, but we have demonstrated that a single ferromagnetic core surrounded by a superconducting shell achieves significant results. Analytical solutions have been found for this simple bilayer, validating the numerical results. Different variations of the hose have been also considered, showing that a hose with various branches and ends would allow the field transfer between different points.

Following this simplified bilayer design, we have built actual magnetic hoses using commercial soft ferromagnets and superconducting coated conductors. Their field transfer properties have been measured, demonstrating a clear improvement with respect to the cases of the ferromagnetic cores or the superconducting shells separately.

The magnetic hoses developed in this chapter, thus, play a role analogous to that of optical fibers for light, allowing the propagation of magnetic fields to long distances. As a consequence, the weak interaction of two distant magnetic systems can be significantly magnified by using magnetic hoses, allowing their fields to interact as if they were close together. Different applications could be envisaged, such as increasing the coupling between nanomagnets in magnetic logic schemes or addressing and controlling internal states of individual quantum systems.

CHAPTER 5

Changing the topology of space: a magnetic wormhole

The versatility offered by transformation optics theory to control the electromagnetic propagation has been applied to very different problems. As we introduced in section 1.3, the theory shows a correspondence between space transformations and electromagnetic materials; from an electromagnetic point of view, a curved space is equivalent to a non-curved regular space full of a particular *transformation media*. This analogy was exploited by Leonhardt and Philbin, who devised the use of electromagnetic metamaterials to mimic celestial mechanics [43]. Since then, different proposals emulating celestial objects like electromagnetic black holes [44, 45, 46, 47, 163] or wormholes [48, 164] have been studied.

In this section we present the theory and the experimental realization of a wormhole for static magnetic fields. Inspired by the theoretical proposal of Greenleaf et al. on electromagnetic wormholes [48], the device allows the transfer of magnetic fields between two points in space through a path that is magnetically undetectable [165].

5.1 The concept

The concept of an electromagnetic wormhole was presented by Greenleaf et al. [48]. In their work they designed a device that acted as an invisible tunnel, allowing electromagnetic wave propagation between its two ends whilst the tunnel itself was not detectable to lateral electromagnetic observations. This device would act as a wormhole with respect to Maxwell equations, effectively changing the topology of the space, since it would make electromagnetic waves propagate as if the $\mathbf{R}^3$ space had a handlebody attached to it [48].

The electromagnetic wormhole was designed applying different space transforma-

tions, which resulted in extremely cumbersome permeability and permittivity distributions required in its whole volume. The difficulty in obtaining such fine-tuned position-dependent material parameters has prevented the electromagnetic wormhole from being experimentally realized.

The concept of an electromagnetic wormhole can be also considered in the static magnetic case. Such device would be able to transfer static magnetic fields between distant regions of space while the region of propagation remains magnetically undetectable. At points near its ends, the device would surely distort the existing background field due to the field that enters and exits them. However, along the rest of its path, the device would be undetectable to lateral magnetic measurements [48].

To design such wormhole for static magnetic fields one could follow a strategy similar to that of [48], considering analogous space transformations and obtaining similar permeability distributions, but the required values would be very complicated to achieve in practice. Differently, here we design a magnetic wormhole not based on transformation optics. We take advantage of the possibilities that magnetic metamaterials offer for shaping static magnetic fields to obtain the desired effect [165].

5.2 A wormhole for the static magnetic case

The magnetostatic wormhole requires constructing a tunnel for magnetic fields acting as if it was outside the usual 3D space. The first property to be satisfied is to magnetically decouple a given volume from the surrounding 3D space. The volume enclosed by an ideal superconducting shell has this property [106], because the external field does not penetrate inside the shell and the field of internal sources does not leak to the exterior. Here we consider a spherical superconducting shell. A second property is that the whole resulting wormhole cannot be magnetically detectable from its exterior. The superconducting spherical shell would distort an applied field and, thus, would be detectable. To address this problem, we consider the results of section 2.2, where we studied the properties of bilayer systems composed of superconducting and ferromagnetic shells to cloak externally applied fields. We demonstrated that the distortion of the SC and the FM parts can be compensated yielding an exact cloaking behavior for uniform fields. In particular, for the spherical bilayer case, we found that the relative permeability of the outer ferromagnetic shell, μ_2, for which there is no distortion is

$$\mu_2 = \frac{2R_2^3 + R_1^3}{2(R_2^3 - R_1^3)}, \tag{5.1}$$

where R_2 is the exterior radius of the FM shell and R_1 is the interior radius of the FM, also corresponding to the exterior radius of the SC shell.

Equation (5.1) was found assuming a uniform external applied field and here we are interested in an arbitrary applied field. To study the behavior of these bilayer cloaks for non-uniform fields we consider the case of a vertical point dipole aligned with the

center of the spherical bilayer at a certain distance d (see Fig. 5.1**b** for a sketch of the geometry). The analytical solution to this problem can be found following an analogous procedure to that for the uniform applied field. A scalar magnetic potential, ϕ, is defined as $\mathbf{H} = -\nabla\phi$, and it is forced to fulfill the Laplace equation in all regions of space. Imposing that the potential at the origin (center of the bilayer shell) is finite, that it tends to the potential created by the bare dipole at infinite, and setting the magnetostatic boundary conditions at the interfaces, the solution of the potential can be found in all regions of space as a summation of infinite terms. In particular, the potential outside the shell is

$$\phi(r,\theta,\varphi) = \phi_{\text{dip}} + \sum_{n=1}^{\infty} \frac{D_n}{r^{n+1}} P_n(\cos\theta), \qquad r > R_2 \tag{5.2}$$

where ϕ_{dip} is the potential created by the bare dipole, $P_n()$ are the Legendre polynomials of integer order n and r, θ, φ are the usual spherical coordinates. D_n are known constants that depend on the geometrical parameters and the permeability of the shells. For the case of a superconducting interior shell with relative permeability $\mu_1 = 0$, it can be found a permeability for the outer FM layer, μ_2, for which $D_n = 0$. This permeability depends on the particular n and is [165]

$$\mu_2 = \frac{(2n+1)}{(n+1)\,(\beta^{2n+1}-1)} + 1, \tag{5.3}$$

where $\beta \equiv R_2/R_1$. This indicates that the different terms of the distortion can be individually canceled by choosing the appropriate permeability of the FM shell, but they cannot be canceled all simultaneously. Interestingly, the permeability for which the dipolar term (n=1) is canceled is that given by Eq. (5.1). Therefore, a spherical bilayer with a permeability fulfilling this equation exactly cloaks a uniform applied field and, for the field of a point dipole, it also cancels the most important term (the dipolar term) of its magnetic response. It can be demonstrated (see the Supplementary Information of [165]) that the rest of terms of the distortion are reduced by making R_2 tend to R_1. This means that a very thin ferromagnetic layer with permeability μ_2 given by Eq. (5.1) surrounding an ideal superconducting shell effectively cancels the global magnetic response.

The spherical bilayer made of an internal SC shell surrounded by a thin FM shell with permeability μ_2 decouples the interior and exterior spaces, and is magnetically undetectable from the exterior. Hence, the overall effect is changing the topology of space [48], as if the interior region had been (magnetically) removed out of the existing 3D space.

A final requirement for the wormhole is that magnetic fields have to propagate through its interior. The transfer of static magnetic fields was addressed in chapter 4, where we developed magnetic hoses that allow to transfer magnetic fields to long distances through any path. We will use one of such hoses to transfer the field between the two ends of the wormhole.

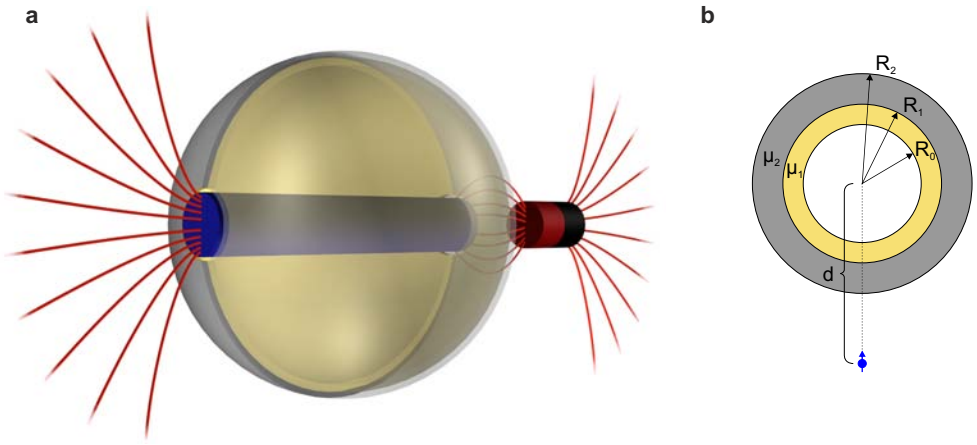

Figure 5.1: (**a**) 3D image of the magnetic wormhole, composed of a cylindrical hose (blue) surrounded by a spherical SC shell (yellow) and FM shell (gray). Half of the device is shown translucent to clarify the different parts. The field of a cylindrical magnet is sketched in red lines, showing how it is transferred through the wormhole. (**b**) Sketch of the geometry considered for the analytical derivation.

The design of the magnetostatic wormhole is, thus, being outlined. A cylindrical magnetic hose will be the core of the device. A spherical SC-FM bilayer with a thin exterior FM shell will cover the hose except in its two ends, where the bilayer cloak will have two openings to allow fields to enter and exit the wormhole (see Fig. 5.1**a**). These openings in the bilayer will affect its cloaking properties and will cause some field distortion. However, if openings are small compared to the size of the sphere, the distortion will be significant only at points very near to the ends, where distortion of the applied field is already expected because of the own ends.

5.2.1 Feasible design of a magnetic wormhole

The magnetic wormhole design requires a further development to be successfully realizable with existing materials. First, the interior hose has to be discretized following one of the strategies proposed in section 4.2.2. We consider here a set of several concentric thin FM cylinders separated by air gaps.

Regarding the exterior thin FM shell of the bilayer, it should be ideally made of a material with homogeneous permeability given by Eq. (5.1). However, materials with constant fine-tuned intermediate relative permeability values (e.g. between 5 and 20) are hard to find. For this reason we design an external *metasurface* consisting of several pieces of thin high-permeability FM foil. The size and distribution of the pieces is determined following an optimization process based on 3D-numerical simulations of the whole device. For this purpose we consider the inner ideal SC shell with $\mu \to 0$ surrounded by different arrangements of thin ideal soft FM pieces with $\mu \to \infty$. The design of the metasurface is tuned to minimize the distortion of an external uniform field

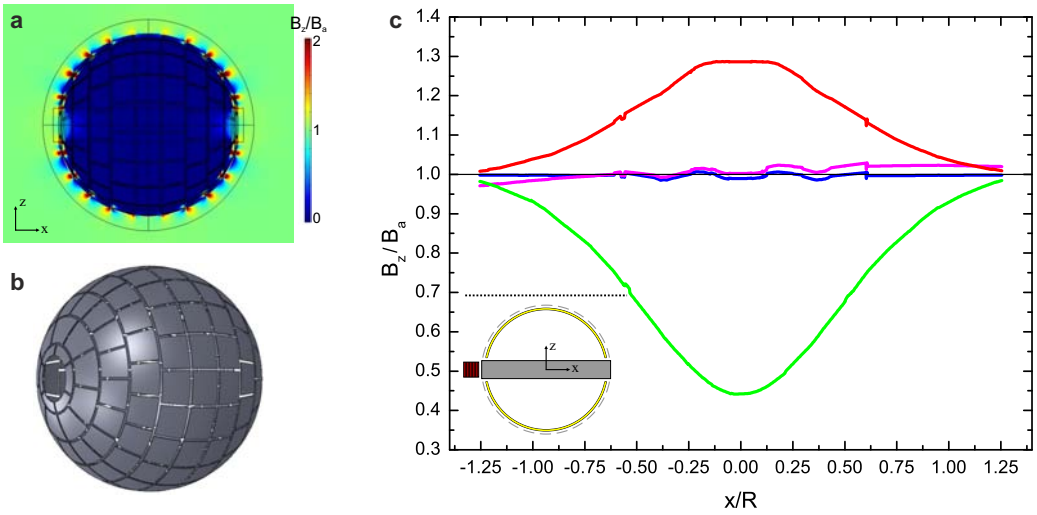

Figure 5.2: (**a**) 3D calculation of the vertical field, B_z, considering an inner spherical ideal superconducting shell ($\mu \to 0$) surrounded by the metasurface composed of thin ideal soft FM pieces ($\mu \to \infty$) distributed as shown in **b**. (**c**) Results of the 3D calculation of the complete wormhole. A cylindrical hose composed of several ideal FM pieces is introduced inside the spherical bilayer and the field is calculated along the horizontal dotted line indicated in the inset sketch. Red, green and blue lines are calculations considering only the FM metasurface, only the interior SC shell and the complete wormhole, respectively, for a uniform field B_a applied in the z-direction. Purple line corresponds to the case of the complete wormhole when the field of a small coil (in red in the inset) is also applied at one of its ends.

applied in the direction perpendicular to the internal hose. The final design is shown in Fig. 5.2**b**, together with the corresponding 3D simulation for a uniform field applied in the z-direction (Fig. 5.2**a**). Calculation shows a null overall magnetic signature, except for some small distortions appearing between the plates of the surface.

The final wormhole design is validated by a numerical calculation of the complete device. The considered hose has a length-to-radius ratio of $l/r = 14.3$ and is made of several cylindrical ideal FM shells ($\mu \to \infty$). An spherical ideal SC shell ($\mu \to 0$) with two transversal openings for the hose is surrounded by the metasurface of thin ideal FM pieces ($\mu \to \infty$). The exterior radius of the wormhole is $R = l/2$. A uniform field is applied in the z-direction (see inset in Fig. 5.2**c**) and the z-field component is calculated along a horizontal line at a distance r from the surface of the wormhole (dotted line in the inset). The cases with only the interior SC and only the exterior FM metasurface are also calculated for comparison. Calculation of the complete device is repeated adding the field of a small coil oriented in the x-direction placed near one of its ends (in red in the inset). Results are shown in Fig. 5.2**c**. They demonstrate that the magnetic signature of the complete device (blue line) is negligible compared to the distortion caused by its parts separately (red and green for the isolated FM and SC, respectively). When the field of the small coil is also present (purple line), the distortion slightly increases. The total B_z field is decreased at positions near the coil (negative x)

whilst it slightly increases at positions close to the other end (positive x). These effects are explained by taking into account that the field lines that are transferred through the wormhole return from the opposite end to the coil. This field increases the total B_z field near the wormhole's end and decreases it near the coil.

5.2.2 Experimental realization

An actual magnetic wormhole based on the presented design was built (Fig. 5.3). The magnetic hose at the core of the wormhole was made of a mu-metal foil 0.2mm thick, folded into a spiral. The different turns were separated by a cardboard sheet. The final hose had a length of 87mm, an exterior diameter of 12mm and had 8 turns of ferromagnetic foil (see Fig. 5.3**d**). The spherical superconducting shell was made of several pieces of type-II SC coated conductor 12mm width (SuperPower SF12050) wrapped around a plastic former (shown in green in Fig. 5.3**e**). In total, 32 pieces of different lengths were used, and they were fixed using small welding points between the strips and also adhesive tape (see their placement in Fig. 5.3**c**). The external metasurface (Fig. 5.3**b**) was made of several pieces of mu-metal foil 0.2mm thick. A plastic support with the appropriate shape was specially designed and 3D-printed in PLA thermoplastic (shown in red in Fig. 5.3**e**), containing the lodgings for each of the pieces. In total, 155 pieces with 6 different shapes were used, and they were placed at a radial distance of 43mm to the center of the sphere.

The experimental setup to demonstrate the wormhole properties (see Fig. 5.4**a**)

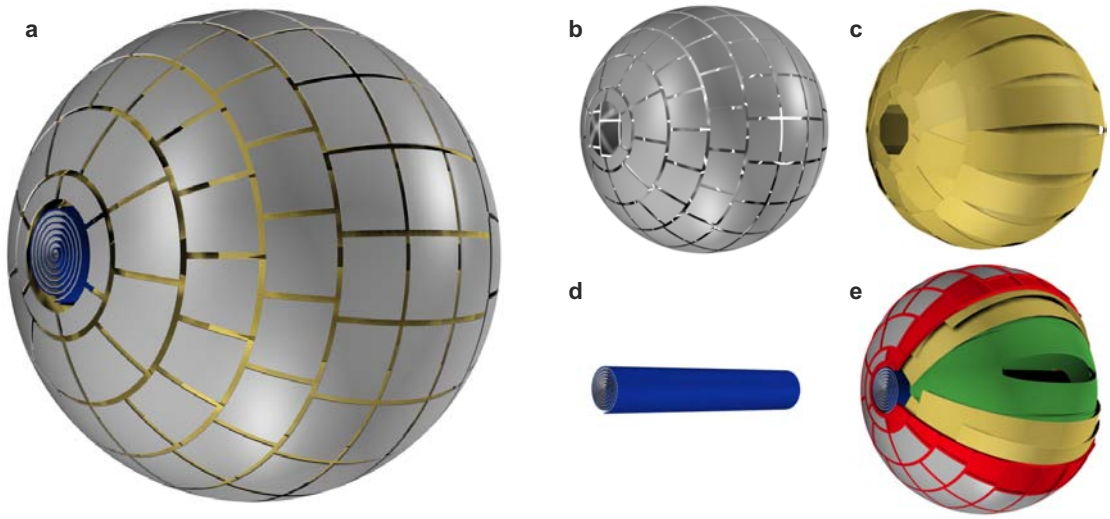

Figure 5.3: (**a**) 3D image of the complete wormhole, formed by the external metasurface made of soft FM pieces (**b**), the internal SC shell made of SC coated conductor (**c**), and the magnetic hose made of FM foil folded into a spiral (**d**). (**e**) Cross-section view of the wormhole, including the plastic formers (in green and red) used to support the SC strips and the FM pieces.

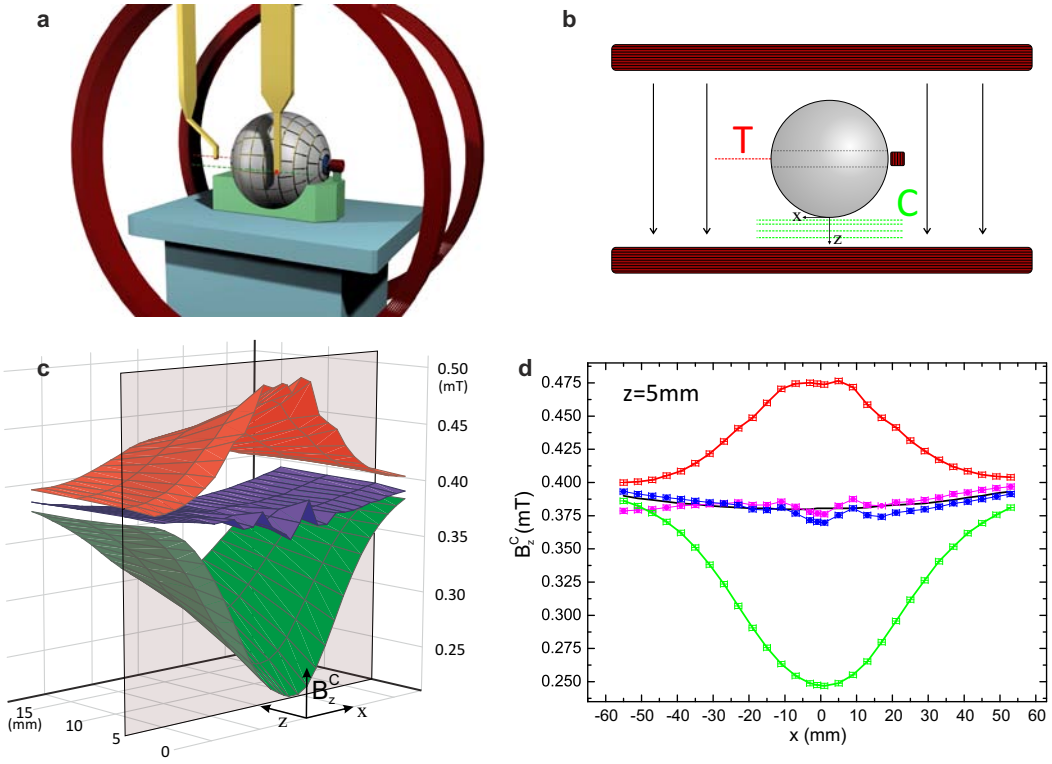

Figure 5.4: (**a**) 3D image of the experimental setup. (**b**) Detailed description of the central plane, including the lines at which probes T (red) and C (green) measured the transferred and cloaked (or distorted) fields, respectively. The uniform applied field was created by the two Helmholtz coils. (**c**) The z-component of magnetic field, B_z^{C}, was measured by probe C as a function of x and for different distances, z, to the wormhole. (**d**) Measurements at $z = 5$ are shown in detail. Red lines are for only the ferromagnetic layer, green for only the superconducting one and blue for the complete device with only the field of the Helmholtz coils. Purple line corresponds to the same measurement of the complete wormhole when the field of the small coil was also applied. Black line represent the measured applied field.

used two Helmholtz coils of radius 150mm, which created a uniform field in the central zone. The wormhole was placed centered between them, oriented with its two ends perpendicular to the applied field. A small coil at one end of the wormhole was fed with a dc current to supply the field to be transferred through it. Two Hall probes were used for the measurements. Probe T, placed at the opposite exit of the wormhole, measured the transferred magnetic field. Probe C scanned the magnetic field in lines close to the surface of the wormhole (see green lines in Fig. 5.4**b**), measuring the distortion of the applied field.

Three types of measurements were performed by probe C: (i) only the superconducting layer, without the ferromagnetic outer layer (submerging the superconductor into liquid nitrogen); (ii) only the ferromagnetic layer (measuring the whole device at room temperature, with the superconductor deactivated); and (iii) the complete wormhole, at

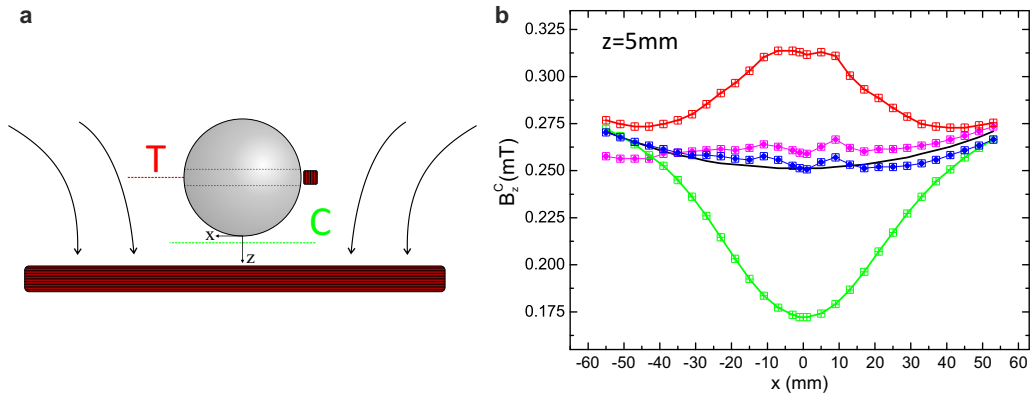

Figure 5.5: Analogous measurements of field distortion for a non-uniform applied field, created by exciting only one of the coils (**a**). Results are shown in **b**. Red lines are for only the ferromagnetic layer, green for only the superconducting one and blue for the complete device with only the field of the Helmholtz coil. Purple line corresponds to the same measurement when the field of the small coil was also applied. Black line represent the measured applied field.

liquid nitrogen temperature.

Measurement results are shown in Fig. 5.4**c** and **d** for a uniform applied field. Although measured simultaneously, we discuss the transmission and field-distortion results separately for clarity. Results of the field distortion for the three cases (i)-(iii) at a distance of 5mm are shown in Fig. 5.4**d**. The complete wormhole (blue line) demonstrated an excellent cloaking behavior, whereas the superconducting and ferromagnetic parts separately yielded clear field distortions. When the small coil was also activated (purple line) the cloaking properties of the wormhole were not significantly affected; the total B_z field near the coil (negative x) slightly decreased and at the opposite end (positive x) it increased. This effect was already found in the calculations, and can be explained by the field transferred through the wormhole. Scans performed at different distances showed very little distortion (see Fig. 5.4**c**), and only at a close distance the effect of the non-uniform ferromagnetic metasurface could be discerned.

We also measured the effect of applying a non-uniform field, created by feeding current in only one of the Helmholtz coils (Fig. 5.5). Even in this case, a very good cancellation of the field distortion was achieved for the full wormhole and not for its components separately. When the small coil was also activated, the distortion increased respect to the case of a uniform applied field. This can be understood considering that the field applied by the single Helmholtz coil was weaker than that created by the two coils. Since the field of the small coil was the same, the relative distortion on the applied field increased.

During the experiments we also measured the field transferred through the wormhole. First, the uniform external field of the Helmholtz coils was applied and then the small coil at the end of the wormhole was fed with a constant current. In these conditions, the

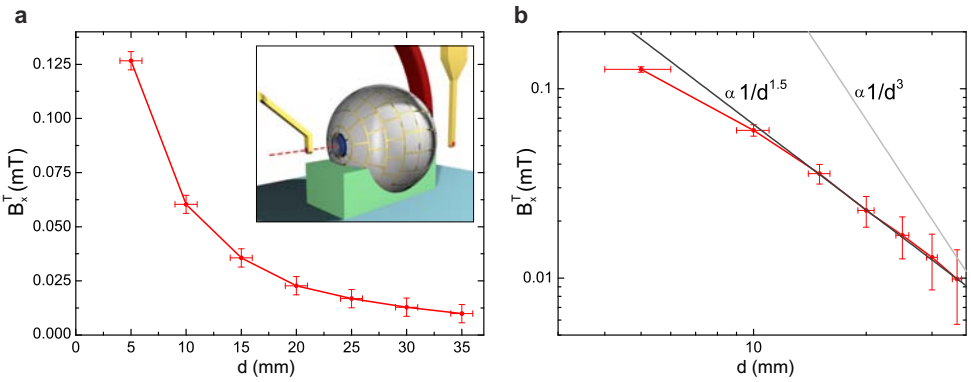

Figure 5.6: Measurements of the horizontal component of magnetic field, B_x^{T}, measured by probe T as a function of distance to the end, d, in (**a**) linear, and (**b**) double-logarithmic scales. Field shows a dependence with the distance roughly as $\sim 1/d^{1.5}$, very different from a dipolar dependence $\sim 1/d^3$.

horizontal component of the field transferred to the opposite end, B_x^{T}, was measured as a function of the distance to the end, d. Results are shown in Fig. 5.6, demonstrating a clear field transfer that decreased with the distance to the end. Interestingly, the dipolar-like magnetic field created by the coil at one end of the wormhole was transformed at the opposite end into a monopolar-like field. Actually, the spacial dependence of the exiting field tended to $\sim 1/d^{1.5}$, since close to the opening the field resembled that of a disk of monopoles (that decreases even smoother with the distance) rather than a single one ($\sim 1/d^2$). This measured monopolar field, already discussed in the original proposal of Greenleaf et al. [48], could represent an alternative to those obtained by exotic spin ices [166] and other systems [167]. Our magnetic wormhole, thus, created the illusion of a magnetic field coming out of nowhere by effectively changing the magnetic topology of space.

Finally, although we constructed a spherical wormhole, similar results could be obtained for the shape of an elongated ellipsoid that could extend to long distances in one direction. These ideas may be applied in devices requiring the local application of magnetic fields in a particular magnetic background that should not be distorted. One particularly relevant application along this line could be in magnetic resonance imaging. Using these ideas, one could foresee ways to apply a magnetic field locally to a patient, without distorting the background magnetic field in the region [48, 168]. They could be useful, for example, in medical operations using simultaneous MRI imaging [48].

Moreover, although our results were experimentally confirmed only for static magnetic fields, both involved ferromagnetic and superconducting materials showed to maintain their properties for low-frequency electromagnetic waves (see the results in sections 2.3 and 3.5). Therefore, a similar wormhole design could also be effective for low-frequency electromagnetic fields.

5.3 Chapter summary and conclusions

The link between space transformations and electromagnetic materials provided by transformation optics has made possible to build electromagnetic devices that mimic celestial objects. One of the most striking theoretical proposals consisted in an electromagnetic wormhole, which would transmit electromagnetic waves between two points in space without being electromagnetically detectable. From an electromagnetic point of view, such device would change the topology of the space. In this chapter we have extended the concept to the static magnetic case, developing and experimentally demonstrating a magnetic wormhole.

Although inspired by transformation optics, our design of a magnetic wormhole has not been based on space transformations but on the properties to shape magnetic fields that magnetic materials offer. Our initial design consisted of a magnetic hose surrounded by a 3D spherical magnetic cloak. A more feasible design has been developed, discretizing the hose into several ferromagnetic shells and the external ferromagnetic layer into a particular *metasurface*. After validating the design using full-3D numerical calculations, we have built an actual magnetic wormhole. We have experimentally demonstrated that a field can be transferred between its ends whilst the whole device is magnetically undetectable. Moreover, when a dipolar field is applied to one of its ends, a monopolar-like field appears at the other end, creating the illusion of a field coming out of nowhere.

These experiments have demonstrated the significant possibilities offered by magnetic materials to shape magnetic fields. The global effect of the wormhole is changing the magnetic topology of the space, as if the region of propagation between its two ends is removed out of the 3D magnetic space. Interestingly, such structure could also have significant applications. It could allow, for example, the application of a local magnetic field in a region with an existing background field without disturbing it.

CHAPTER 6

Conclusions

In this thesis we have introduced different new ways to shape and control magnetic fields. In addition to addressing different particular problems, like magnetic cloaking, concentration or magnetic field transfer, this research has resulted in a whole new "toolbox" to shape static magnetic fields in a general way. The theoretical design of these tools has combined transformation optics theory with solutions directly arising from Maxwell equations. Interestingly, final designs have been realized simply with combinations of ferromagnetic and superconducting materials. The complementary properties of these two kinds of materials have allowed the realization of devices that achieve very different effects.

First we have studied the cloaking of magnetic fields, presenting a theoretical design based on transformation optics (*antimagnet*) and a simpler bilayer scheme consisting of a superconducting shell surrounded by a ferromagnetic one. This bilayer cloak has been experimentally tested for both static and low-frequency magnetic fields.

Then, we have addressed the concentration of magnetic fields and have designed, by transformation optics, a magnetic concentrating shell. We have demonstrated its properties to concentrate external applied fields and also to expel the field of internal sources. A feasible design made of superconducting and ferromagnetic pieces has been studied and experimentally realized, demonstrating its ability to shape magnetic fields in the static case and also for low-frequency electromagnetic waves.

The transfer of static magnetic fields has also been studied, initially finding an ideal but unfeasible solution by transformation optics. After a further development, we have shown that a cylindrical ferromagnetic core surrounded by a superconducting shell (forming a *magnetic hose*) can transfer magnetic fields to long distances. The experimental demonstration of this property has also been conducted.

Finally, we have designed a magnetic wormhole, a device that allows to transfer magnetic fields between two points in space without being magnetically detectable. Although inspired by a proposal based on transformation optics, our design has relied on the properties of magnetic metamaterials to shape magnetic fields instead. An actual magnetic wormhole has been built using superconductors and ferromagnetic materials, and their features have been experimentally confirmed.

It is worth to remark that all the experimental realizations presented in this work have been performed as proof-of-principle experiments to demonstrate the theoretical ideas we have introduced. Further developments of these ideas could turn them into practical devices that could be applied in actual technologies.

The results of this thesis may also reveal the importance that the research in magnetostatic metamaterials can have in the near future. Transformation optics and metamaterials have provided unprecedented phenomena in many regions of the electromagnetic spectrum. However, the static magnetic case has been traditionally seen as a simpler limit that deserves much less interest. The results of this work indicate, on the contrary, that static magnetic conditions constitute an ideal case to apply transformation optics and metamaterial concepts. There are several reasons for this.

First, in the static magnetic case one can find alternative and much simpler solutions to control and manipulate fields than those for electromagnetic waves. We have demonstrated, for example, that magnetic fields can be cloaked with simply two homogeneous and isotropic layers, in contrast to electromagnetic cloaks that require cumbersome inhomogeneous and anisotropic material parameters. The magnetic concentrating shell, realizable using pieces of two commercial materials, is another good example; an analogous concentrator for electromagnetic fields would require complicated fine-tuned permeability and permittivity distributions, also in the interior space of the concentrator.

Another important advantage of the magnetic case is that natural materials exist with a wide range of magnetic permeabilities, including extreme values like $\mu = 0$ and $\mu = \infty$. Superconducting materials play a key role in this point, because they provide a magnetic shielding effect that has no direct counterpart for electromagnetic waves. Moreover, when different magnetic materials are properly combined, we have shown that tunable anisotropic effective properties can be obtained. For this reason, most of the devices conceived for shaping magnetic fields can be realized with existing materials.

And, finally, the magnetic case has a particular importance because magnetism is found at the basis of many essential scientific and industrial applications. Therefore, novel strategies to shape and control magnetic fields, as the "toolbox" presented in this thesis, could provide important advantages in many of them. The application of our magnetic bilayer cloak to actual nuclear physics experiments, or the extension of some of this research to other science areas (allowing the cloaking of diffusive light or the concentration of thermal fields) are examples of this importance. It is worth to mention that the research contained in this thesis has resulted in the filing of two

European patents, indicating the practical side of this research. Moreover, we have shown that results found in static conditions can also be applied to electromagnetic waves of low frequency. This result has a special relevance because many of the existing electromagnetic technologies rely on this low-frequency range of the electromagnetic spectrum. The novel strategies to control static magnetic fields, thus, could be directly exported to these technologies in a simple and natural way.

To sum up, the work contained in this thesis presents a set of new tools to manipulate, control and shape magnetic fields. Results provide a new horizon in which some traditional limitations for manipulating magnetic fields fade and can eventually disappear. One hundred and fifty years after the formulation of Maxwell's equations, magnetism shows there is still much to be explored.

Bibliography

[1] J. D. Jackson and J. D. Jackson, *Classical electrodynamics*, vol. 3. Wiley New York etc., 1962.

[2] H. K. Onnes *Leiden Comm.*, vol. 120b, 122b, 124c, 1911.

[3] W. Meissner and R. Ochsenfeld, "Ein neuer effekt bei eintritt der supraleitfähigkeit," *Naturwissenschaften*, vol. 21, no. 44, pp. 787–788, 1933.

[4] M.-K. Wu, J. R. Ashburn, C. Torng, P. H. Hor, R. L. Meng, L. Gao, Z. J. Huang, Y. Wang, and C. Chu, "Superconductivity at 93 k in a new mixed-phase y-ba-cu-o compound system at ambient pressure," *Physical Review Letters*, vol. 58, no. 9, p. 908, 1987.

[5] H. Maeda, Y. Tanaka, M. Fukutomi, and T. Asano, "A new high-tc oxide superconductor without a rare earth element," *Japanese Journal of Applied Physics*, vol. 27, no. 2A, p. L209, 1988.

[6] G. Blatter, M. Feigel'Man, V. Geshkenbein, A. Larkin, and V. M. Vinokur, "Vortices in high-temperature superconductors," *Reviews of Modern Physics*, vol. 66, no. 4, p. 1125, 1994.

[7] E. H. Brandt, "The flux-line lattice in superconductors," *Reports on Progress in Physics*, vol. 58, no. 11, p. 1465, 1995.

[8] J. Bardeen, L. N. Cooper, and J. R. Schrieffer, "Theory of superconductivity," *Physical Review*, vol. 108, no. 5, p. 1175, 1957.

[9] V. Ginzburg and L. Landau *Zhurnal Eksperimentalnoi i Teoreticheskoi Fiziki*, vol. 20, pp. 1064–1082, 1950.

[10] F. London and H. London, "The electromagnetic equations of the supraconductor," in *Proceedings of the Royal Society of London A: Mathematical, Physical and Engineering Sciences*, vol. 149, pp. 71–88, The Royal Society, 1935.

[11] C. Bean, "Magnetization of hard superconductors," *Physical Review Letters*, vol. 8, no. 6, pp. 250–253, 1962.

[12] C. P. Bean, "Magnetization of high-field superconductors," *Reviews of Modern Physics*, vol. 36, no. 1, pp. 31–38, 1964.

[13] D.-X. Chen and R. Goldfarb, "Kim model for magnetization of type-ii superconductors," *Journal of Applied Physics*, vol. 66, no. 6, pp. 2489–2500, 1989.

[14] D.-X. Chen and A. Sanchez, "Theoretical critical-state susceptibility spectra and their application to high-tc superconductors," *Journal of Applied Physics*, vol. 70, no. 10, pp. 5463–5477, 1991.

[15] Y. Fukumoto, H. Wiesmann, M. Garber, M. Suenaga, and P. Haldar, "Alternating-current losses in silver-sheathed (bi, pb) 2sr2ca2cu3o10 tapes ii: Role of interfilamentary coupling," *Applied Physics Letters*, vol. 67, no. 21, pp. 3180–3182, 1995.

[16] F. Gömöry, R. Tebano, A. Sanchez, E. Pardo, C. Navau, I. Husek, F. Strycek, and P. Kovac, "Current profiles and ac losses of a superconducting strip with an elliptic cross-section in a perpendicular magnetic field," *Superconductor Science and Technology*, vol. 15, no. 9, p. 1311, 2002.

[17] A. Palau, T. Puig, X. Obradors, E. Pardo, C. Navau, A. Sanchez, A. Usoskin, H. Freyhardt, L. Fernandez, B. Holzapfel, *et al.*, "Simultaneous inductive determination of grain and intergrain critical current densities of yba2cu3o7- x coated conductors," *Applied Physics Letters*, vol. 84, no. 2, pp. 230–232, 2004.

[18] N. B. Kundtz, D. R. Smith, and J. B. Pendry, "Electromagnetic design with transformation optics," *Proceedings of the IEEE*, vol. 99, no. 10, pp. 1622–1633, 2011.

[19] J. Pendry, A. Aubry, D. Smith, and S. Maier, "Transformation optics and subwavelength control of light," *Science*, vol. 337, no. 6094, pp. 549–552, 2012.

[20] J. B. Pendry, D. Schurig, and D. R. Smith, "Controlling electromagnetic fields," *Science*, vol. 312, no. 5781, pp. 1780–1782, 2006.

[21] D. Schurig, J. Pendry, and D. R. Smith, "Calculation of material properties and ray tracing in transformation media," *Optics Express*, vol. 14, no. 21, pp. 9794–9804, 2006.

[22] G. W. Milton, M. Briane, and J. R. Willis, "On cloaking for elasticity and physical equations with a transformation invariant form," *New Journal of Physics*, vol. 8, no. 10, p. 248, 2006.

[23] T. J. Cui, D. R. Smith, and R. Liu, *Metamaterials*. Springer, 2010.

[24] A. Ward and J. Pendry, "Refraction and geometry in maxwell's equations," *Journal of Modern Optics*, vol. 43, no. 4, pp. 773–793, 1996.

[25] S. A. Cummer, B.-I. Popa, D. Schurig, D. R. Smith, and J. Pendry, "Full-wave simulations of electromagnetic cloaking structures," *Physical Review E*, vol. 74, no. 3, p. 036621, 2006.

[26] D. Schurig, J. Mock, B. Justice, S. A. Cummer, J. Pendry, A. Starr, and D. Smith, "Metamaterial electromagnetic cloak at microwave frequencies," *Science*, vol. 314, no. 5801, pp. 977–980, 2006.

[27] W. Cai, U. K. Chettiar, A. V. Kildishev, and V. M. Shalaev, "Optical cloaking with metamaterials," *Nature Photonics*, vol. 1, no. 4, pp. 224–227, 2007.

[28] S. A. Cummer, R. Liu, and T. J. Cui, "A rigorous and nonsingular two dimensional cloaking coordinate transformation," *Journal of Applied Physics*, vol. 105, no. 5, p. 056102, 2009.

[29] W. X. Jiang, T. J. Cui, G. X. Yu, X. Q. Lin, Q. Cheng, and J. Y. Chin, "Arbitrarily elliptical–cylindrical invisible cloaking," *Journal of Physics D: Applied Physics*, vol. 41, no. 8, p. 085504, 2008.

[30] D.-H. Kwon and D. H. Werner, "Two-dimensional eccentric elliptic electromagnetic cloaks," *Applied Physics Letters*, vol. 92, no. 1, p. 013505, 2008.

[31] M. Rahm, D. Schurig, D. A. Roberts, S. A. Cummer, D. R. Smith, and J. B. Pendry, "Design of electromagnetic cloaks and concentrators using form-invariant coordinate transformations of maxwell's equations," *Photonics and Nanostructures-fundamentals and Applications*, vol. 6, no. 1, pp. 87–95, 2008.

[32] W. X. Jiang, J. Y. Chin, Z. Li, Q. Cheng, R. Liu, and T. J. Cui, "Analytical design of conformally invisible cloaks for arbitrarily shaped objects," *Physical Review E*, vol. 77, no. 6, p. 066607, 2008.

[33] W. Wang, L. Lin, J. Ma, C. Wang, J. Cui, C. Du, and X. Luo, "Electromagnetic concentrators with reduced material parameters based on coordinate transformation," *Optics Express*, vol. 16, no. 15, pp. 11431–11437, 2008.

[34] W. X. Jiang, T. J. Cui, Q. Cheng, J. Y. Chin, X. M. Yang, R. Liu, and D. R. Smith, "Design of arbitrarily shaped concentrators based on conformally optical transformation of nonuniform rational b-spline surfaces," *Applied Physics Letters*, vol. 92, no. 26, p. 264101, 2008.

[35] Y. Luo, H. Chen, J. Zhang, L. Ran, and J. A. Kong, "Design and analytical full-wave validation of the invisibility cloaks, concentrators, and field rotators created with a general class of transformations," *Physical Review B*, vol. 77, no. 12, p. 125127, 2008.

[36] H. Chen and C. Chan, "Transformation media that rotate electromagnetic fields," *Applied Physics Letters*, vol. 90, no. 24, p. 241105, 2007.

[37] D.-H. Kwon and D. H. Werner, "Polarization splitter and polarization rotator designs based on transformation optics," *Optics Express*, vol. 16, no. 23, pp. 18731–18738, 2008.

[38] W. X. Jiang, T. J. Cui, H. F. Ma, X. Y. Zhou, and Q. Cheng, "Cylindrical-to-plane-wave conversion via embedded optical transformation," *Applied Physics Letters*, vol. 92, no. 26, p. 261903, 2008.

[39] U. Leonhardt and T. Tyc, "Superantenna made of transformation media," *New Journal of Physics*, vol. 10, no. 11, p. 115026, 2008.

[40] L. Lin, W. Wang, J. Cui, C. Du, and X. Luo, "Design of electromagnetic refractor and phase transformer using coordinate transformation theory," *Optics Express*, vol. 16, no. 10, pp. 6815–6821, 2008.

[41] M. Rahm, S. A. Cummer, D. Schurig, J. B. Pendry, and D. R. Smith, "Optical design of reflectionless complex media by finite embedded coordinate transformations," *Physical Review Letters*, vol. 100, no. 6, p. 063903, 2008.

[42] W. X. Jiang, T. J. Cui, X. Y. Zhou, X. M. Yang, and Q. Cheng, "Arbitrary bending of electromagnetic waves using realizable inhomogeneous and anisotropic materials," *Physical Review E*, vol. 78, no. 6, p. 066607, 2008.

[43] U. Leonhardt and T. G. Philbin, "General relativity in electrical engineering," *New Journal of Physics*, vol. 8, no. 10, p. 247, 2006.

[44] D. A. Genov, S. Zhang, and X. Zhang, "Mimicking celestial mechanics in metamaterials," *Nature Physics*, vol. 5, no. 9, pp. 687–692, 2009.

[45] E. E. Narimanov and A. V. Kildishev, "Optical black hole: Broadband omnidirectional light absorber," *Applied Physics Letters*, vol. 95, no. 4, p. 041106, 2009.

[46] Q. Cheng, T. J. Cui, W. X. Jiang, and B. G. Cai, "An omnidirectional electromagnetic absorber made of metamaterials," *New Journal of Physics*, vol. 12, no. 6, p. 063006, 2010.

[47] H. Chen, R.-X. Miao, and M. Li, "Transformation optics that mimics the system outside a schwarzschild black hole," *Optics Express*, vol. 18, no. 14, pp. 15183–15188, 2010.

[48] A. Greenleaf, Y. Kurylev, M. Lassas, and G. Uhlmann, "Electromagnetic wormholes and virtual magnetic monopoles from metamaterials," *Physical Review Letters*, vol. 99, no. 18, p. 183901, 2007.

[49] P. A. Huidobro, M. L. Nesterov, L. Martin-Moreno, and F. J. Garcia-Vidal, "Transformation optics for plasmonics," *Nano Letters*, vol. 10, no. 6, pp. 1985–1990, 2010.

[50] A. Aubry, D. Y. Lei, A. I. Fernández-Domínguez, Y. Sonnefraud, S. A. Maier, and J. B. Pendry, "Plasmonic light-harvesting devices over the whole visible spectrum," *Nano Letters*, vol. 10, no. 7, pp. 2574–2579, 2010.

[51] A. Fernández-Domínguez, S. Maier, and J. Pendry, "Collection and concentration of light by touching spheres: a transformation optics approach," *Physical Review Letters*, vol. 105, no. 26, p. 266807, 2010.

[52] A. Fernández-Domínguez, A. Wiener, F. García-Vidal, S. Maier, and J. Pendry, "Transformation-optics description of nonlocal effects in plasmonic nanostructures," *Physical Review Letters*, vol. 108, no. 10, p. 106802, 2012.

[53] U. Leonhardt, "Optical conformal mapping," *Science*, vol. 312, no. 5781, pp. 1777–1780, 2006.

[54] M. Kadic, T. Bückmann, R. Schittny, and M. Wegener, "Metamaterials beyond electromagnetism," *Rep. Prog. Phys*, vol. 76, no. 126501, p. 126501, 2013.

[55] S. A. Cummer and D. Schurig, "One path to acoustic cloaking," *New Journal of Physics*, vol. 9, no. 3, p. 45, 2007.

[56] H. Chen and C. Chan, "Acoustic cloaking in three dimensions using acoustic metamaterials," *Applied Physics Letters*, vol. 91, no. 18, p. 183518, 2007.

[57] S. A. Cummer, B.-I. Popa, D. Schurig, D. R. Smith, J. Pendry, M. Rahm, and A. Starr, "Scattering theory derivation of a 3d acoustic cloaking shell," *Physical Review Letters*, vol. 100, no. 2, p. 024301, 2008.

[58] B.-I. Popa, L. Zigoneanu, and S. A. Cummer, "Experimental acoustic ground cloak in air," *Physical Review Letters*, vol. 106, no. 25, p. 253901, 2011.

[59] L. Sanchis, V. García-Chocano, R. Llopis-Pontiveros, A. Climente, J. Martínez-Pastor, F. Cervera, and J. Sánchez-Dehesa, "Three-dimensional axisymmetric cloak based on the cancellation of acoustic scattering from a sphere," *Physical Review Letters*, vol. 110, no. 12, p. 124301, 2013.

[60] M. Farhat, S. Enoch, S. Guenneau, and A. Movchan, "Broadband cylindrical acoustic cloak for linear surface waves in a fluid," *Physical Review Letters*, vol. 101, no. 13, p. 134501, 2008.

[61] H. Chen, J. Yang, J. Zi, and C. Chan, "Transformation media for linear liquid surface waves," *EPL (Europhysics Letters)*, vol. 85, no. 2, p. 24004, 2009.

[62] M. Brun, S. Guenneau, and A. B. Movchan, "Achieving control of in-plane elastic waves," *Applied Physics Letters*, vol. 94, no. 6, p. 061903, 2009.

[63] M. Farhat, S. Guenneau, S. Enoch, and A. B. Movchan, "Cloaking bending waves propagating in thin elastic plates," *Physical Review B*, vol. 79, no. 3, p. 033102, 2009.

[64] M. Farhat, S. Guenneau, and S. Enoch, "Ultrabroadband elastic cloaking in thin plates," *Physical Review Letters*, vol. 103, no. 2, p. 024301, 2009.

[65] S. Brûlé, E. Javelaud, S. Enoch, and S. Guenneau, "Experiments on seismic metamaterials: Molding surface waves," *Physical Review Letters*, vol. 112, no. 13, p. 133901, 2014.

[66] S. Guenneau, C. Amra, and D. Veynante, "Transformation thermodynamics: cloaking and concentrating heat flux," *Optics Express*, vol. 20, no. 7, pp. 8207–8218, 2012.

[67] S. Narayana and Y. Sato, "Heat flux manipulation with engineered thermal materials," *Physical Review Letters*, vol. 108, no. 21, p. 214303, 2012.

[68] R. Schittny, M. Kadic, S. Guenneau, and M. Wegener, "Experiments on transformation thermodynamics: molding the flow of heat," *Physical Review Letters*, vol. 110, no. 19, p. 195901, 2013.

[69] J. Pendry, A. Holden, W. Stewart, and I. Youngs, "Extremely low frequency plasmons in metallic mesostructures," *Physical Review Letters*, vol. 76, no. 25, p. 4773, 1996.

[70] J. B. Pendry, A. J. Holden, D. Robbins, and W. Stewart, "Magnetism from conductors and enhanced nonlinear phenomena," *Microwave Theory and Techniques, IEEE Transactions on*, vol. 47, no. 11, pp. 2075–2084, 1999.

[71] R. A. Shelby, D. R. Smith, and S. Schultz, "Experimental verification of a negative index of refraction," *Science*, vol. 292, no. 5514, pp. 77–79, 2001.

[72] V. G. Veselago, "The electrodynamics of substances with simultaneously negative values of ε and μ," *Physics-Uspekhi*, vol. 10, no. 4, pp. 509–514, 1968.

[73] J. B. Pendry, "Negative refraction makes a perfect lens," *Physical Review Letters*, vol. 85, no. 18, p. 3966, 2000.

[74] D. R. Smith, W. J. Padilla, D. Vier, S. C. Nemat-Nasser, and S. Schultz, "Composite medium with simultaneously negative permeability and permittivity," *Physical Review Letters*, vol. 84, no. 18, p. 4184, 2000.

[75] J. Pendry, "Optics: Positively negative," *Nature*, vol. 423, no. 6935, pp. 22–23, 2003.

[76] D. R. Smith, J. B. Pendry, and M. C. Wiltshire, "Metamaterials and negative refractive index," *Science*, vol. 305, no. 5685, pp. 788–792, 2004.

[77] C. M. Soukoulis, S. Linden, and M. Wegener, "Negative refractive index at optical wavelengths," *Science*, vol. 315, no. 5808, pp. 47–49, 2007.

[78] A. Greenleaf, M. Lassas, and G. Uhlmann, "Anisotropic conductivities that cannot be detected by eit," *Physiological measurement*, vol. 24, no. 2, p. 413, 2003.

[79] A. Alu and N. Engheta, "Plasmonic and metamaterial cloaking: physical mechanisms and potentials," *Journal of Optics A: Pure and Applied Optics*, vol. 10, no. 9, p. 093002, 2008.

[80] J. Perczel, T. Tyc, and U. Leonhardt, "Invisibility cloaking without superluminal propagation," *New Journal of Physics*, vol. 13, no. 8, p. 083007, 2011.

[81] P. Alitalo, F. Bongard, J.-F. Zürcher, J. Mosig, and S. Tretyakov, "Experimental verification of broadband cloaking using a volumetric cloak composed of periodically stacked cylindrical transmission-line networks," *Applied Physics Letters*, vol. 94, no. 1, p. 014103, 2009.

[82] F. Monticone and A. Alù, "Do cloaked objects really scatter less?," *Physical Review X*, vol. 3, no. 4, p. 041005, 2013.

[83] R. Fleury and A. Alù, "Cloaking and invisibility: A review," in *Forum Electromagn. Res. Methods Appl. Technol.(FERMAT)*, vol. 1, pp. 1–24, 2014.

[84] U. Leonhardt and T. Tyc, "Broadband invisibility by non-euclidean cloaking," *Science*, vol. 323, no. 5910, pp. 110–112, 2009.

[85] J. Li and J. Pendry, "Hiding under the carpet: a new strategy for cloaking," *Physical Review Letters*, vol. 101, no. 20, p. 203901, 2008.

[86] R. Liu, C. Ji, J. Mock, J. Chin, T. Cui, and D. Smith, "Broadband ground-plane cloak," *Science*, vol. 323, no. 5912, pp. 366–369, 2009.

[87] T. Ergin, N. Stenger, P. Brenner, J. B. Pendry, and M. Wegener, "Three-dimensional invisibility cloak at optical wavelengths," *Science*, vol. 328, no. 5976, pp. 337–339, 2010.

[88] M. Gharghi, C. Gladden, T. Zentgraf, Y. Liu, X. Yin, J. Valentine, and X. Zhang, "A carpet cloak for visible light," *Nano Letters*, vol. 11, no. 7, pp. 2825–2828, 2011.

[89] H. Chen and B. Zheng, "Broadband polygonal invisibility cloak for visible light," *Scientific reports*, vol. 2, 2012.

[90] H. Chen, B. Zheng, L. Shen, H. Wang, X. Zhang, N. I. Zheludev, and B. Zhang, "Ray-optics cloaking devices for large objects in incoherent natural light," *Nature Ccommunications*, vol. 4, 2013.

[91] A. Alù and N. Engheta, "Achieving transparency with plasmonic and metamaterial coatings," *Physical Review E*, vol. 72, no. 1, p. 016623, 2005.

[92] P.-Y. Chen, J. Soric, and A. Alu, "Invisibility and cloaking based on scattering cancellation," *Advanced Materials*, vol. 24, no. 44, pp. OP281–OP304, 2012.

[93] D. Rainwater, A. Kerkhoff, K. Melin, J. Soric, G. Moreno, and A. Alù, "Experimental verification of three-dimensional plasmonic cloaking in free-space," *New Journal of Physics*, vol. 14, no. 1, p. 013054, 2012.

[94] J. Soric, P. Chen, A. Kerkhoff, D. Rainwater, K. Melin, and A. Alù, "Demonstration of an ultralow profile cloak for scattering suppression of a finite-length rod in free space," *New Journal of Physics*, vol. 15, no. 3, p. 033037, 2013.

[95] M. Wegener, "Metamaterials beyond optics," *Science*, vol. 342, no. 6161, pp. 939–940, 2013.

[96] J. Li, Y. Gao, and J. Huang, "A bifunctional cloak using transformation media," *Journal of Applied Physics*, vol. 108, no. 7, p. 074504, 2010.

[97] H. Xu, X. Shi, F. Gao, H. Sun, and B. Zhang, "Ultrathin three-dimensional thermal cloak," *Physical Review Letters*, vol. 112, no. 5, p. 054301, 2014.

[98] T. Han, X. Bai, D. Gao, J. T. Thong, B. Li, and C.-W. Qiu, "Experimental demonstration of a bilayer thermal cloak," *Physical Review Letters*, vol. 112, no. 5, p. 054302, 2014.

[99] R. Schittny, M. Kadic, T. Bückmann, and M. Wegener, "Invisibility cloaking in a diffusive light scattering medium," *Science*, vol. 345, no. 6195, pp. 427–429, 2014.

[100] B. Wood and J. Pendry, "Metamaterials at zero frequency," *Journal of Physics: Condensed Matter*, vol. 19, no. 7, p. 076208, 2007.

[101] C. Navau, D.-X. Chen, A. Sanchez, and N. Del-Valle, "Magnetic properties of a dc metamaterial consisting of parallel square superconducting thin plates," *Applied Physics Letters*, vol. 94, no. 24, p. 242501, 2009.

[102] F. Magnus, B. Wood, J. Moore, K. Morrison, G. Perkins, J. Fyson, M. Wiltshire, D. Caplin, L. Cohen, and J. Pendry, "A dc magnetic metamaterial," *Nature Materials*, vol. 7, no. 4, pp. 295–297, 2008.

[103] F. Yang, Z. L. Mei, T. Y. Jin, and T. J. Cui, "Dc electric invisibility cloak," *Physical Review Letters*, vol. 109, no. 5, p. 053902, 2012.

[104] M. Liu, Z. L. Mei, X. Ma, and T. J. Cui, "dc illusion and its experimental verification," *Applied Physics Letters*, vol. 101, no. 5, p. 051905, 2012.

[105] Z. L. Mei, Y. S. Liu, F. Yang, and T. J. Cui, "A dc carpet cloak based on resistor networks," *Optics Express*, vol. 20, no. 23, pp. 25758–25765, 2012.

[106] A. Sanchez, C. Navau, J. Prat-Camps, and D.-X. Chen, "Antimagnets: controlling magnetic fields with superconductor–metamaterial hybrids," *New Journal of Physics*, vol. 13, no. 9, p. 093034, 2011.

[107] A. Greenleaf, Y. Kurylev, M. Lassas, and G. Uhlmann, "Cloaking devices, electromagnetic wormholes, and transformation optics," *SIAM review*, vol. 51, no. 1, pp. 3–33, 2009.

[108] H. Chen, C. Chan, and P. Sheng, "Transformation optics and metamaterials," *Nature Materials*, vol. 9, no. 5, pp. 387–396, 2010.

[109] U. Leonhardt, "To invisibility and beyond," *Nature*, vol. 471, no. 7338, pp. 292–293, 2011.

[110] J. Prat-Camps, A. Sanchez, and C. Navau, "Superconductor–ferromagnetic metamaterials for magnetic cloaking and concentration," *Superconductor Science and Technology*, vol. 26, no. 7, p. 074001, 2013.

[111] S. Narayana and Y. Sato, "Dc magnetic cloak," *Advanced Materials*, vol. 24, no. 1, pp. 71–74, 2012.

[112] F. Gömöry, M. Solovyov, J. Šouc, C. Navau, J. Prat-Camps, and A. Sanchez, "Experimental realization of a magnetic cloak," *Science*, vol. 335, no. 6075, pp. 1466–1468, 2012.

[113] J. Prat-Camps, C. Navau, D.-X. Chen, and A. Sanchez, "Exact analytical demagnetizing factors for long hollow cylinders in transverse field," *Magnetics Letters, IEEE*, vol. 3, pp. 0500104–0500104, 2012.

[114] A. Deshpande and N. Feege, "Magnetic field cloaking device rd2013-2 progress report," January 2014.

[115] B. Coe, K. Dehmelt, A. Deshpande, and N. Feege, "A compact magnetic cloaking device for future collider experiments," *Bulletin of the American Physical Society*, vol. 58, 2013.

[116] J. Souc, M. Solovyov, F. Gömöry, J. Prat-Camps, C. Navau, and A. Sanchez, "A quasistatic magnetic cloak," *New Journal of Physics*, vol. 15, no. 5, p. 053019, 2013.

[117] J. Šouc, F. Gömöry, and M. Vojenčiak, "Calibration free method for measurement of the ac magnetization loss," *Superconductor Science and Technology*, vol. 18, no. 5, p. 592, 2005.

[118] S. Chikazumi, *Physics of Ferromagnetism 2e.* No. 94, Oxford University Press, 2009.

[119] R. A. Hein, T. L. Francavilla, and D. H. Liebenberg, *Magnetic susceptibility of superconductors and other spin systems.* Springer Science & Business Media, 1991.

[120] W. L. Barnes, A. Dereux, and T. W. Ebbesen, "Surface plasmon subwavelength optics," *Nature*, vol. 424, no. 6950, pp. 824–830, 2003.

[121] E. Moreno, S. G. Rodrigo, S. I. Bozhevolnyi, L. Martin-Moreno, and F. Garcia-Vidal, "Guiding and focusing of electromagnetic fields with wedge plasmon polaritons," *Physical Review L*, vol. 100, no. 2, p. 023901, 2008.

[122] J. A. Schuller, E. S. Barnard, W. Cai, Y. C. Jun, J. S. White, and M. L. Brongersma, "Plasmonics for extreme light concentration and manipulation," *Nature Materials*, vol. 9, no. 3, pp. 193–204, 2010.

[123] C. Navau, J. Prat-Camps, and A. Sanchez, "Magnetic energy harvesting and concentration at a distance by transformation optics," *Physical Review Letters*, vol. 109, no. 26, p. 263903, 2012.

[124] S. X. Wang and G. Li, "Advances in giant magnetoresistance biosensors with magnetic nanoparticle tags: review and outlook," *Magnetics, IEEE Transactions on*, vol. 44, no. 7, pp. 1687–1702, 2008.

[125] V. Pizzella, S. Della Penna, C. Del Gratta, and G. L. Romani, "Squid systems for biomagnetic imaging," *Superconductor Science and Technology*, vol. 14, no. 7, p. R79, 2001.

[126] R. Fagaly, "Superconducting quantum interference device instruments and applications," *Review of scientific instruments*, vol. 77, no. 10, p. 101101, 2006.

[127] P.-A. Besse, G. Boero, M. Demierre, V. Pott, and R. Popovic, "Detection of a single magnetic microbead using a miniaturized silicon hall sensor," *Applied Physics Letters*, vol. 80, no. 22, pp. 4199–4201, 2002.

[128] D. Robbes, "Highly sensitive magnetometers a review," *Sensors and Actuators A: Physical*, vol. 129, no. 1, pp. 86–93, 2006.

[129] M. Pannetier, C. Fermon, G. Le Goff, J. Simola, and E. Kerr, "Femtotesla magnetic field measurement with magnetoresistive sensors," *Science*, vol. 304, no. 5677, pp. 1648–1650, 2004.

[130] P. Ripka and M. Janošek, "Advances in magnetic field sensors," 2010.

[131] J. Lenz and A. S. Edelstein, "Magnetic sensors and their applications," *Sensors Journal, IEEE*, vol. 6, no. 3, pp. 631–649, 2006.

[132] W. C. Griffith, R. Jimenez-Martinez, V. Shah, S. Knappe, and J. Kitching, "Miniature atomic magnetometer integrated with flux concentrators," *Applied Physics Letters*, vol. 94, no. 2, pp. 023502–023502, 2009.

[133] R. Kleiner, D. Koelle, F. Ludwig, and J. Clarke, "Superconducting quantum interference devices: State of the art and applications," *Proceedings of the IEEE*, vol. 92, no. 10, pp. 1534–1548, 2004.

[134] A. A. B. Brojeny, Y. Mawatari, M. Benkraouda, and J. R. Clem, "Magnetic fields and currents for two current-carrying parallel coplanar superconducting strips in a perpendicular magnetic field," *Superconductor Science and Technology*, vol. 15, no. 10, p. 1454, 2002.

[135] A. Kurs, A. Karalis, R. Moffatt, J. D. Joannopoulos, P. Fisher, and M. Soljačić, "Wireless power transfer via strongly coupled magnetic resonances," *Science*, vol. 317, no. 5834, pp. 83–86, 2007.

[136] D. Huang, Y. Urzhumov, D. R. Smith, K. H. Teo, and J. Zhang, "Magnetic superlens-enhanced inductive coupling for wireless power transfer," *Journal of Applied Physics*, vol. 111, no. 6, p. 064902, 2012.

[137] M. Kobayashi and A. Pascual-Leone, "Transcranial magnetic stimulation in neurology," *The Lancet Neurology*, vol. 2, no. 3, pp. 145–156, 2003.

[138] G. Bonmassar, S. W. Lee, D. K. Freeman, M. Polasek, S. I. Fried, and J. T. Gale, "Microscopic magnetic stimulation of neural tissue," *Nature Communications*, vol. 3, p. 921, 2012.

[139] J. Prat-Camps, C. Navau, and A. Sanchez, "Experimental realization of magnetic energy concentration and transmission at a distance by metamaterials," *Applied Physics Letters*, vol. 105, no. 23, p. 234101, 2014.

[140] F. Sun and S. He, "Create a uniform static magnetic field over 50 t in a large free space region," *Progress In Electromagnetics Research*, vol. 137, pp. 149–157, 2013.

[141] F. Sun and S. He, "Static magnetic field concentration and enhancement using magnetic materials with positive permeability," *Progress In Electromagnetics Research*, vol. 142, pp. 579–590, 2013.

[142] F. Sun and S. He, "Dc magnetic concentrator and omnidirectional cascaded cloak by using only one or two homogeneous anisotropic materials of positive permeability," *Progress In Electromagnetics Research*, vol. 142, pp. 683–699, 2013.

[143] F. Sun and S. He, "Transformation inside a null-space region and a dc magnetic funnel for achieving an enhanced magnetic flux with a large gradient," *Progress In Electromagnetics Research*, vol. 146, pp. 143–153, 2014.

[144] K. Liu, W. Jiang, F. Sun, and S. He, "Experimental realization of strong dc magnetic enhancement with transformation optics," *Progress In Electromagnetics Research*, vol. 146, pp. 187–194, 2014.

[145] R. Bjørk, A. Smith, and C. R. Bahl, "Metamaterial anisotropic flux concentrators and magnetic arrays," *Journal of Applied Physics*, vol. 114, no. 5, p. 053912, 2013.

[146] T. Han, H. Ye, Y. Luo, S. P. Yeo, J. Teng, S. Zhang, and C.-W. Qiu, "Manipulating dc currents with bilayer bulk natural materials," *Advanced Materials*, vol. 26, no. 21, pp. 3478–3483, 2014.

[147] T. Han, J. Zhao, T. Yuan, D. Y. Lei, B. Li, and C.-W. Qiu, "Theoretical realization of an ultra-efficient thermal-energy harvesting cell made of natural materials," *Energy & Environmental Science*, vol. 6, no. 12, pp. 3537–3541, 2013.

[148] J. Prat-Camps, C. Navau, and A. Sanchez, "Magnetic coupling enhancement by effective space cancellation," *preprint*, 2015.

[149] N. Tesla, "Colorado springs notes 1899-1900," *Nilola Tesla Museum, Beograd: Nolit*, p. 395, 1978.

[150] Y. Urzhumov and D. R. Smith, "Metamaterial-enhanced coupling between magnetic dipoles for efficient wireless power transfer," *Physical Review B*, vol. 83, no. 20, p. 205114, 2011.

[151] G. Lipworth, J. Ensworth, K. Seetharam, D. Huang, J. S. Lee, P. Schmalenberg, T. Nomura, M. S. Reynolds, D. R. Smith, and Y. Urzhumov, "Magnetic metamaterial superlens for increased range wireless power transfer," *Scientific reports*, vol. 4, 2014.

[152] B. Wang, K. H. Teo, T. Nishino, W. Yerazunis, J. Barnwell, and J. Zhang, "Experiments on wireless power transfer with metamaterials," *Applied Physics Letters*, vol. 98, no. 25, p. 254101, 2011.

[153] J. D. Irwin and R. M. Nelms, *Basic engineering circuit analysis*. John Wiley & Sons, 2007.

[154] J. M. Coey, *Magnetism and magnetic materials*. Cambridge University Press, 2010.

[155] D. B. Carlton, N. C. Emley, E. Tuchfeld, and J. Bokor, "Simulation studies of nanomagnet-based logic architecture," *Nano Letters*, vol. 8, no. 12, pp. 4173–4178, 2008.

[156] C. Navau, J. Prat-Camps, O. Romero-Isart, J. I. Cirac, and A. Sanchez, "Long-distance transfer and routing of static magnetic fields," *Physical Review Letters*, vol. 112, p. 253901, Jun 2014.

[157] Y. Levin and F. B. Rizzato, "Superconducting pipes and levitating magnets," *Physical Review E*, vol. 74, no. 6, p. 066605, 2006.

[158] R. Cowburn and M. Welland, "Room temperature magnetic quantum cellular automata," *Science*, vol. 287, no. 5457, pp. 1466–1468, 2000.

[159] R. Cowburn, A. Adeyeye, and M. Welland, "Controlling magnetic ordering in coupled nanomagnet arrays," *New Journal of Physics*, vol. 1, no. 1, p. 16, 1999.

[160] D. A. Allwood, G. Xiong, C. Faulkner, D. Atkinson, D. Petit, and R. Cowburn, "Magnetic domain-wall logic," *Science*, vol. 309, no. 5741, pp. 1688–1692, 2005.

[161] J. Stajic, "The future of quantum information processing," *Science*, vol. 339, no. 6124, pp. 1163–1163, 2013.

[162] T. Gaebel, M. Domhan, I. Popa, C. Wittmann, P. Neumann, F. Jelezko, J. R. Rabeau, N. Stavrias, A. D. Greentree, S. Prawer, *et al.*, "Room-temperature coherent coupling of single spins in diamond," *Nature Physics*, vol. 2, no. 6, pp. 408–413, 2006.

[163] W. Lu, J. Jin, Z. Lin, and H. Chen, "A simple design of an artificial electromagnetic black hole," *Journal of Applied Physics*, vol. 108, no. 6, p. 064517, 2010.

[164] M. Kadic, G. Dupont, S. Enoch, and S. Guenneau, "Invisible waveguides on metal plates for plasmonic analogs of electromagnetic wormholes," *Physical Review A*, vol. 90, no. 4, p. 043812, 2014.

[165] J. Prat-Camps, C. Navau, and A. Sanchez, "A magnetic wormhole," *preprint*, 2015.

[166] C. Castelnovo, R. Moessner, and S. L. Sondhi, "Magnetic monopoles in spin ice," *Nature*, vol. 451, no. 7174, pp. 42–45, 2008.

[167] M. Ray, E. Ruokokoski, S. Kandel, M. Möttönen, and D. Hall, "Observation of dirac monopoles in a synthetic magnetic field," *Nature*, vol. 505, no. 7485, pp. 657–660, 2014.

[168] S. M. Anlage, "Magnetic hose keeps fields from spreading," *Physics*, vol. 7, p. 67, 2014.

List of publications by Jordi Prat-Camps

1. A. Sanchez, C. Navau, J. Prat-Camps and D.-X. Chen
"Antimagnets: controlling magnetic fields with superconductor-metamaterial hybrids", *New Journal of Physics* **13**, 093034 (2011).

2. F. Gömöry, M. Solovyov, J. Šouc, C. Navau, J. Prat-Camps, and A. Sanchez
"Experimental realization of a magnetic cloak", *Science* **335**, 1466 (2012).

3. J. Prat-Camps, C. Navau, D.-X. Chen and A. Sanchez
"Exact Analytical Demagnetizing Factors for Long Hollow Cylinders in Transverse Field", *IEEE Magnetics Letters* **3**, 5000104 (2012).

4. C. Navau, J. Prat-Camps and A. Sanchez
"Magnetic Energy Harvesting and Concentration at a Distance by Transformation Optics", *Physical Review Letters* **109**, 263903 (2012).

5. J. Šouc, M. Solovyov, F. Gömöry, J. Prat-Camps, C. Navau and A. Sanchez
"A quasistatic magnetic cloak", *New Journal of Physics* **15**, 053019 (2013).

6. J. Prat-Camps, C. Navau and A. Sanchez
"Superconductor-ferromagnetic metamaterials for magnetic cloaking and concentration", *Superconductor Science and Technology* **26**, 074001 (2013).

7. C. Navau, J. Prat-Camps, O.Romero-Isart, J.I. Cirac and A. Sanchez
"Long-Distance Transfer and Routing of Static Magnetic Fields", *Physical Review Letters* **112**, 253901 (2014).

8. J. Prat-Camps, C. Navau and A. Sanchez
"Experimental realization of magnetic energy concentration and transmission at a distance by metamaterials", *Applied Physics Letters* **105**, 234101 (2014).

9. J. Prat-Camps, C. Navau and A. Sanchez
"A magnetic wormhole", *preprint* (2015).

10. J. Prat-Camps, C. Navau and A. Sanchez
"Magnetic coupling enhancement by effective space cancellation", *preprint* (2015).